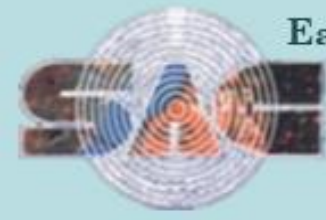
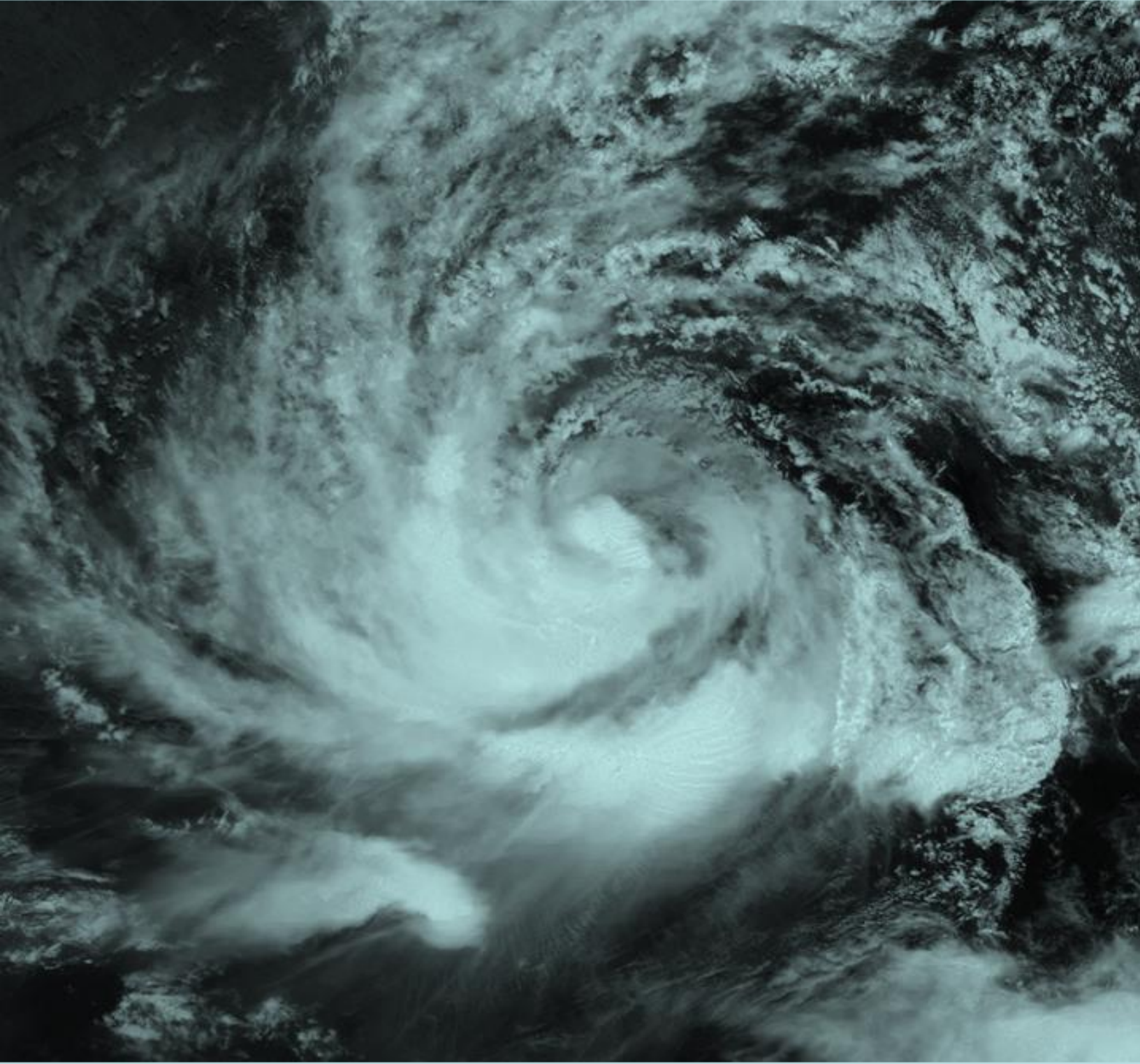




TROPICAL CYCLONE YAAS

PREDICTION, MONITORING AND ANALYSIS OF AFTER EFFECTS

SAC/EPSA/SR-01/2021



Earth, Ocean, Atmosphere, Planetary Sciences and Applications Area
Space Applications Centre (ISRO), Ahmedabad-380015

June, 2021

Document Control and DATA Sheet

Report No.	SAC/EPSA/ SR-01/2021
Date	June, 2021
Title	Tropical Cyclone YAAS: Prediction, Monitoring and Analysis of After Effects
Type of Report	Scientific Report
No. of Pages	109
Authors	Team
Number of Figures	58
Number of Tables	13
Number of References	52
Originating Unit	EPSA/SAC
Abstract	On May 23, 2021 a Very Severe Cyclonic Storm (VSCS) YAAS developed over the Bay of Bengal (BoB) that hit the Odisha coast to the south of Balasore with maximum sustained wind speed (MSW) of 75 kts on May 26, 2021. Cyclone was continuously monitored in the real-time and forecasts were generated using a combination of satellite observations, statistical and dynamical models at Space Applications Centre (SAC/ISRO), Ahmedabad. Post-landfall effects of cyclone on coastal zone and resources, agricultural crops, forest regions, inland water inundation, and ocean primary productivity were analysed using in-situ observations, satellite data and numerical models. The role of satellite data in understanding different processes related to cyclone has been brought out in this report.
Key words	cyclone, prediction, satellite observations, sea surface temperature, storm surge, inundation, wave prediction, salinity, rainfall, flood, hydrological modelling, upwelling, biological productivity, chlorophyll, damage assessment, crops, forest
Security classification	Unrestricted

Team

1. Neeru Jaiswal
2. Shivani Shah
3. Anup Kumar Mandal
4. Seemanth M.
5. Jishad M.
6. Suchandra Aich Bhowmick
7. Neerja Sharma
8. Shard Chander
9. Amit K. Dubey
10. Vibhuti B. Jha
11. Rohit Pradhan
12. Nimisha Singh
13. Debojyoti Ganguly
14. R.K. Sarangi
15. N. Jaiganesh
16. Arvind Sahay
17. Saroj Maity
18. Rojalin Tripathy
19. Nikhil V. Lele
20. Ayan Das
21. Mukesh Kumar
22. Neeraj Agarwal
23. Mehul Pandya
24. Mini Raman
25. Bimal Bhattacharya
26. R.P. Singh
27. A K Varma
28. Rashmi Sharma
29. I. M. Bahuguna

Acknowledgements

The preparation of this report on various aspects of cyclone YAAS was jointly carried out by scientists of a task team constituted by, Deputy Director, Earth, Ocean, Atmosphere and Planetary Science Applications Area (EPSA), SAC (ISRO).

Task team members wish to express sincere gratitude to the Director, SAC (ISRO), for his keen interest, overall guidance and encouragement for the work undertaken in this report.

Encouragement and persistent support with guidance given by Deputy Director, Earth, Ocean, Atmosphere and Planetary Science Applications Area (EPSA), SAC (ISRO) during the course of this work is gratefully acknowledged. He was instrumental in formation of the task teams with specific objectives and provided full support for successfully executing the study objectives.

It was not possible to complete the study without the support of various national and international agencies. We sincerely thank India Meteorological Department (IMD) for the real-time cyclone updates and for providing the best estimates of cyclone track and intensity. The data provided by Indian National Centre for Ocean Information Services (INCOIS) for oceanic studies is very much acknowledged. Authors are thankful to NDC/NRSC, Hyderabad for providing Oceansat-2 OCM datasets. Thanks are due to the National Center for Environmental Prediction (NCEP) for providing the valuable data for the models, JTWC for providing real-time cyclone track and intensity estimation, JAXA for providing GSMAp rainfall data, NASA archive for providing MODIS AQUA, VIIRS and OLCI data datasets which has been used to produce chlorophyll images and TRMM3B42 datasets which has been used to validate the rain products. The authors also acknowledge the Environmental Modeling Center (EMC) of NCEP for providing HWRF modeling system.

Summary

On May 23, 2021 a Very Severe Cyclonic Storm (VSCS) YAAS developed over the Bay of Bengal (BoB) that hit the Odisha coast to the south of Balasore with maximum sustained wind speed (MSW) of 75 kts on May 26, 2021. Cyclone was continuously monitored in the real-time and forecasts were generated using a combination of satellite observations, statistical and dynamical models at Space Applications Centre (SAC/ISRO), Ahmedabad. Post-landfall effects of cyclone on coastal zone and resources, agricultural crops, forest regions, inland water inundation, and ocean primary productivity were analysed using in-situ observations, satellite data and numerical models. The role of satellite data in understanding different processes related to cyclone has been brought out in this report. Accurate predictions of cyclogenesis, intensification and landfall as well as the prediction of ocean state helped in saving many lives, due to appropriate measures by disaster management authorities.

The genesis potential parameter (GPP) using NCEP-GFS data showed the signatures of tropical cyclogenesis in BoB on May 20. Once declared as a tropical storm by IMD, prediction of cyclone track and intensity were made at SAC using in-house dynamical-numerical modelling system comprising of SAC-Lagrangian Advection Model and Hurricane Weather Research Forecast (HWRF) model. These real-time predictions were validated using observations from India Meteorological Department. The 24 hour lead time prediction error in landfall position and time was about 19 km and 6 hour (early), respectively. Apart from this, cyclone structural parameters and rapid changes in the inner core of TC were estimated using INSAT-3D data. The surface wind speed derived from SMAP satellite was also analyzed to study cyclone wind asymmetry.

Since the cyclogenesis takes place over oceans, the ocean heat and associated features are important parameters for cyclone predictions. Warm (positive) SST anomaly ($\sim 2^{\circ}\text{C}$) was observed in the central Bay of Bengal in the observations from INSAT-3D and GHRSST. Correspondingly there was high positive TCHP anomaly ($(\sim 60\text{kJ/cm}^2)$ seen in the satellite data assimilative numerical ocean model outputs. Real-time in-house simulations from Advanced Circulation Model (ADCIRC) and Simulating wave nearshore (SWAN)

predicted high storm surge and severe inundation in the low-lying areas of Sundarbans. These simulations were validated using the tide gauge data at Dharma port. The wave model WAVEWATCH-III predicted high cyclonic wave height up to 5.6m.

Precipitation during Yaas was well captured by H-E rainfall algorithm based on INSAT-3D satellite measurements. Tropical cyclone (TC) rain structure was captured well from genesis to dissipation. High-intensity rain was recorded on 25th and 26th May 2021, when YAAS achieved its ‘very severe cyclonic storm’ status. The rainfall estimates were validated using surface based rain gauge observations over three states (Odisha, Jharkhand and West Bengal). Heavy rain from Yaas created flood like situation in the coastal districts of Orissa and West Bengal. It also impacted Jharkhand, Bihar and Eastern parts of Uttar Pradesh.

In this report, various hydrological aspects are also analyzed with the help of remote sensing dataset with the aim of potential identification of most vulnerable areas for flood. The cyclone induced flood inundation probability was derived by making use of in-house developed SACHYDRO hydrological model. Surface inundation after Cyclone Yaas in the Eastern Coast of India was mapped using Sentinel-1, C band SAR data at a 10 m resolution. AMSR2 36GHz MPDI based flood index maps were generated for Cyclone Yaas during 27-28 May 2021. Sentinel-2 multispectral dataset were analysed to understand the changes in the turbidity due to cyclone.

Remote sensing based data analysis was carried out to study the upwelling and impact of cyclone on Ocean biological productivity in central BoB and off Odisha coast using OCM-2 data. It was observed that upwelling velocity during cyclone Yaas was 4-6 m/day and dropped to less than 1 m/day in the post landfall week. SST data analysis showed decrease of up to 1.8°C . A localized patch of 200-250 percent enhanced chlorophyll concentration was observed near Chilka, which extended offshore up to 100 km, which, subsequently dissipated and thus absent in 8-day composite image of 2-9 June 2021. This increased chlorophyll concentration was observed left of the track in 8-day composite image and extended from coast to offshore waters and appears to be in the direction of surface currents. Thermocline displacement of up to 24m was observed along cyclone track.

The damage to agricultural crops and forest region due to cyclone YAAS was assessed in the coastal regions of Odisha and West Bengal using microwave and optical sensors data. The systematic data from optical Mx and SAR instruments in the form of Analysis Ready Data and polarimetric signatures at 10m spatial resolution at 6-day interval from twin satellites of Sentinel-1A/1B and Sentinel-2A/2B were analyzed and used for damage detection and mapping affected areas with various levels of possible disturbances.

Table of Contents

1.	PREDICTION AND MONITORING OF CYCLONE YAAS.....	1 -
1.1.	INTRODUCTION	2
1.1.1	<i>Brief overview of TC YAAS.....</i>	2
1.2	CYCLOGENESIS PREDICTION.....	4
1.2.1	<i>Prediction of cyclogenesis using Genesis Potential Parameter</i>	4
1.2.1	<i>Prediction of cyclogenesis using Scatterometer Data</i>	6
1.3.	CYCLONE TRACK AND INTENSITY PREDICTION	9
1.3.1	<i>Real-time track prediction using SAC-Lagrangian Advection Model</i>	9
1.3.2	<i>Track error analysis of Lagrangian Advection Model.....</i>	12
1.3.3	<i>Cyclone Intensity Prediction.....</i>	14
1.3.4	<i>Error analysis of the intensity prediction by HWRF model.....</i>	16
1.4	SHIP AVOIDANCE REGION ADVISORIES	17
1.5	ANALYSIS OF INSAT-3D AND INSAT-3DR OBSERVATIONS DURING TC YAAS.....	18
1.5.1	<i>Cyclone structure observations using INSAT3D satellite data.....</i>	19
1.5.2	<i>Cyclone Geo-location.....</i>	20
1.5.3	<i>Cyclone Intensity estimation using ADT with INSAT-3D data</i>	21
1.6	TROPICAL CYCLONE YAAS OBSERVED BY INSAT-3DR RAPID SCAN DATA	22
1.7	SMAP SATELLITE OBSERVATION OVER TC YAAS	24
1.8	FORECAST DISSEMINATION THROUGH WEB PORTAL SCORPIO/MOSDAC	25
1.9	COVERAGE OF CYCLONE YAAS BY MEDIA.....	26
1.10	CONCLUSIONS	26
	REFERENCES	27
2.	TROPICAL CYCLONE ‘YAAS’: RESEARCH AND OPERATIONAL ACTIVITIES FROM OCEAN PERSPECTIVE.....	29
2.1	INTRODUCTION	30
2.2	CYCLONE INDUCED SEA SURFACE COOLING AND DENSITY CHANGES IN THE OCEAN	30
2.3	OPERATIONAL ACTIVITIES.....	37
2.3.1.	<i>Storm surge forecast for YAAS cyclone</i>	37
2.3.2	<i>Coastal inundation forecast.....</i>	39
2.3.3	<i>Extreme wave prediction during ‘YAAS’</i>	41
2.4	CONCLUSIONS	46
	REFERENCES	46

3. RAINFALL ESTIMATION OVER TROPICAL CYCLONE YAAS48

3.1	INTRODUCTION	49
-----	--------------------	----

THE MAIN OBJECTIVE OF THIS SECTION IS TO SHOW THE USEFULNESS AND RELIABILITY OF H-E RAINFALL PRODUCTS FROM INSAT-3D/3DR ON VERY SEVERE TC YAAS WHICH FORMED IN THE BAY OF BENGAL AND PERSISTED FROM 21 MAY -28 MAY 2021. THE SECTION ALSO PROVIDES VALIDATION STATISTICS OF H-E RAIN WITH SURFACE RAIN GAUGES OBSERVATIONS FROM INDIAN METEOROLOGICAL DEPARTMENT (IMD) AND OTHER SATELLITES PRODUCTS. IN ADDITION, A BRIEF EXPLANATION OF H-E RAINFALL RETRIEVAL TECHNIQUE IS ALSO PROVIDED.49

3.2	H-E RETRIEVAL TECHNIQUE	49
3.3	H-E RAIN DURING TROPICAL CYCLONE YAAS	51
3.3.1	<i>Validation of H-E rain estimates</i>	52
3.4	CONCLUSION	56
	REFERENCES	57

4. ASSESSMENT OF SURFACE INUNDATION AND CHANGES IN WATER TURBIDITY ASSOCIATED WITH CYCLONE YAAS.....58

4.1	INTRODUCTION	59
4.2	DATA USED	60
4.3	ANALYSIS OF CYCLONE INDUCED FLOODING USING HYDROLOGICAL MODELLING.....61	
4.3	SURFACE INUNDATION MAPPING USING SAR	62
4.5	SURFACE INUNDATION MAPPING USING MICROWAVE RADIOMETRY	63
4.6	IMPACT ASSESSMENT OF WATER QUALITY USING OPTICAL DATASET:.....65	
4.7	CONCLUSION	66
	REFERENCES	67

5. CYCLONE YAAS INDUCED UPWELLING AND CHANGES IN OCEAN BIOLOGICAL PRODUCTIVITY68

5.1	INTRODUCTION	69
5.2	DATA USED	69
5.3.	METHODOLOGY	70
5.4	RESULTS	71
5.4.1	<i>Chlorophyll from Ocean Colour Monitor (OCM-2) imagery before and after TC Yaas.....74</i>	
5.4.2	<i>Thermocline displacement following the passage of cyclone Yaas</i> 75	
5.5	DISCUSSION	75
5.6	CONCLUSION	76

REFERENCES	76
6. DAMAGE ASSESSMENT OF AGRICULTURAL CROPS AND FOREST IN COASTAL REGIONS OF ODISHA AND WEST BENGAL	79
6.1. INTRODUCTION	80
A. DAMAGE ASSESSMENT STUDY FOR CROP USING OPTI-SAR	80
<i>A.1. Study Area</i>	81
<i>A.2. Data Used</i>	81
<i>A.3. Scientific Approaches</i>	82
<i>A.4. Results</i>	85
B. DAMAGE ASSESSMENT STUDY FOR FOREST REGION	90
<i>B.1. Study area and datasets</i>	90
<i>B.2 Methodology</i>	91
<i>B.3 Results</i>	92
6.2 CONCLUSIONS	97
REFERENCES	97

1. Prediction and Monitoring of cyclone YAAS

Neeru Jaiswal, Shivani Shah and A K Varma

1.1. Introduction

Tropical cyclones (TCs) are one of the most violent weather manifestations that include number of different hazards like storm surge, flooding, extreme winds, torrential rains, thunderstorms, and lightening and cause devastation along the coastal regions. Each year tremendous economy losses and deaths are caused by the TCs throughout the world. To overcome/reduce such losses, the accurate prediction of TC formation, is required so that precautionary measures can be taken. TC formation involves interaction between synoptic scale as well as the mesoscale process. The North Indian Ocean (NIO) is a potentially energetic region for the development of TCs. Prediction of the development of any cyclonic system in the NIO is being done as a regular exercise at Space Applications Centre, Ahmedabad (SAC-ISRO) using the indigenously developed algorithms. Once the system is developed, prediction of its track and intensity are generated in real-time and disseminated through a web based application “Satellite based cyclone observation and real-time prediction over Indian ocean” (SCORPIO) (<https://mosdac.gov.in/scorpio>), available on the MOSDAC portal (<https://mosdac.gov.in>). The similar exercise was performed during the formation of TC YAAS, and discussed in the present report.

1.1.1 Brief overview of TC YAAS

Tropical cyclone YAAS was a second tropical cyclone of the year 2021 that formed in the North Indian Ocean. It was developed from a low-pressure system formed over east central Bay of Bengal (BoB) in the morning (0830 IST/0300 UTC) of May 22, 2021. Under favorable environmental conditions, it concentrated into a depression over east central BoB in the noon (1130 IST/0600 UTC) of May 23, 2021. It moved northwestwards and intensified into a deep depression (DD) over east central BoB in the midnight (2330 IST/1800 UTC) of May 23. It turned into the cyclonic storm in the early morning (0530 IST/0000 UTC) of May 24 over the same region and named by IMD as TC ‘YAAS’. Thereafter, it moved north-northwestwards, attained a peak intensity of 75 kts, and lay centered over northwest BoB about 30 km east of Dhamra Port, Odisha during early morning (0530 IST/0000 UTC) of May 26. It Continued moving north-northwestwards, and crossed north Odisha coast near latitude 21.35°N and longitude 86.95°E, about 20 km to the south of Balasore as a VSCS with maximum sustained wind speed (MSW) of 75 kts gusting to 85 kts (130 -140 kmph gusting to 155 kmph) between 1030-1130 IST(0500-

0600 UTC) of 26th May (IMD report , 2021). The best track of TC YAAS provided by India Meteorological Department (IMD), Delhi with its intensity categories is shown in Fig.1.1. The IMD classification of cyclone categories is given in Table 1.1.

Table 1.1: IMD classification of categories of cyclonic system

System	Associated wind speed (knots)
Low pressure area	<17
Depression	17-27
Deep Depression	28-33
Cyclonic Storm	34-47
Severe Cyclonic Storm (SCS)	48-63
Very SCS (VSCS)	64-85
Extremely SCS (ESCS)	86-119
Super Cyclonic Storm(SuC)	>119

Cyclone name “YAAS”, was given by Oman. As per global convention, the thirteen countries that make up the Indian Ocean Region—Bangladesh, India, Iran, Maldives, Myanmar, Oman, Pakistan, Qatar, Saudi Arabia, Sri Lanka, Thailand, United Arab Emirates, Yemen—have drawn up a list of names for tropical cyclones, which are assigned serially with the alphabetic order of the nation’s name. The word “YAAS” has its origin in the Persian language and means the flower jasmine in English.

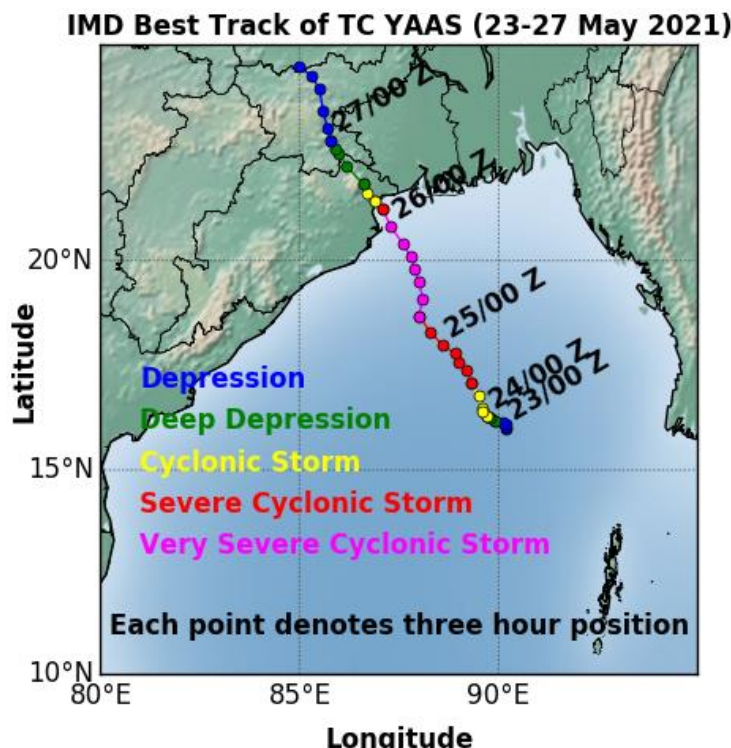


Figure 1.1: Three-hourly IMD best track of TC YAAS with its intensity.

1.2 Cyclogenesis Prediction

The prediction of tropical cyclogenesis (TCG) of cyclonic systems that develop in the NIO is being done at SAC using in-house developed technique. This technique is based on wind pattern matching of the scatterometer derived surface wind observations and provides 1-4 days advance TCG prediction (Jaiswal and Kishtawal, 2011; 2013). During cyclone active months of the NIO i.e. April-June and October-December, the cyclogenesis prediction technique is regularly run to detect the earliest signatures of any possibility of cyclonic activity in the Bay of Bengal (BoB) and Arabian Sea (ARB) region. Due to unavailability of SCATSAT-1 satellite data, this technique could not be run and the cyclogenesis of TC YAAS could not be predicted. The model forecasts can be examined to investigate the signatures of tropical cyclogenesis. Advanced prediction of tropical cyclogenesis based on model forecasted parameters is discussed in the next section.

1.2.1 Prediction of cyclogenesis using Genesis Potential Parameter

A cyclone genesis parameter, termed the genesis potential parameter (GPP), for the Indian Sea was proposed by Kotal et al. 2019. The parameter is defined as the product of four variables, namely vorticity at 850 hPa, middle tropospheric relative humidity, middle tropospheric instability, and the inverse of vertical wind shear. The variables are calculated using the National Centers for Environmental Prediction (NCEP), USA, reanalysis data, averaged within a circle of 2.5° radius around the centre of cyclonic system. The GPP, at early development stage of a cyclonic storm provides a useful predictive signal for intensification of the system.

$$GPP = \begin{cases} \frac{\zeta_{850} \times M \times I}{S} & \text{if } \zeta_{850} > 0, M > 0 \\ 0 & \text{otherwise} \end{cases} \quad (1)$$

$$M = \frac{(RH - 40)}{30}$$

Where, ζ_{850} is low level relative vorticity (at 850 hPa in 10^{-5} s^{-1}), S is vertical wind shear (between 200 and 850 hPa in s^{-1}), RH is the mean relative humidity (between 700 and 500 hPa) and I is middle-tropospheric instability (temperature difference between 850 hPa and 500 hPa). All the variables are estimated by computing the grided values and averaging it over an area of radius 2.5° . The maximum value of GPP in the NIO region was compared to the pre-determined threshold value for cyclogenesis. The threshold value to detect

cyclogenesis was determined by maximizing the probability of detection (POD) and minimizing the false alarm ratio (FAR). POD is the ratio of the total number of detected TC formation and total number of formed cases and FAR is the ratio of the total number of predicted TC formation that does not occur (develop) and total number of non-developed cases. For threshold determination, GFS analysis fields, during nine TCs formed in the NIO during the period 2009-10 and 100 non-developed cases were analyzed. The GPP was estimated using the 850 hPa wind fields, deep vertical wind shear (850-200 hPa), warm core (850-500 hPa), and mean relative humidity (700-500 hPa). The TC formation has been determined by varying the different threshold values of GPP, which are obtained by minimum of the maximum values of GPP using the GFS analysis fields on the day of TC formation of all cyclones. These thresholds have also been used to predict the TCG by the GFS analysis fields of 100 non-developed cases. The optimum threshold values for GPP was found as “2” which is then used to identify the TCG in GFS forecasted fields (Singh et al., 2013). The GPP value was computed in NIO with the GFS data prior to the formation of TC YAAS to detect its cyclogenesis signatures. The spatial plots of GPP with the required parameters used in GPP computations (as given in Eq. 1) are shown in Fig. 1.2 for 00 UTC and 12 UTC forecasts of GFS on 20, 21 and 22 May 2021. The maximum GPP values for all analyzed forecasts are summarized in Table 1.2:

Table 1.2: Maximum GPP computed in BoB region before formation of TC YAAS

Date	00 UTC 20 MAY	12 UTC 20 MAY	00 UTC 21 MAY	12 UTC 21 MAY	00 UTC 22 MAY	12 UTC 22 MAY
Maximum GPP	2.18	3.80	3.98	5.86	8.09	9.32

The values of GPP are increasing, which shows the strengthening of cyclogenesis conditions.

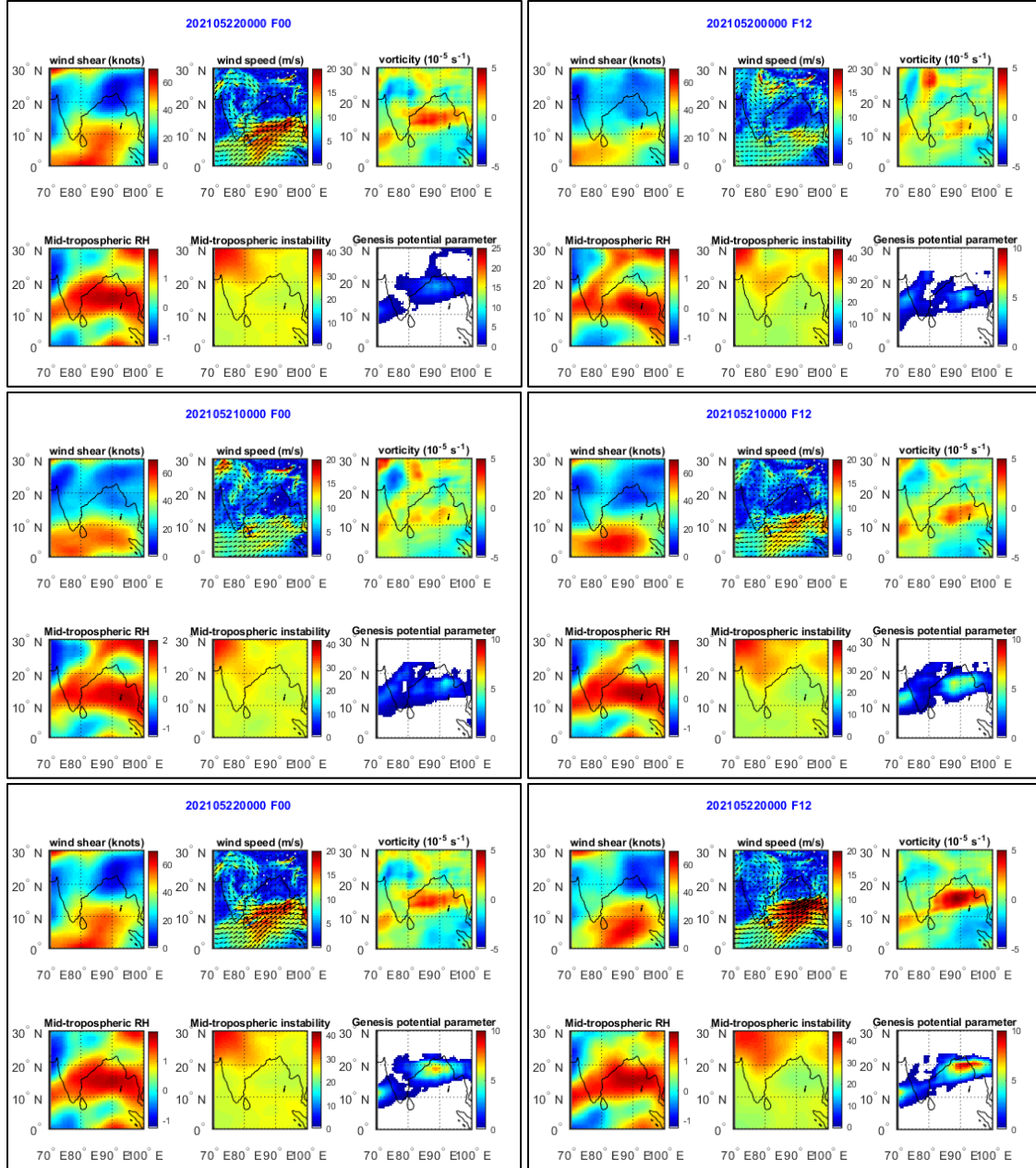


Figure 1.2: Spatial plot of parameters responsible for cyclogenesis and GPP values for 00 and 12 UTC of 20, 21 and 22 May 2021.

1.2.1 Prediction of cyclogenesis using Scatterometer Data

A technique has been developed at SAC for cyclogenesis prediction using scatterometer data. This technique is based on the premise that there is some similarity between the low-level wind pattern of the developing systems, which can be detected and used to identify the developing and non-developing low-pressure systems. In this technique, the real-time observed winds are matched to the wind patterns archived within the database of all

developed systems in the past and the most similar wind pattern was selected. This similarity was quantified using a matching index as given in the following expression.

$$cc = \frac{\frac{1}{N} \sum_{i=1}^N (A_i - \bar{A})^* (B_i - \bar{B})}{\sqrt{\frac{1}{N} \sum_i^N |A_i - \bar{A}|^2} \times \sqrt{\frac{1}{N} \sum_i^N |B_i - \bar{B}|^2}} \quad (1)$$

where \bar{A} and \bar{B} represents the mean value of the complex vectors A and B respectively. N is the dimension of vector A (or B) and A and B are the complex numbers formed using the wind vectors [*for example $A = (u+iv)$*].

If the matching index value is found to be greater or equal to some pre-defined threshold values (0.6 for NIO), the cyclogenesis is predicted. The scatterometer data of QuikSCAT and OSCAT were used in the development and testing of the algorithm (Jaiswal and Kishtawal, 2011; 2013). During the years 2010-13, OSCAT data was used for the real-time cyclogenesis prediction using the above-discussed approach. In the year 2014 the OSCAT stopped working and thereafter the surface wind observations from RAPIDSCAT were being used in the real-time prediction of TCG in NIO at SAC. SCATSAT1 (Scatterometer Satellite1) satellite was launched on 26th September, 2016 to provide weather forecasting, cyclone prediction, and tracking services to India. The SCATSAT-1 data was being utilized operationally in the real-time for TCG prediction. Recently this satellite stopped working and due to unavailability of any other satellite data with such wider swath, the above technique could not be used for the TCG prediction. However, the passes of NASA scatterometer ASCAT onboard metopA, metopB and metopC were processed to get the signature of low-level wind circulation. Due to the narrow swath of ASCAT (unlike OSCAT, SCATSAT-1 and QuickSCAT), there is a least possibility to capture the complete low-level wind circulation in a single pass, thus the above discussed technique cannot be applied over ASCAT dataset. The earliest signatures of low-level circulation were found on all the three ASCAT passes of May 23. Wind vectors overlaid on the wind speed (m/s) by the passes of ASCAT from metopA, metopB and metopC during the genesis of TC YAAS are shown in the Fig. 1.3. The strong circulation can be seen in all these passes, which may indicate to the development of this circulation into a tropical cyclone.

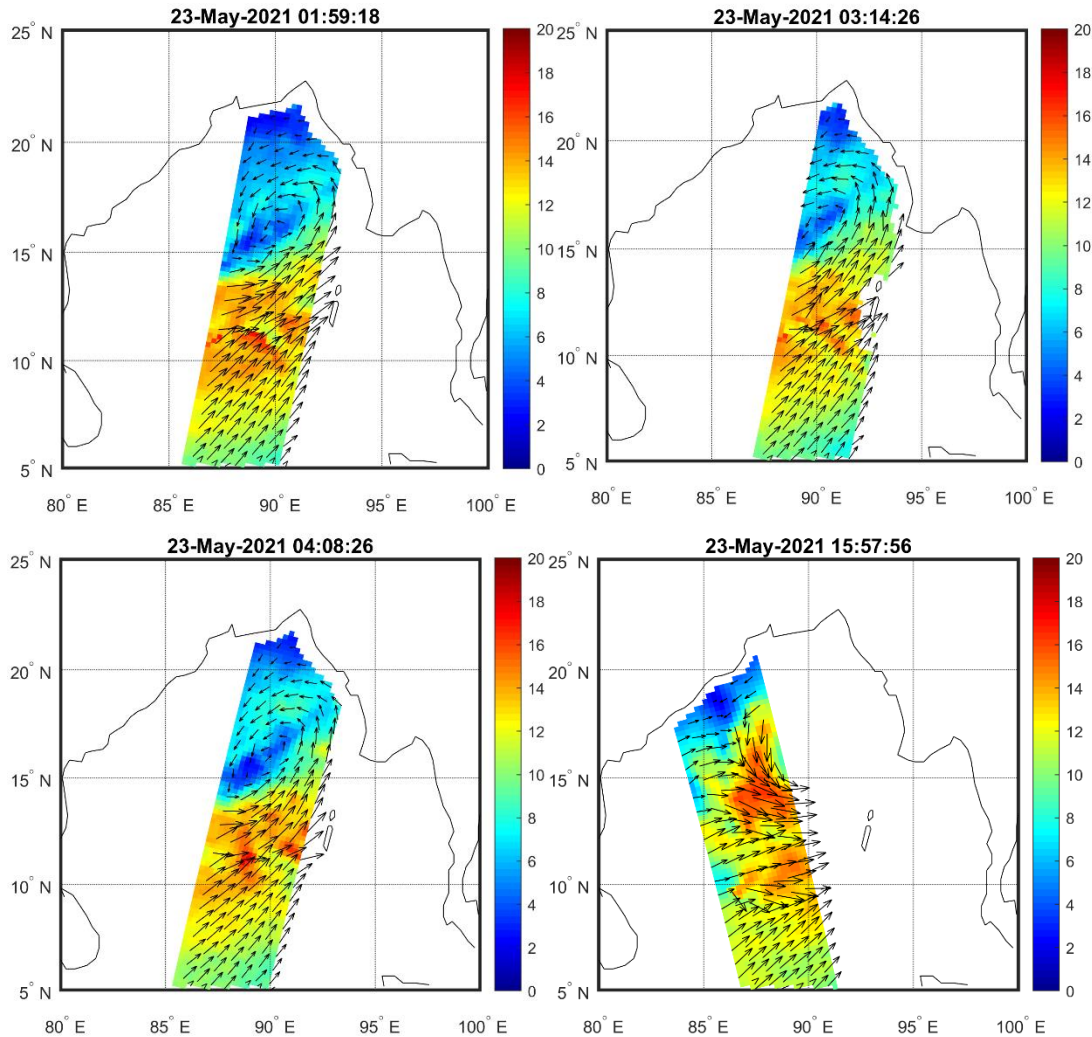


Figure 1.3: Wind vectors overlaid on the wind speed (m/s) by the passes of ASCAT from metopA (top left), metopB (top right) and metopC (bottom left and right) during the genesis of TC YAAS.

1.3. Cyclone Track and Intensity Prediction

A system has been developed in SAC for monitoring, analysis and prediction of tropical cyclones over the Indian Ocean. The results of analysis and prediction are disseminated through SCORPIO web-portal linked to MOSDAC server. After the formation of tropical cyclone over the Indian Ocean, track predictions are carried out using three different models. (a) indigenously developed Lagrangian advection cyclone track prediction model (LAGAM), (b) Hurricane Weather Research and Forecasting (HWRF), a coupled land-ocean-atmosphere model customized for Indian ocean region, and (c) WRF model, used for daily real-time predictions of all-India weather at 5 km resolution. The HWRF model is used for prediction of tropical cyclone intensity. The track and intensity prediction of cyclone YAAS was initiated on MAY 23, 2021 and were continued until cyclone made landfall. Real-time track prediction of cyclone YAAS by SAC-Lagrangian advection Model, WRF and HWRF models are discussed in the following sections.

1.3.1 Real-time track prediction using SAC-Lagrangian Advection Model

SAC-Lagrangian Advection model is dynamical framework based computationally efficient model (Singh et al, 2011; 2012). It requires the high resolution $0.5^{\circ} \times 0.5^{\circ}$ forecasted atmospheric winds and temperature from Global forecast System (GFS), which is global numerical weather prediction model, run by NOAA, and the initial position of cyclone, which is obtained from Joint Typhoon Warning Centre (JTWC) for track prediction. Cyclone track prediction is provided using this model upto 96 hour with 6 hour interval. As a first step, the steering flow has been computed for every 6-hour forecast interval up to 96 hours, using the analysis as well as forecast wind fields data at 21 pressure levels (100-1000 mb) by the weighted average scheme. The weight for each level was assigned by estimating the potential vorticity (PV) which is adapted from the study by Hoover et al., 2006. Then a cyclonic vortex is removed using a synthetic cyclone, which is constructed by using the vorticity equation (Chan and Williams, 1987):

$$\frac{\partial \zeta}{\partial t} + V \cdot \nabla (\zeta + f) = 0$$

Where ζ is the vorticity and $f = \beta y + f_0$. Here y denotes latitudinal displacement, f_0 is the value of coriolis parameter at $y = 0$ and β is the rate of change of coriolis parameter with

latitude. In case of axisymmetric vortex, the velocity is calculated using the equation (Chan and Williams, 1987):

$$V(r) = V_m \left(\frac{r}{r_m} \right) \exp \left[\frac{1}{b} \left(1 - \left(\frac{r}{r_m} \right)^b \right) \right]$$

Where V_m and r_m denote the maximum value of tangential velocity and the radius at which V_m occurs, respectively. This synthetic cyclone was used to remove the existing cyclonic wind fields present in the steering flow to achieve the residual steering current. To avoid the discontinuity of wind fields due to removal of cyclonic circulation, tapered weights $W(k)$ are used for generation of residual flow fields. Now, resulting steering flow that is obtained after removing the cyclonic vortex from steering flow is used in Lagrangian Advection Model to forecast cyclone track. The computation for the trajectory of cyclone (or cyclone track) is initiated by interpolating the steering wind from model grid points to the initial location of cyclone (Brand, 1981). The real time predicted tracks for cyclone YAAS have been shown in Fig. 1.4.

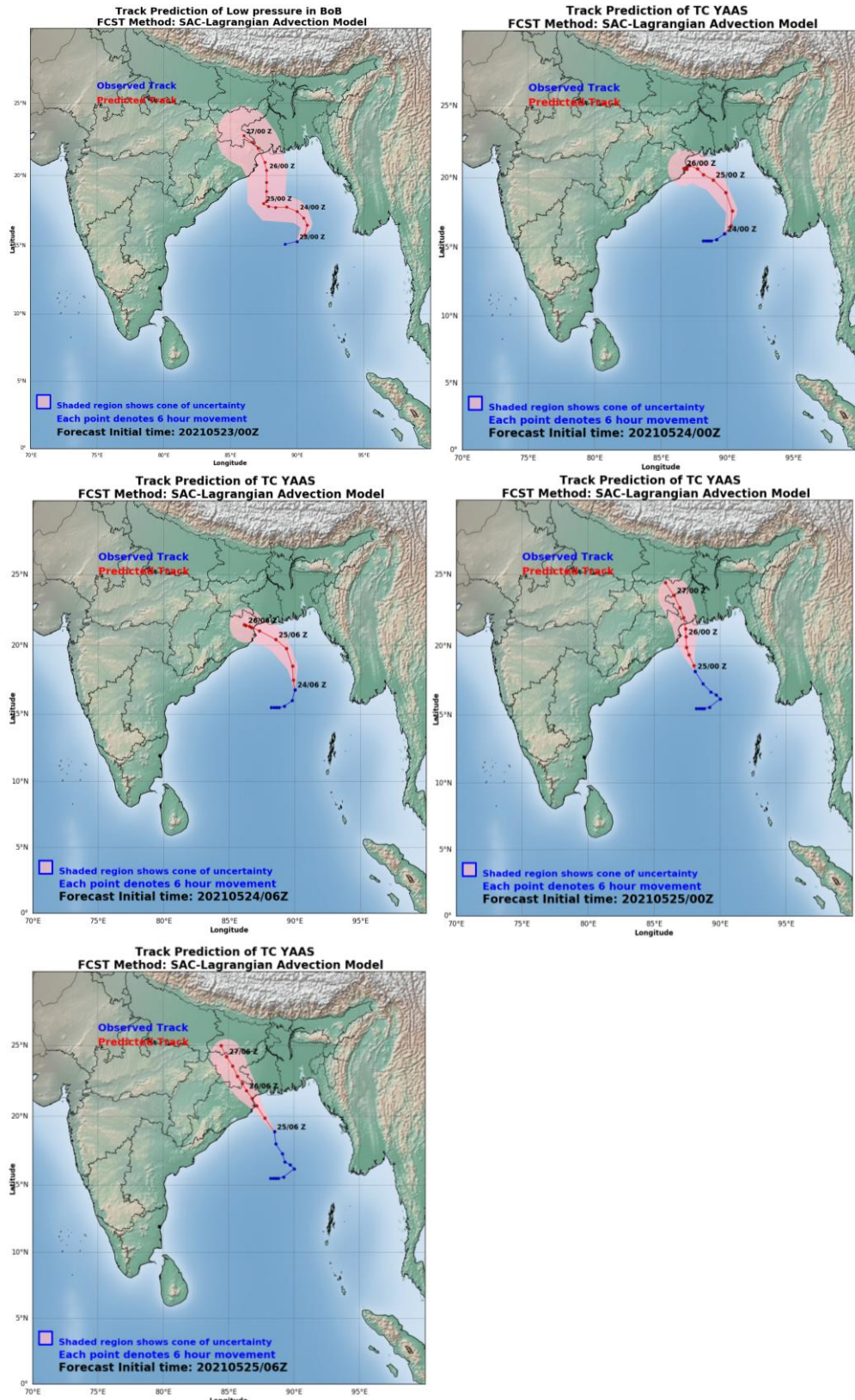


Figure 1.4: Track prediction of cyclone YAAS for different initial conditions by SAC-Lagrangian advection model (Real- time generated products).

1.3.2 Track error analysis of Lagrangian Advection Model

The real time predicted tracks of cyclone YAAS by SAC-Lagrangian Advection Model for different initial times have been shown with the observed track of IMD in Fig. 1.5. The track forecast error for all the forecasts were computed w.r.t IMD observed track positions. The error values have been summarized in Table 1.3. IMD reported the landfall point of cyclone YAAS near Balasore, Odisha (landfall point: 21.35 N, 86.95 E) between 0500 and 0600 UTC (IMD, Report). The landfall position error for all the forecasts have been computed and reported in the Table 1.4. For 24-hour lead prediction, the landfall position error of Lagrangian advection model was found as ~19 km and landfall time error was ~6 hour.

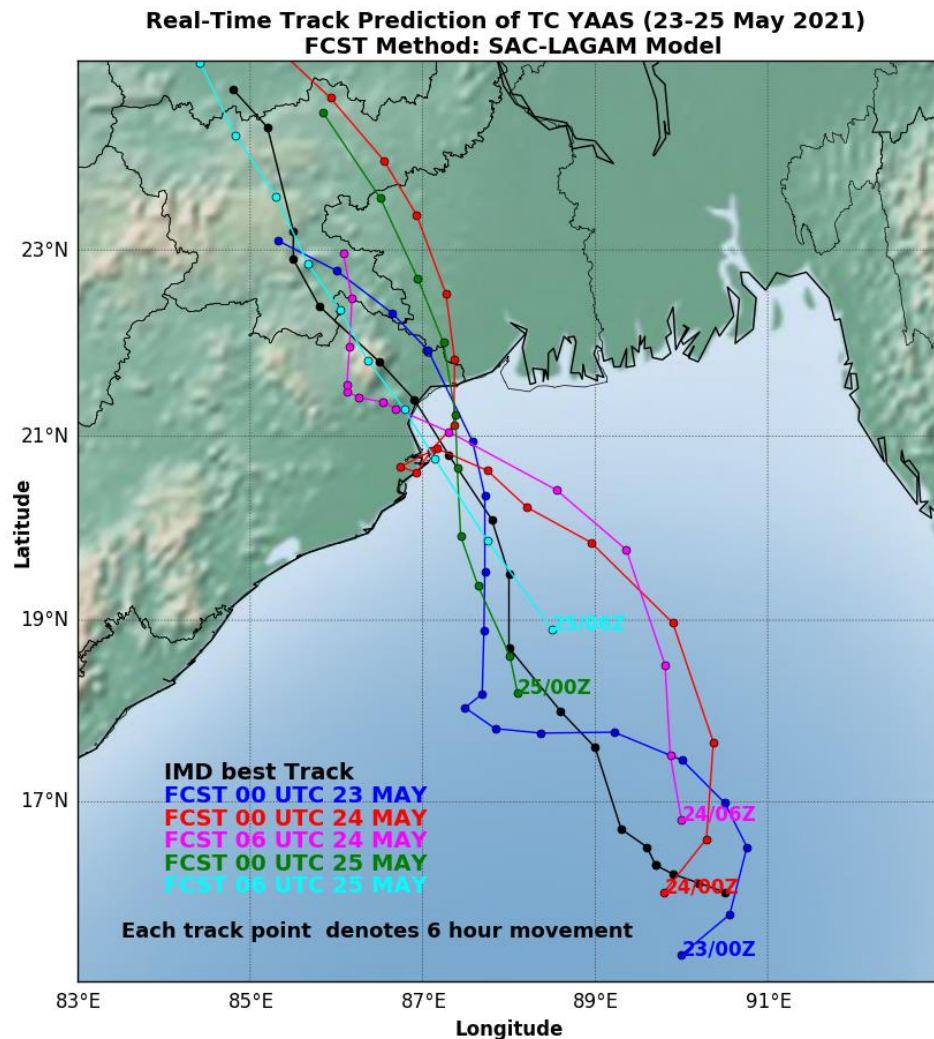


Figure 1.5: IMD best track and real-time predicted track of cyclone YAAS by SAC-Lagrangian advection model for different initial time (23-MAY-00Z, 24 MAY-00Z, 24 MAY-06Z, 25 MAY-00 Z, 25 MAY-06Z).

Table 1.3: Track Forecast Error (km) of SAC-Lagrangian Advection track prediction Model w.r.t IMD observed track positions

FCST Initial time \ FCST Hour	00 UTC 23 MAY	00 UTC 24 MAY	06 UTC 24MAY	00 UTC 25 MAY	06 UTC 25 MAY	Mean Error
6	54.74	74.23	109.47	10.06	44.04	58.51
12	97.64	155.93	132.56	30.35	100.58	103.41
24	123.93	208.98	199.75	18.72	72.78	124.83
36	153.78	126.62	177.13	79.83	51.79	117.83
48	117.46	60.00	66.29	126.00	126.41	99.23
72	65.61	226.12	113.13			134.95
96	52.95					52.95

Table 1.4: Landfall Prediction Error (km) of SAC-Lagrangian advection track prediction Model for TC YAAS.

Forecast Time/Date		Landfall Time/Date/Location				Landfall Error	
Date	Time	Date	Time	Long	Lat	Location Error (km)	Time Error (Hrs)
23MAY	00 UTC	26MAY	09 UTC	87.27	21.54	39.28	+5 hour
24MAY	00 UTC	25MAY	21 UTC	86.99	20.79	62.40	-8 hour
24MAY	06 UTC	25MAY	16 UTC	86.86	21.23	16.27	-13 hour
25MAY	00 UTC	26MAY	08 UTC	87.33	21.50	42.73	+2 hour
25MAY	06 UTC	26MAY	23 UTC	86.84	21.21	19.29	-6 hour

Cyclone landfall (IMD): Latitude: 21.35, Longitude 86.95 at 04 UTC 26 MAY

1.3.3 Cyclone Intensity Prediction

For cyclone intensity prediction numerical weather prediction model WRF and HWRF are utilized. WRF model is regularly run at SAC, its output are analyzed to get cyclone related parameters.

The HWRF model is a primitive-equation, non-hydrostatic, coupled atmosphere-ocean model with an atmospheric component that employs the Non-hydrostatic Mesoscale Model (NMM) dynamic core of the WRF model (WRF-NMM), with a parent and two nest domains (Biswas et al. 2018). The parent domain covers roughly 77.2° x 77.2° on a rotated latitude/longitude E-staggered grid. The location of the parent domain is determined based on the initial position of the storm provided by NHC/Joint Typhoon Warning Center (JTWC). The middle nest domain, of about 17.8° x 17.8° , and the inner nest domain, of about 5.9° x 5.9° , move along with the storm using two-way interactive nesting. The stationary parent domain has a grid spacing of 0.099° (about 13.5 km) while the middle nest grid spacing is 0.033° (about 4.5 km) and the inner nest grid spacing is 0.011° (about 1.5 km). The dynamic time steps are 30, 10, and 3.33 s, respectively, for the parent, middle nest, and inner nest domains. Starting 2018, all the basins have their model top at 10 hPa and 75 levels are used.

HWRF v4.0a includes a scale-aware Arakawa-Schubert scheme for cumulus parameterization and a Ferrier-Aligo cloud microphysics package for explicit moist physics. The Global Forecasting System (GFS) Eddy-diffusivity Mass flux scheme is used for the planetary boundary layer, along with the modified Geophysical Fluid Dynamics Laboratory (GFDL) surface layer scheme. The Monin-Obukhov scheme is used for surface flux calculations, which employs an improved air-sea momentum flux parameterization in strong wind conditions. The Noah land surface model is used to represent the land surface for calculating the surface fluxes and the amount of upwelling radiation at the lower atmospheric model boundary. Radiation effects are evaluated by the Rapid Radiative Transfer Model for General Circulation Models (RRTMG) scheme, which includes diurnal variations and interactive effects of clouds. The HWRF physics operational suite also includes parameterization of dissipative heating. The time integration is performed with a forward-backward scheme for fast waves, an implicit scheme for vertically propagating sound waves, and the Adams-Bashforth scheme for horizontal advection and for the Coriolis force. In the vertical, the hybrid pressure-sigma coordinate is used.

The NCEP Global Forecast System (GFS) analysis is used to generate the initial conditions (ICs) for the hurricane model parent domain in the operational configuration.

Numerical Experiments and Data Used

The HWRF4.0a model, used in the present study, is obtained from the NCEP website www.dtcenter.org. The model is installed and evaluated for its default configuration for NIO tropical cyclones. The present study summarizes the results of TC BULBUL for three different initial conditions i.e. 00 UTC 23, 24 and 25 MAY. The NCEP Global Forecast System (GFS) analysis and forecasts ($0.25^0 \times 0.25^0$) have been used to provide the initial and lateral boundary conditions. All the three experiments were performed in the uncoupled ocean mode and without the data assimilation module.

The intensity of simulated cyclone from different experiments is evaluated in terms of the maximum sustained wind speed (MSW). The real time intensity prediction of cyclone for all initial conditions (00 UTC 23-25 MAY) was provided on the SCORPIO web-portal (Fig. 1.6).

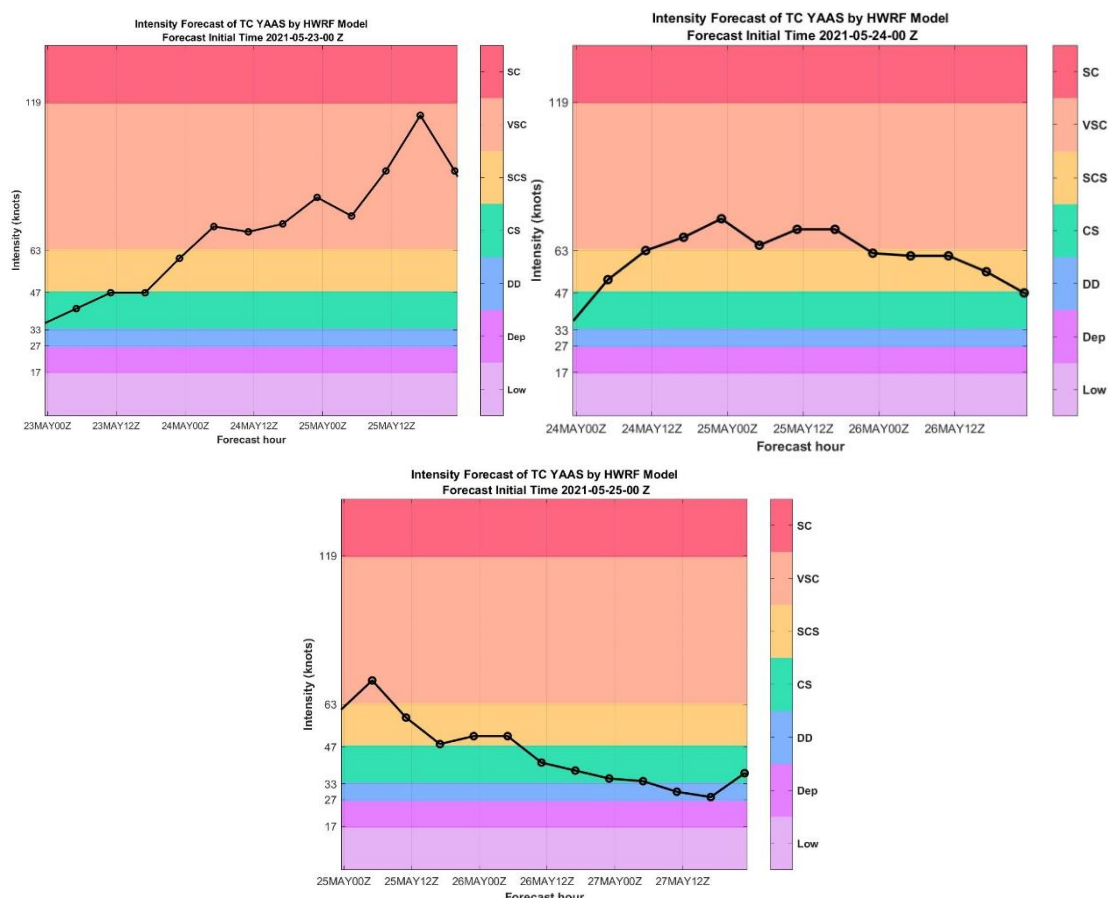


Figure 1.6: Real time forecast of cyclone intensity by HWRF model.

1.3.4 Error analysis of the intensity prediction by HWRF model

The model simulated intensity of cyclone YAAS for different initial conditions are presented in Fig. 1.7 along with real-time intensity estimates of IMD. The error in model-simulated intensity (MSW) with respect to the IMD estimated MSW for all initial conditions are presented in Fig. 1.8. The results suggest that the model overestimated the intensity for all forecast hour w.r.t. initial condition of 00 UTC 23 MAY. This may be due to the reason that cyclone was not formed on 23 May; it was in a depression stage, that may lead to less accurate wind structure simulations. However, the forecasts initiated on 00 UTC 24 and 25 MAY, are relatively close to the observed intensity values by IMD.

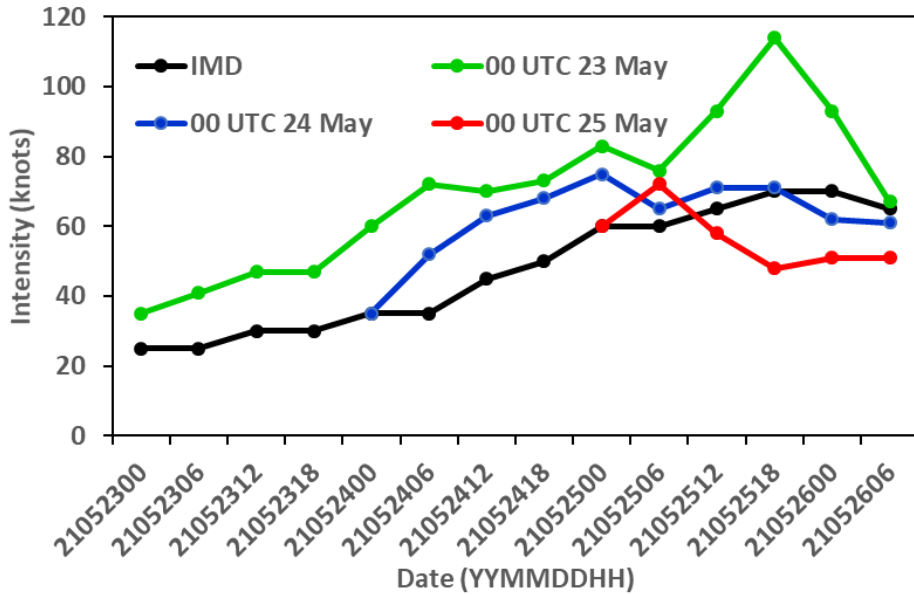


Figure 1.7: Cyclone intensity simulated by HWRF model for different initial conditions with IMD estimates.

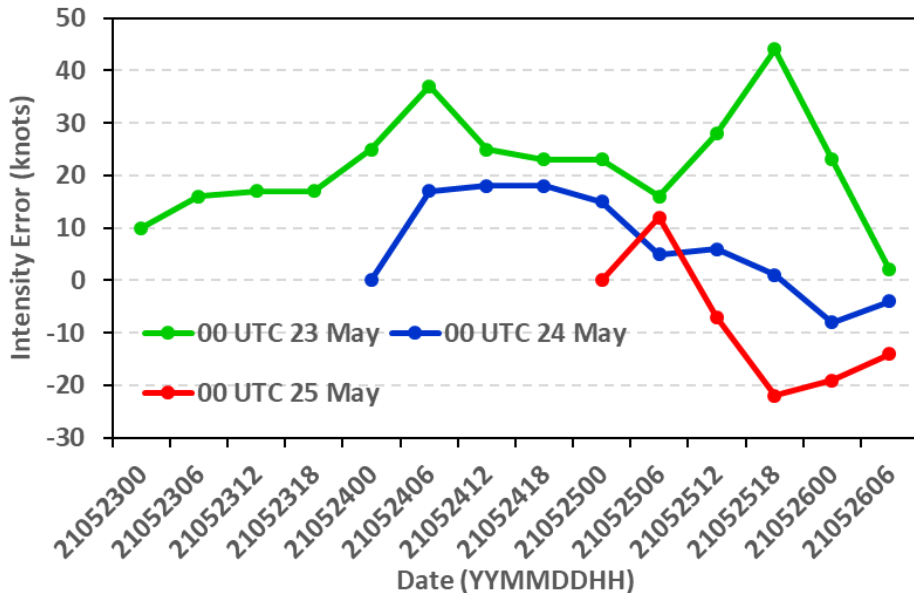


Figure 1.8: Cyclone intensity error by HWRF model w.r.t. JTWC observed intensity estimates for different initial conditions.

1.4 Ship Avoidance Region Advisories

For vessels at sea, avoiding the 34-knot wind field of a tropical cyclone is paramount. Based on operational HWRF model, 34-knot wind radial distances the graphical inputs of ship avoidance region were generated for cyclone and disseminated through SCORPIO server. The real-time generated ship avoidance region advisory products are shown in Fig. 1.9.

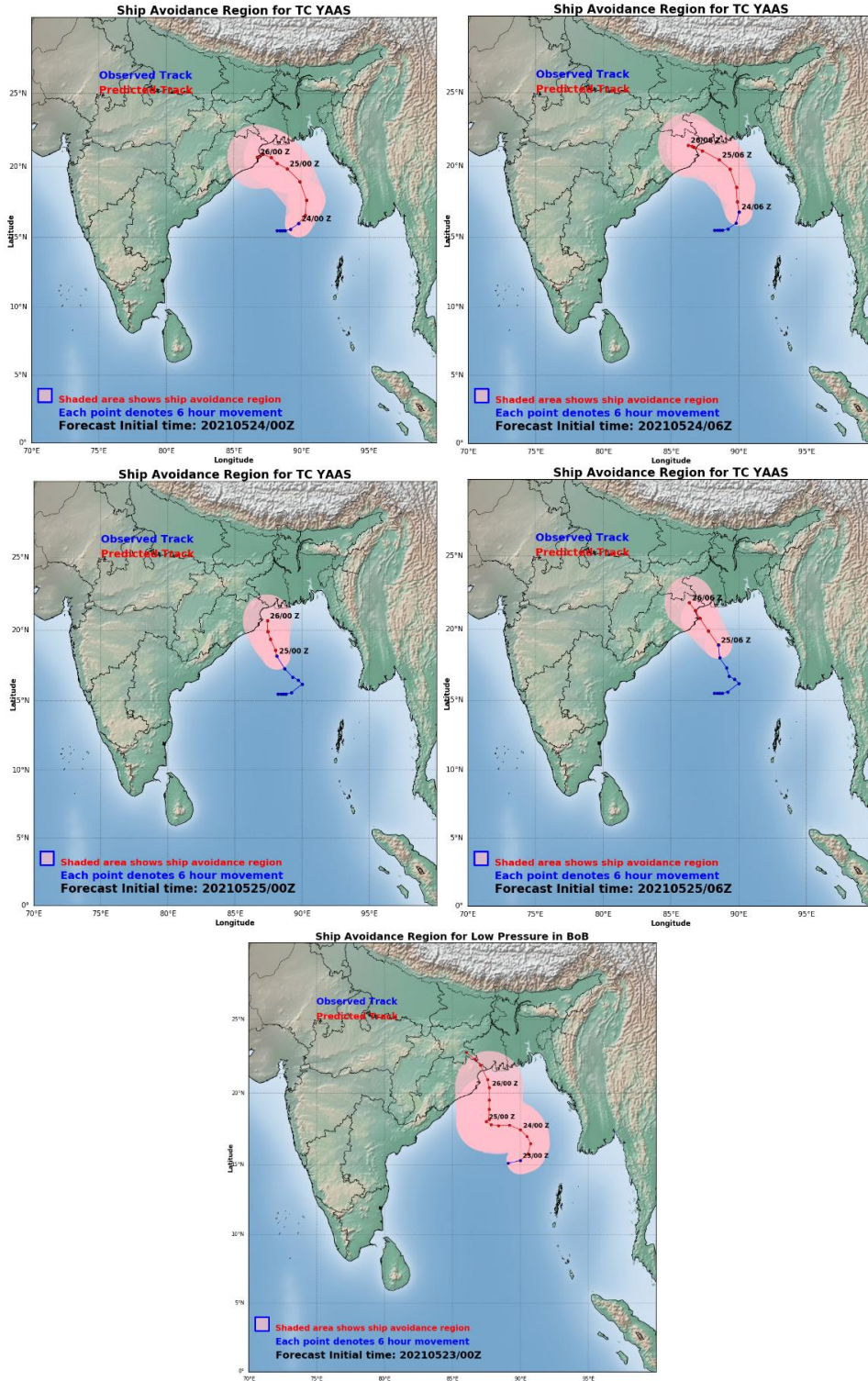


Figure 1.9: Ship avoidance region forecast advisories generated at 00, 06 UTC of 23-25 MAY

1.5 Analysis of INSAT-3D and INSAT-3DR observations during TC YAAS

India's two meteorological geostationary satellites viz., INSAT3D and INSAT3DR provides coverage over India and surrounding regions including the oceans. INSAT-3D/3DR are meteorological satellite of ISRO, an exclusive next generation mission designed for enhanced meteorological observations and monitoring of land and ocean surfaces for weather forecasting and disaster warnings. INSAT-3D and INSAT-3DR both have two meteorological payloads, an Imager (with 6 channels) and a Sounder (with 18 infrared channels and a visible channel for daytime cloud detection). The Imager has capability of taking observations of full earth-disk from geostationary orbit in one visible channel (VIS, 0.55-0.75 μm) and five infrared (IR) channels: Shortwave infrared (SWIR, 1.55-170 μm), Mid-wave infrared (MIR, 3.8-4.0 μm), Water Vapor absorption channel (WV, 6.5-7.1 μm), and two split-window thermal infrared channels (TIR1, 10.2-11.2 μm and TIR2, 11.5 to 12.5 μm). The observations from VIS and SWIR channels are available at 1 km x 1 km ground resolution at nadir, whereas MIR, TIR1, and TIR2 has resolution of 4 km x 4 km. The WV channel has coarser resolution of 8 km x 8 km at nadir. The sub-satellite points of INSAT3D and INSAT3DR are at 82° E and 74° E, respectively. Enhanced resolution and multi-spectral capability of INSAT-3D/3DR imager and sounder instruments provide unique opportunity to observe the development and intensification of tropical cyclones. One of the essential ingredients to the intensification of tropical cyclones is vigorous convection with associated latent-heat release through condensation processes. Identifying and quantifying active convection in geostationary satellite images can be potentially useful to the prediction of cyclone intensification. The coverage of cyclone YAAS by TIR-1 and visible channels of INSAT-3D satellite on 06 UTC 25-MAY-2021 are shown in the Fig. 1.10.

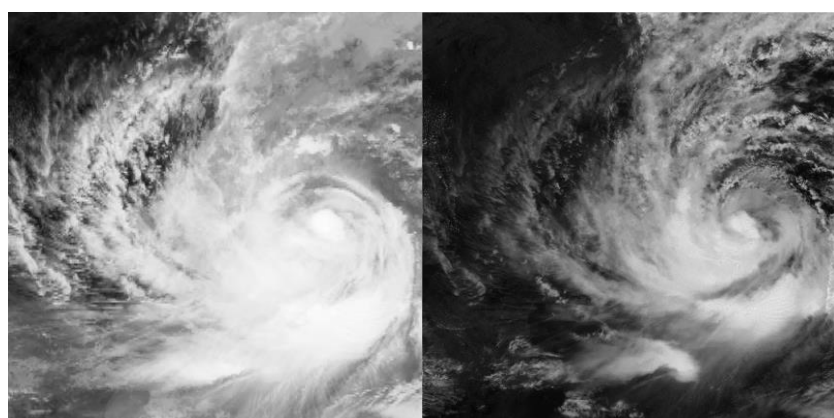


Figure 1.10: Coverage of cyclone YAAS by TIR-1 and visible channels of INSAT-3D satellite on 06 UTC 25-MAY-2021.

1.5.1 Cyclone structure observations using INSAT3D satellite data

Cyclone structural parameters are estimated using INSAT3D observations from different channels. Cyclone centric products from INSAT-3D imager channels are generated to visualize cyclone structure viz., its center, temperature of eye and its environment. Radius of Maximum Winds (R_{max}) is one of the most critical parameters that determine the tropical cyclone wind structure. This information is often required to assess the area of damage after the landfall of cyclone. The radius of maximum winds is normally very small (~ 30 km) compared to the size of cyclone, but can vary in a large range under specific circumstances. In infrared satellite images, the central region of cyclone is mostly obscured by high level cirrus clouds that cause difficulty in precise identification of R_{max} . High resolution observations from Visible and SWIR channels provide unique opportunity to identify the cloud structure near the center of cyclone. A procedure has been developed to produce cyclone centric products from each half hourly image of INSAT3D satellite. These images are very useful to study the structural changes in the core of tropical cyclone. A sample product generated on 0830 UTC 25 MAY, 2021 have been presented in the Fig. 1.11.

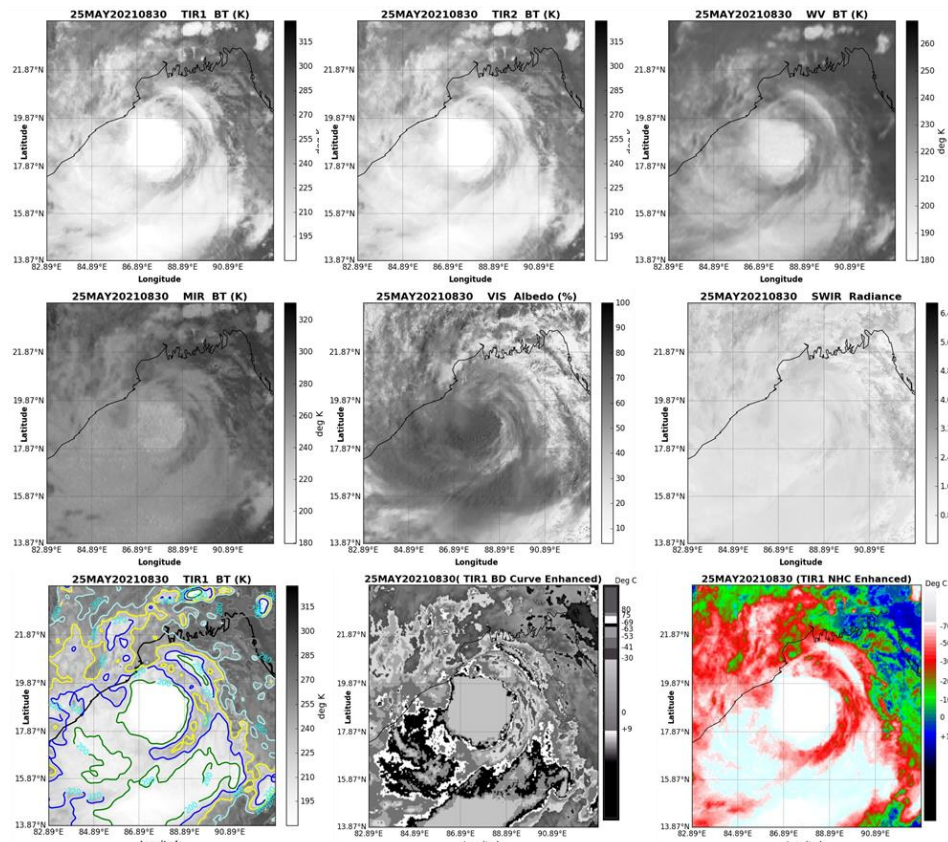


Figure 1.11: Cyclone Centric product generated using INSAT-3D imager channel. The nine panels show (a) TIR1 BT, (b) TIR2 BT, (c) WV BT, (d) MIR BT, (e) Vis Albedo, (f) SWIR radiances, (g) TIR1 BT Contours, (h) TIR1 BT BD enhanced, and (i) TIR1 BT NHC enhanced images.

1.5.2 Cyclone Geo-location

TC YAAS was continuously observed by the half hourly acquisition of INSAT-3D satellite. In half hourly TIR imageries of INSAT 3D satellite the center location of cyclone was estimated by center determination algorithm developed at SAC. The results were disseminated through SCORPIO web-server. One of the sample products generated in the real-time has been shown in the Fig. 1.12.

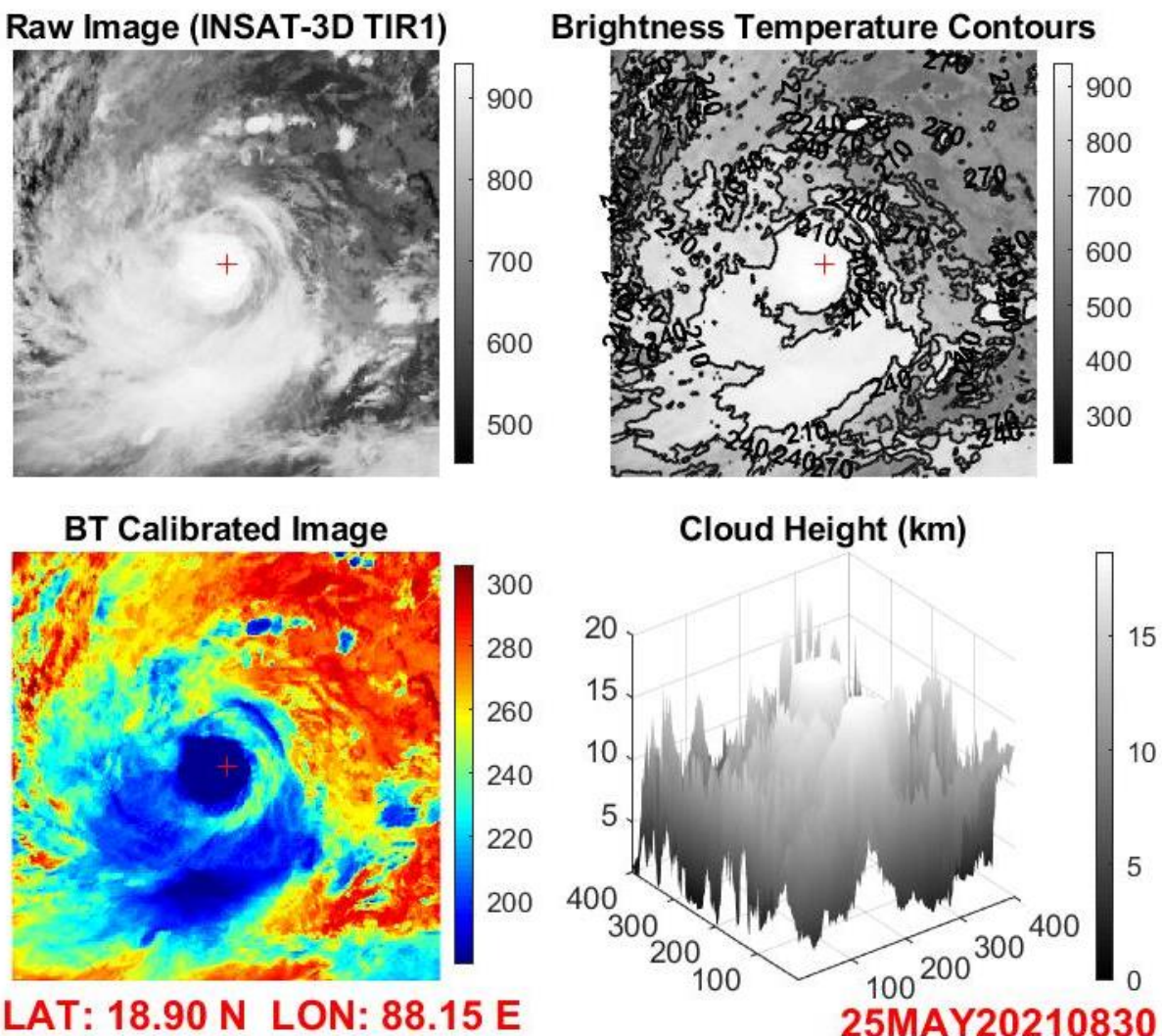


Figure 1.12: Cyclone center estimation using INSAT-3D TIR1 data. The four panels show a) INSAT-3D TIR1 raw image, (b) TIR1 BT contours, (c) BT calibrated image, and (d) cloud height (km).

1.5.3 Cyclone Intensity estimation using ADT with INSAT-3D data

Advanced Dvorak Technique (ADT) was originally developed within the Man computer Interactive Data Access System (McIDAS) architecture. The algorithm utilizes McIDAS library functions and routines to ingest infrared satellite data, display textual and graphical results, read various input data files, and write various output files. The ADT version 8.2.1, software package has been obtained from CIMSS and is installed in the “Non-McIDAS” mode (Jaiswal et al., 2021). The modules to ingest INSAT-3D satellite data in the software (version 8.2.1) are developed at Space applications Center (SAC-Ahmedabad, ISRO). The ADT was run in offline mode to estimate intensity values of TC YAAS using INSAT3D satellite data (SAC_ADT). ADT is run operationally for all global cyclones using half-hourly images of geo-stationary satellite images by CIMSS and provided at their web page in the near real time. SAC_ADT values were compared with the operational values of intensity obtained from the ADT run at CIMSS (CIMSS_ADT) and the real-time intensity values provided by IMD (Fig. 1.13). The error analysis were performed and the results shows that intensity of cyclones using INSAT-3D data by ADT are comparable to CIMSS_ADT and the best track estimates. However, there is an underestimation during 12 UTC 24 MAY to 06 UTC 25 MAY. The peak intensity of cyclone YAAS as observed by IMD (75 knots) was estimated as 70 knots by SAC_ADT between 18 UTC 25 MAY to 00 UTC 26 MAY.

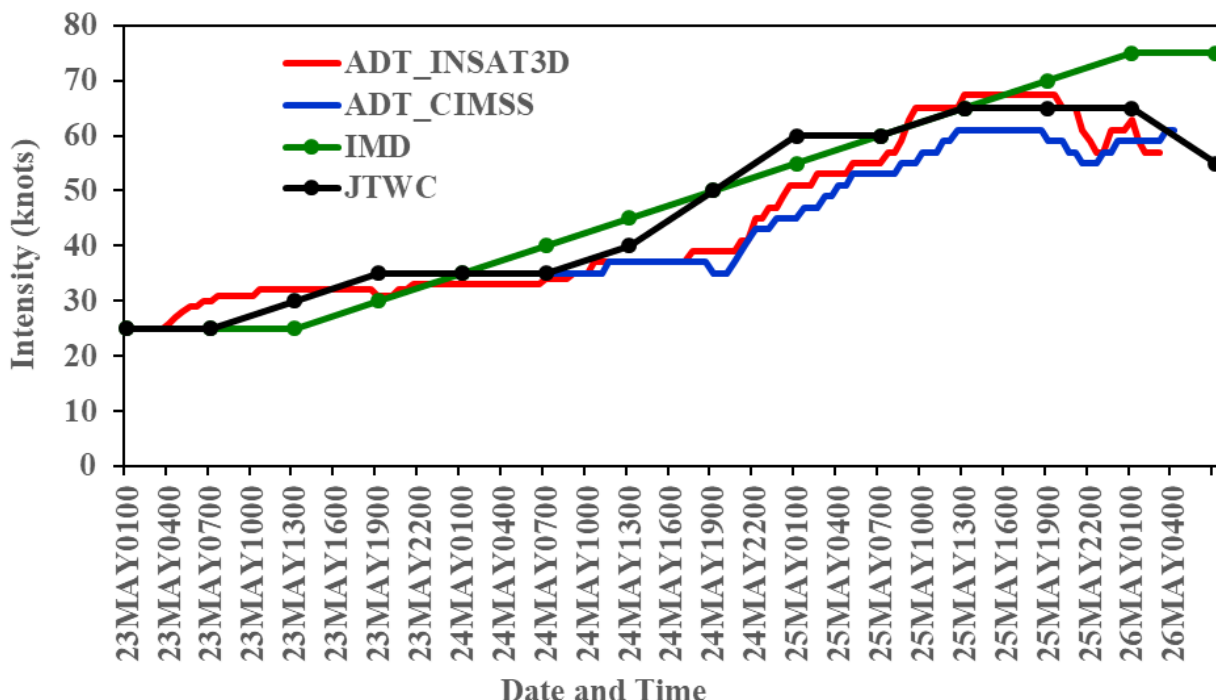


Figure 1.13: Intensity estimated by ADT using INSAT3D satellite data (SAC_ADT), CIMSS operational ADT (CIMSS_ADT) products and real-time observed values of IMD (IMD) during life time of TC YAAS.

1.6 Tropical cyclone YAAS observed by INSAT-3DR Rapid Scan Data

The rapid scan images from geostationary satellites have been proven to be useful tools in weather applications like the derivation of atmospheric motion winds, analysis of wildfires, convective initiation nowcasting, and identification of overshooting convective cloud tops. These images are useful for monitoring the convective features of storms that evolve on shorter time scales i.e. less than 15 or 30-minutes (Dworak et al. 2012; Cintineo et al. 2013). Several unique signatures have been identified within satellite imagery of severe convective storm tops, which include rapid cloud-top cooling (Cintineo et al. 2013), overshooting tops (Dworak et al. 2012), above-anvil cirrus plumes (Levizzani and Setvák 1996), the cold ring (Setvák et al. 2010) etc.

The Indian geostationary satellite INSAT3DR is being operated in rapid scan operation mode during high impact weather activities like TCs to capture the images in every 4-minutes interval. These satellite observations may be helpful in observing the rapidly changing features over TCs and thus determining its movement, structure and intensity. The atmospheric motion winds generated using rapid scan images during tropical cyclone time shows potential for providing very good quality winds information over Indian Ocean by increasing the amount of wind data availability and by capturing atmospheric movement that are too short-lived to be depicted by routine 30-minute scans. During the very severe TC YAAS, in the Bay of Bengal during 24-26 May 2021, the INSAT3DR satellite was operated in rapid scan mode. This TC was developed near the North Bay region and made landfall at the Odisha coast after achieving severe tropical cyclone category. The visual animation of TIR1, WV, visible and differenced “TIR1-WV” imageries over TC were also extensively analysed to observe the deep convective cloud-top movement, out flow characteristics and other structural features. The pattern of large-scale circulation around cyclone is also analysed by using atmospheric motion winds in rapid scan mode.

The differenced BT (IR-WV) values of two channels during the entire life of cyclone was computed and analyzed (Fig. 1.14). These images well represents the asymmetric clouds within eyewall and inner core region of TC. The presence of over shooting clouds at some locations is found rapidly changing as it alters in the next 4 minute imageries. The deep overshooting clouds (blue in colour, with differenced BT $<-20^{\circ}\text{C}$) were observed in the southern part of the eyewall whereas the low clouds (red in colour, with differenced BT close to 0°C) were present in the norther part. The extent of differenced BT was found to be changing in every 4 minute images.

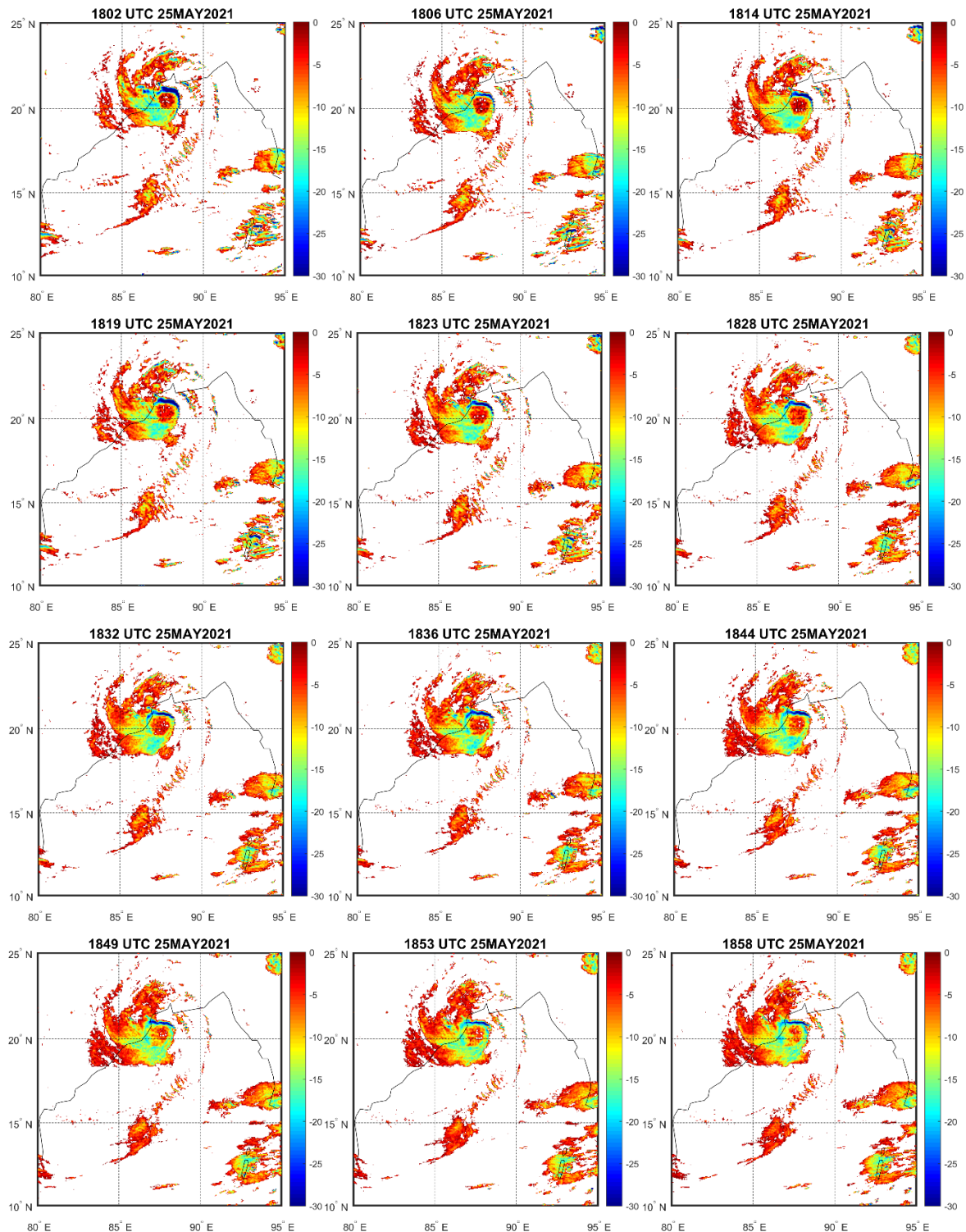


Figure 1.14: Asymmetric clouds within inner core region of TC YAAS during its peak intensity stage 1802-1858 UTC 25 May 2021.

The INSAT3D rapid acquisition images shows the rapidly changing pattern within inner core region of cyclone.

1.7 SMAP satellite observation over TC YAAS

Soil Moisture Active Passive (SMAP) is a United States environmental research satellite launched on 31 January 2015. The SMAP observatory includes a dedicated spacecraft and instrument suite in a near-polar, Sun-synchronous orbit. The SMAP measurement system consists of a radiometer (passive) instrument and a synthetic aperture radar (active) instrument operating with multiple polarizations in the L-band range. The combined active and passive measurement approach takes advantage of the spatial resolution of the radar and the sensing accuracy of the radiometer. The observations from L band radiometers, being in low frequency are uncontaminated by rain.

SMAP provides two wind speed products e.g. (i) Near-Real Time (NRT) wind speed and (ii) Final wind speed product. The NRT wind processing uses ancillary fields of shorter latency but lower quality. A final wind Speed version, reprocessed with a 1-month delay, which uses higher quality ancillary data. Additionally, SMAP also provide Tropical Cyclones (TC) ASCII files with SMAP 10-min maximum-sustained winds (in kn) and wind radii (in nm) for the 34 kn (17 m/s), 50 kn (25 m/s), and 64 kn (33 m/s) winds for each SMAP pass over a TC in all tropical ocean basins. The wind speed from NRT product of SMAP over TC YAAS has been shown in the Fig. 1.15. There was only one pass of SMAP over the TC YAAS 01 UTC 24MAY. The maximum intensity observed by SMAP was 25.82 m/s (50 knots). The high asymmetric winds were observed over southern region of cyclone.

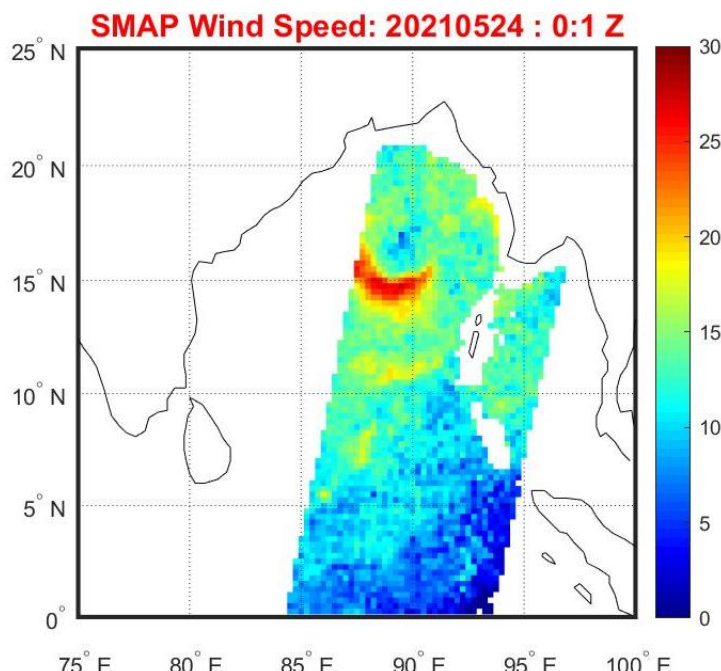


Figure 1.15: Wind speed over TC YAAS (01 UTC 24 MAY 2021) observed by SMAP satellite (NRT product).

1.8 Forecast Dissemination through web portal SCORPIO/MOSDAC

Satellite based cyclone observation and real-time prediction over Indian ocean (SCORPIO) (<https://mosdac.gov.in/scorpio>) is a web based application designed to provide Web-GIS available on the MOSDAC portal (<https://mosdac.gov.in>). It works as a decision support system to support the disaster management system. For cyclone YAAS, the scorpio website was updated in the real-time with following information:

- Cyclone track prediction
- Cyclone intensity prediction
- Ship avoidance region due to cyclonic winds
- Cyclone center estimation product using INSAT 3D data
- Cyclone centric images generated using INSAT3D imager channels
- ADCIRC based Storm surge forecast as animated Gif
- Coastal Inundation as jpeg image
- Coastal Inundation as GIS layer along with other thematic layers to aid the Decision Support system
- Tropical Cyclone Heat Potential anomaly as GIS layer along with other thematic layers

The webpage of scorpio web-portal during cyclone YAAS has been shown in the Fig. 1.16.

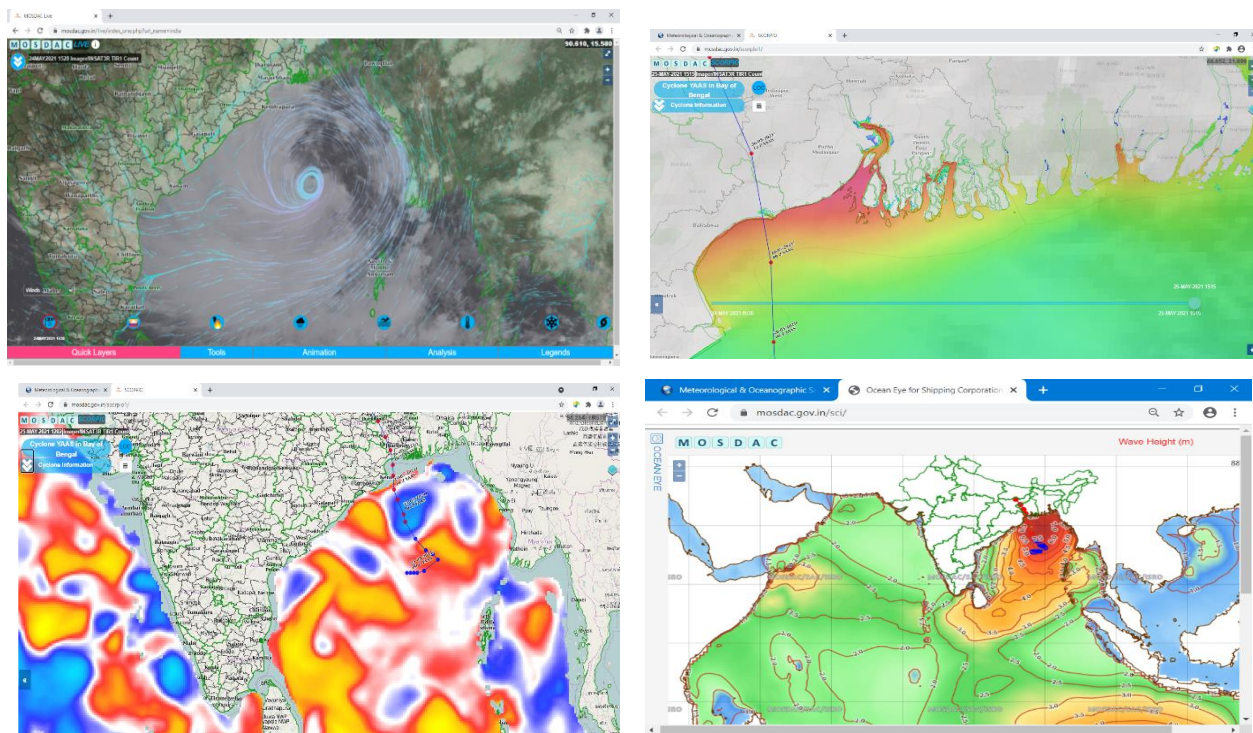


Figure 1.16: Cyclone YAAS forecast products disseminated through webserver SCORPIO.

1.9 Coverage of cyclone YAAS by media

Due to the advancement in cyclone prediction models the alerts were timely generated for cyclone YAAS and government took the preventive measures. Cyclone track and intensity until the landfall was continuously broadcasted via media channels, which made the wide publicity and awareness among the people. The personal interviews and live press conferences from IMD for the updates of cyclone YAAS was telecasted during the whole day as cyclone was approaching the coast of Odisha. The timely information saved the human loss and result the better preparedness to overcome the post-cyclone impacts. The media reports were providing the updates based on the foreign weather agencies as well as the India Meteorological Department.

1.10 Conclusions

The real time predictions of cyclogenesis, track and intensity of cyclone YAAS have been discussed in this report. The real time generated forecasts were disseminated through SCORPIO web-portal linked with MOSDAC site (www.mosdac.gov.in).

The Cyclogenesis signatures of TC YAAS was detected earliest on 20th May by GFS based Genesis Potential parameter. The track and intensity prediction of cyclone based on dynamical and numerical models viz. SAC-Lagrangian Advection Model and Hurricane Weather Research Forecast (HWRF) model, were provided continuously till cyclone made landfall. The real time forecasts were compared to the real-time observed estimates obtained from India Meteorological Department and Joint typhoon Warning Centre (JTWC). The error analysis for all the forecasts have been performed and presented in the report. The landfall position and time forecast error in 24 hour was about 19 km and 6 hour (early), respectively. The INSAT-3D visible and infrared data were analyzed to retrieve cyclone structural parameter viz., center. INSAT3D TIR-1 data was used in ADT to estimate cyclone intensity. INSAT3DR TIR-1 and water vapor images were processed to generate the differenced image (TIR-1 –WV) to study the rapid changes in the inner core of TC. The surface wind speed of SMAP satellite was also analyzed to study cyclone wind asymmetry. Our plans consist of utilizing multi-satellite multi-sensor approach to retrieve key parameters of tropical cyclone e.g. accurate location, surface wind structure, asymmetry, and size of cyclone, and develop methodology to assimilate this information in NWP models for improving the prediction of cyclone track and intensity. It is also planned to utilize key satellite observations of atmospheric and oceanic parameters to improve the accuracy of the prediction of location and intensity of cyclone at the time of its landfall.

References

1. Cintineo M. J., Pavolonis J., Sieglaff M., and Heidinger A. K. (2013): Evolution of severe and nonsevere convection inferred from GOES-derived cloud properties. *J. Appl. Meteor. Climatol.*, vol. 52, 2009–2023.
2. Chan, J. C. L. and Williams R. T. (1987): Tropical cyclone movement and surrounding flow relationship. *Mon Wea Rev* 110:1354-1374.
3. Dworak, R., Bedka K. M., Brunner J., and Feltz W. (2012): Comparison between GOES-12 overshooting top detections, WSR-88D radar reflectivity, and severe storm reports. *Weather and Forecasting*, Vol. 27, 684–699.
4. Hoover, B.T. and Morgan M.C. (2006). Effects of cumulus parameterization on tropical cyclone potential vorticity structure and steering flow. *Preprints of the 27th AMS Conference on Hurricanes and Tropical Meteorology*. April 23-28 Monterey, CA, paper 8B.5.
5. Jaiswal, Neeru and Kishtawal, C. M. (2011): Prediction of tropical cyclogenesis using scatterometer data, *IEEE Transaction on Geoscience and Remote Sensing*, vol. 49, Issue 12, pp. 4904 -4909.
6. Jaiswal, Neeru and Kishtawal, C. M. and Pal, P. K. (2013): Prediction of Tropical Cyclogenesis in North Indian Ocean using Oceansat-2 scatterometer (OSCAT) winds. *Meteorology and atmospheric Physics*, Vol. 119, pp. 137-149. DOI: 10.1007/s00703-012-0230-8.
7. Jaiswal Neeru, Kaushik Nitesh and Varma A. K. (2021): Advanced Dvorak Technique for Tropical Cyclone Intensity Estimation using INSAT-3D Satellite Data. SAC-Report: SAC/EPSA/AOSG/ASD/SR/05/2021.
8. Kotal, S.D., Kundu, P.K. and Roy Bhowmik, S.K. (2009): Analysis of cyclogenesis parameter for developing and non-developing low pressure systems over the Indian Sea, *Nat. Hazards*, 50:389-402
9. Kossin, J. P., Knaff, J. A., Berger, H. I., Herndon, D. C., Cram, T. A., Velden, C. S., Murnane, R. J. and Hawkins, J. D. (2007): Estimating Hurricane Wind Structure in the Absence of Aircraft Reconnaissance. *Weather and Forecasting*, 22, 89-101.
10. Singh, Sanjeev Kumar, Kishtawal, C.M. and Pal, P.K. (2011): Track Prediction of Indian Ocean cyclones using Lagrangian Advection Model. *Natural Hazards* DOI 10.1007/s11069-012-0121-9.

11. Singh, S. K., Kishtawal, C. M., Singh, R. Jaiswal, Neeru and Pal, P. K. (2012): Impact of Vortex-Removal from Environmental Flow in cyclone Track Prediction using Lagrangian Advection Model. *Meteorology and Atmospheric Physics*, 117,103–120. DOI 10.1007/s00703-012-0198-4
12. Singh, S. K., Jaiswal Neeru, Kishtawal, C. M., Singh R., Pal., P. K. (2013): Early detection of cyclogenesis signature using global model products, *IEEE Transactions on geoscience and remote sensing* 52(8), 5116-5121.

2. Tropical Cyclone ‘YAAS’: Research and Operational activities from ocean perspective

**Anup Kumar Mandal, Seemanth M., Jishad M., Suchandra Aich
Bhowmick and Neeraj Agarwal**

2.1 Introduction

India has an extensive coastline; therefore, a significant portion of its sustainable development depends on the ocean conditions. The subcontinent is surrounded by Indian Ocean and is vulnerable to devastations from tropical storms and cyclones. The ruinous impact of tropical cyclones (TC) is much more pronounced in the east coast of India, as compared to the west coast. The Bay of Bengal (BoB) is an enclosed ocean basin, and is a part of the north Indian Ocean. The distribution of tropical storms/cyclones in BoB is bimodal. Peak cyclonic activity is noticed during the post monsoon months of September to December and the secondary peak is during premonsoon months from April to June. For BoB, seasonal and intra-seasonal variability in both ocean and atmosphere plays key role in genesis, intensification and movement of tropical cyclones. In this report, we present a detailed research and operational activity carried out at SAC (ISRO), on the pre-monsoon cyclone YAAS, which evolved over Bay of Bengal on 23rd May 2021.

2.2 Cyclone induced Sea Surface cooling and density changes in the ocean

Daily Sea Surface Temperature (SST) data from the INSAT -3D, which is based on 30 min SST observations, and GHRSST have been used for this study. Indian satellites for met-ocean applications, INSAT-3D and INSAT-3DR (both are in geostationary orbit) having a six-band imager paired with a 19-band sounder. SST is derived with a spatial resolution of 4 km from split thermal window channels (10.2- 11.3 μ m and 11.5 –12.5 μ m) during daytime and using additional mid-IR window channel (3.7 – 4.1 μ m) during night time over cloud-free oceanic regions ([Gangwar and Thapliyal, 2020](#); [Walton et al., 1998](#)). Both the satellites provide images at every 30-minute inter-satellite temporal difference of around 15 minutes. So effectively, we get an SST image at high temporal resolution (every 15 minutes) that has a definite advantage ([Agarwal et al., 2019](#)) over polar-orbiting sensors, which only provide observations in a specific region two times a day. In this study, thermal fronts are computed using the daily averaged image of SST from INSAT-3D. The SST data sets were downloaded from MOSDAC (Meteorological and Oceanographic Satellite Data Archival Centre, <https://mosdac.gov.in/>).

The Group for High-Resolution Sea Surface Temperature (GHRSST) data merges SST observations from all kinds of available sources. It is a merged SST product, which includes SST from all the available microwave and infrared sensors. The Level-4 (L4) product is generated using various objective analysis techniques to produce gap-free SST maps over the global oceans. The SST product used in this study is generated by Jet Propulsion Laboratory

(JPL) using an optimum interpolation approach on a global 0.011° grid ([Reynolds et al., 2007](#)). This is version 4 multiscale ultrahigh resolution (MUR) product that has inputs from all possible sources of SST such as NASA Advanced Microwave Scanning Radiometer-EOS (AMSR-E), the Moderate Resolution Imaging Spectroradiometer (MODIS) on the NASA Aqua and Terra platforms, the US Navy microwave WindSat radiometer and in situ SST observations from the NOAA iQuam project. GHRSST SST Products blended from multiple satellites or multiple passes of satellites. The data downloaded from (<https://podaac-tools.jpl.nasa.gov/drive/files/allData/ghrsst/data/GDS2/L4/GLOB/JPL/MUR/v4.1>). The sea surface salinity (SSS) datasets are available at NASA Physical Oceanography Distributed Active Archive Center (PO.DAAC) (<http://podaac.jpl.nasa.gov>). The eight-day averaged SMAP L3 product having spatial resolution of 0.250×0.250 have been used for this study. The eight-day product is created by averaging eight days of L2 data.

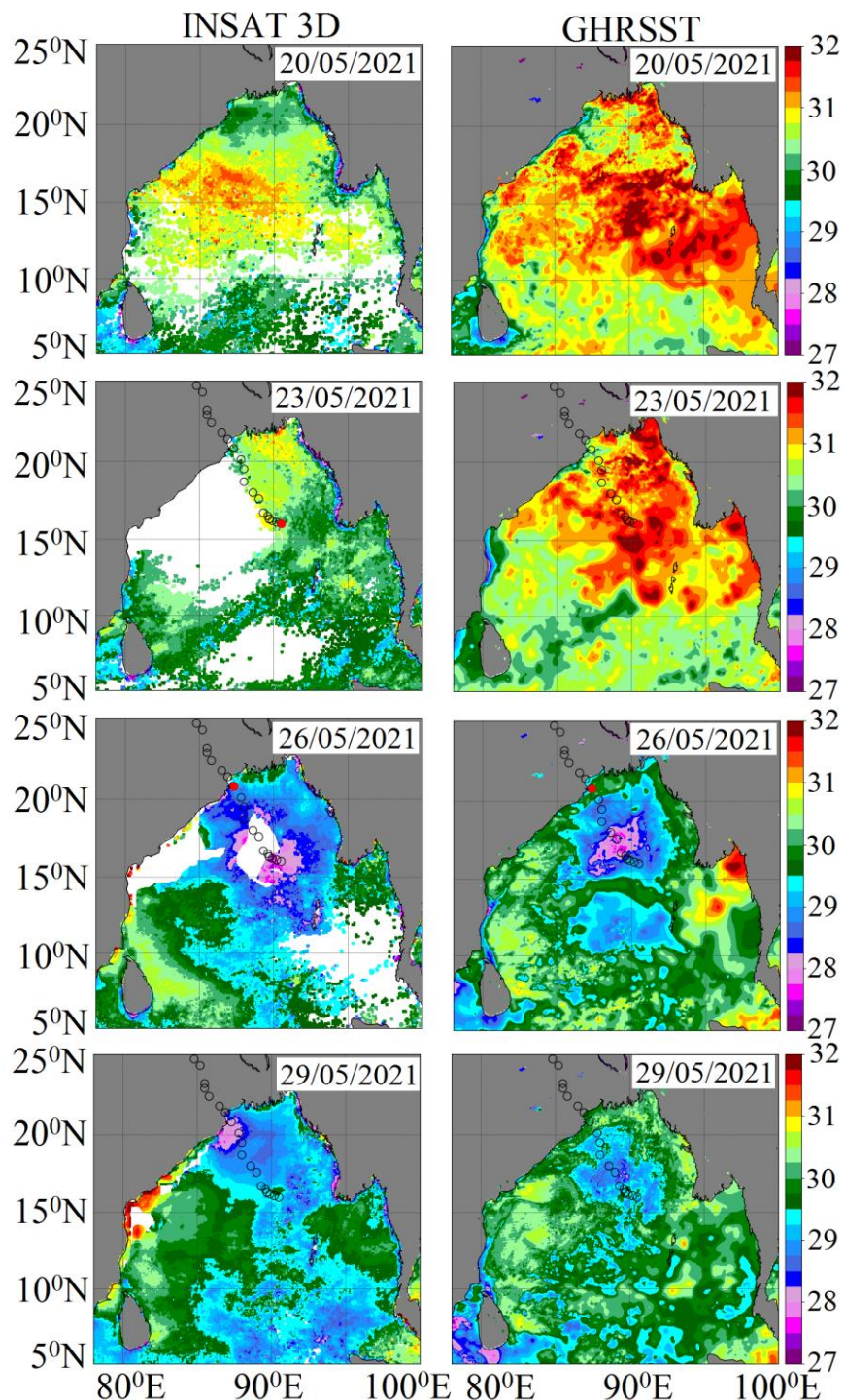


Figure 2.1a: The SST data from INSAT and GHRSST before, during and after Yaas Cyclone. The circles are indicating the path of Yaas cyclone and red circle is pointing cyclone position.

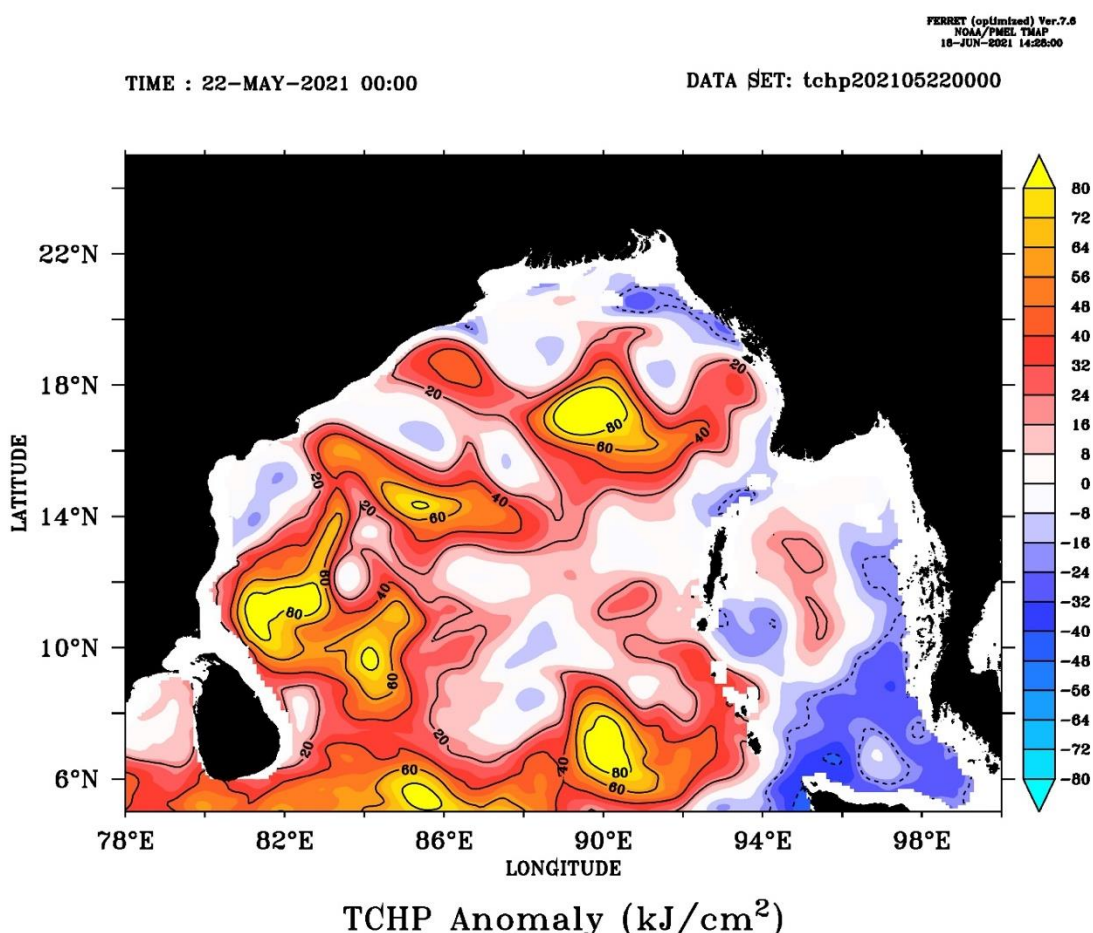


Figure 2.1b: TCHP anomaly (kJ/cm^2) over BoB as observed on 22nd May 2021 using Modular Ocean Model (MOM3)

The spatial plot of the INSAT SST and GHRSST before, during and after Yaas is shown in Fig. 2.1a. Fig. 2.1b shows the tropical cyclone heat potential (TCHP) anomaly calculated using the temperature and salinity profile simulated from data assimilative modular ocean model (MOM3) operational in- house at the Space Applications Centre. On May 20, the ocean was very warm having a high temperature $>30^{\circ}\text{C}$ in the central BoB. Correspondingly, TCHP anomaly as seen from model simulations were high positive (40-80 kJ/cm^2), making the oceanic conditions conducive for cyclogenesis. A deep depression was formed at $16^{\circ}\text{N}; 90.5^{\circ}\text{E}$ on 23rd May. Later, the system further intensified as it turned to the northeast, becoming a severe cyclonic storm on May 24. Yaas moved northeast ward, strengthening to a Category 1-equivalent tropical cyclone and to a very severe cyclonic storm on May 25. On May 26, Yaas crossed the northern Odisha coast and further weakened inland while turning north-northwestwards.

The INSAT SST data has been analysed for May 2021 to understand the pre-cyclonic conditions and the Hovmöller plot of SST anomaly is shown in Fig. 2.2. Fig. 2.2 shows a high temperature anomaly (+1.2 °C) just before the formation of cyclone (on 21 and 22 May 2021). The SST data from INSAT is missing at 80-85°N during 23-25 May due to the cloud cover. SST reduced rapidly after the passage of cyclone and the cool SST prevailed until the end of May 2021.

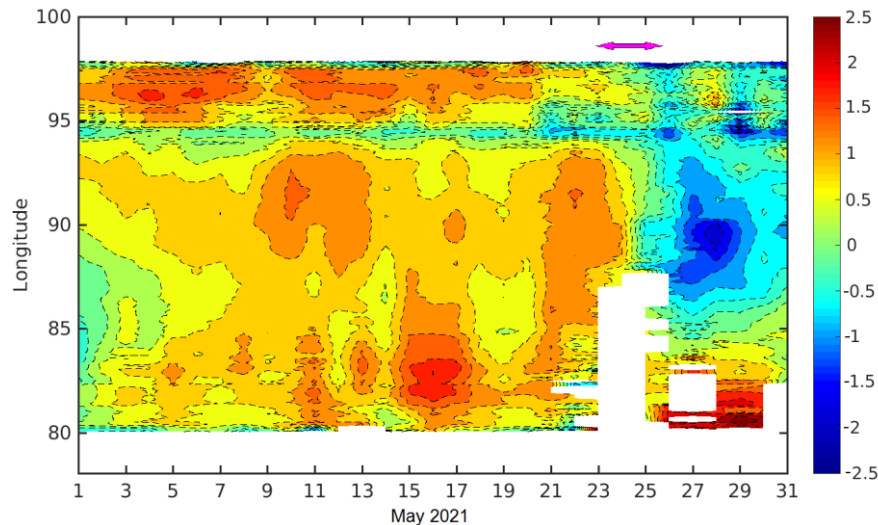


Figure 2.2: The SST Anomaly during May 2021 that showing a high temperature anomaly (+1.2°C) prior to the formation of Yaas. The magenta arrow is showing the duration of cyclone Yaas.

The time series of INSAT SST data from 16°N; 86°E for April –May months for 2019, 2020 and 2021 is shown in Fig. 2.3. Interestingly, Fani, Amphan and Yaas cyclones were formed in the same season of 2019, 2020 and 2021, respectively. Fani originated as a tropical depression on April 26, 2019, and dissipated on May 4, 2019. The temperature was about 30 °C during April and decreased rapidly (by 3 °C) after Fani Cyclone. In 2020, cyclone Amphan originated as a tropical depression on May 16 and dissipated on May 21, 2020. The temperature was about 30 °C on May 15 and declined after cyclone. For Yaas, The SST has drastically reduced by about 2.25 °C after the pass of cyclone.

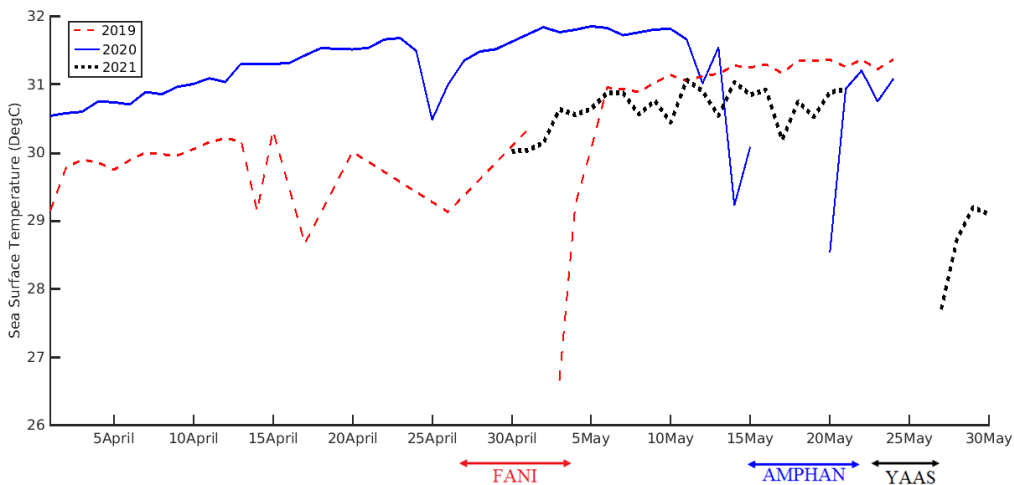


Figure 2.3: The SST data during April and May from 2019-2021 from 16°N ; 86°E . The arrows are indicating the duration of cyclones Fani, Amphan and Yaas from 2019, 2020 and 2021, respectively.

Fig. 2.4 shows the snapshot of daily averaged SST, 8-day averaged SSS and estimated density for 20th May 2021 and 28th May 2021, i.e. prior to cyclone. Large scale, low salinity features ($< 32 \text{ psu}$) in the central Bay of Bengal can be clearly seen in the sea surface salinity image for 20th May 2021. This low salinity results in strong surface stratification, which results in surface heating due to high solar insolation. This can be clearly seen in the SST image in the central Bay of Bengal, where large scale warming ($\sim 32^{\circ}\text{C}$) can be seen consistent with the low salinity region. Hence, it can be seen that the ocean surface conditions were conducive for the formation and sustainability of cyclone in the region. The seas surface density is also low as compared to the surroundings in the region.

After the passage of cyclone, surface becomes cool and saline due to Ekman pumping associated with high cyclonic winds. There is a drastic change in the physical properties after the passage of cyclone, which can be seen in the SST, SSS and density difference maps post and pre cyclone. There is a temperature drop of $\sim 3^{\circ}\text{C}$ from 20th to 28th May, while the salinity increases by $\sim 1 \text{ psu}$, due to which the density increases by $\sim 2 \text{ Kg/m}^3$.

Density changes are associated with both salinity and temperature changes, surface cooling and salinification can increase the density, however, which physical parameter (SST or SSS) contributed more to changes in density is not known.

Density changes were computed in two ways, one by keeping fixed SST and another, by keeping fixed SSS (both corresponding to 20th May) in order to assess the individual contribution of SST and SSS in density change and the results are shown in Fig. 2.4 and 2.5, respectively. It can be clearly seen that density changes ($> 50\%$) resulted mainly due to cooling

of SST, while the salinity changes resulted in only marginal change ($\sim 15\%$) in the total density changes.

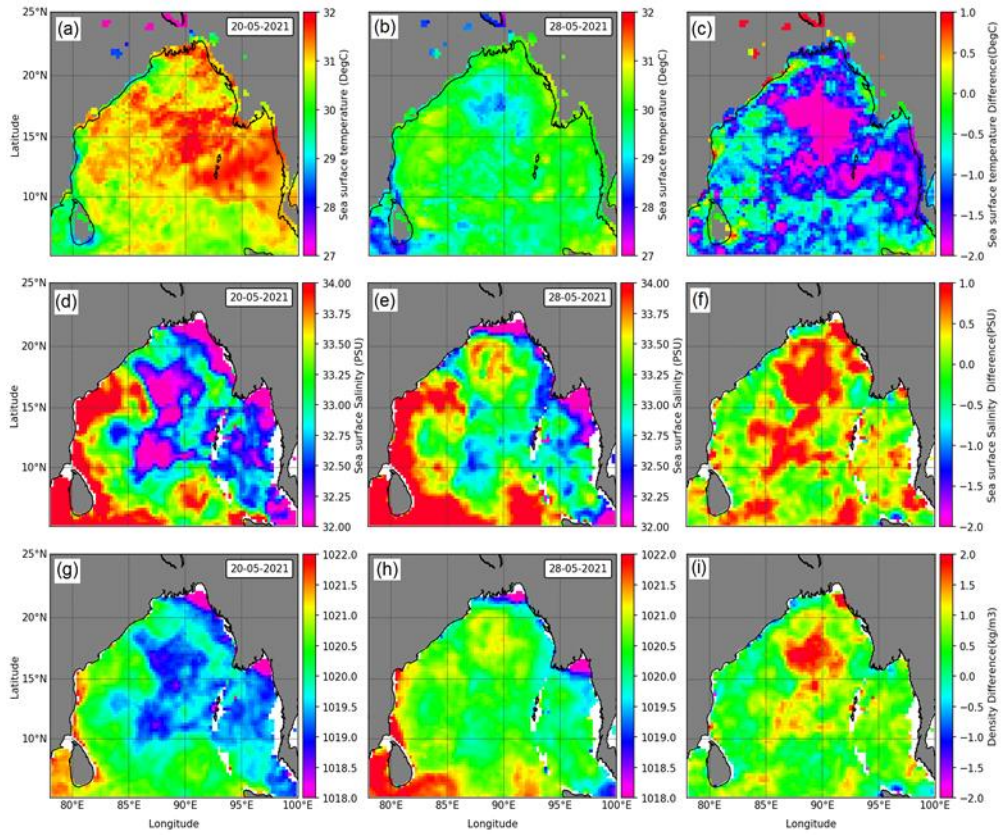


Figure 2.4: Maps of (upper panel) Surface temperature ($^{\circ}\text{C}$), (middle panel) salinity (psu) and (lower panel) density (Kg/m^3) during (a,d,g) pre-cyclone (20/05/2021) and (b,e,h) post-cyclone (28/05/2021). The differences (post – pre cyclone) are in c, f and i, respectively

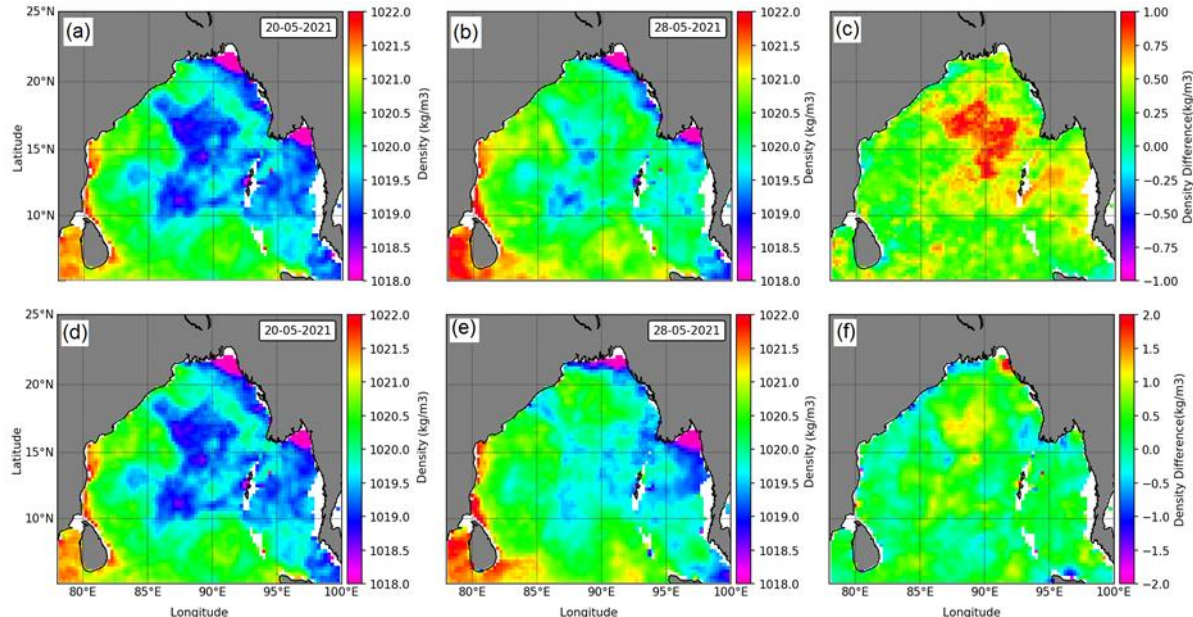


Figure 2.5: Density using temperature and constant salinity from 20/05/2021 (a-c) and salinity and constant temperature from 20/05/2021 (d-f) pre (20/05/2021), and post (28/05/2021) cyclone Yaas and the difference, respectively.

2.3 Operational Activities

Accurate prediction of Ocean state has paramount importance for different applications such as naval operations, ship routing, tourism, fisheries, port and harbour construction, offshore industries, disaster management etc. This becomes more relevant when there occurs an extreme weather event like a tropical cyclone. Storm surge induced coastal inundation maybe considered the worst disaster caused by a cyclone. Here at SAC, storm surge forecast is being generated whenever there is a tropical cyclone occurs in the North Indian Ocean region. Recently, an early warning system for coastal inundation forecast due to tropical cyclone along the east coast of India has also been established (Mandal et al., 2020). In addition, forecasting of extreme waves induced by strong cyclonic winds is also very important for different applications. A very high resolution data assimilative wave forecasting system is operational at SAC since 01st June 2018 (Seemanth and Suchandra, 2018). Routine wave forecasts generated from this system are operationally disseminated to different stake holders through MOSDAC. Storm surge and inundation forecasts are also disseminated through MOSDAC, whenever there is a tropical cyclone. Moreover, a 3-dimensional ocean circulation model is also operational at SAC which provides six hourly forecasts of ocean state parameters for next 120 hours at a horizontal resolution of 0.1° in the North Indian Ocean region. Operational activities carried out at Oceanic Sciences Division during the tropical cyclone ‘YAAS’ are discussed in the following sections.

2.3.1. Storm surge forecast for YAAS cyclone

The storm surge forecast was generated using state of the art coupled ADCIRC+SWAN model. The ADCIRC model discretizes the shallow-water equations using finite element methods defined on unstructured meshes (Luettich and Westrink 2004). The shallow-water equations are derived from the incompressible Navier-Stokes equations while assuming hydrostatic pressure and solve for surface water elevation and surface water currents. The accurate description of coastal geometry is much needed for storm surge forecasts. For this,ETOPO-2 global relief model data was used to prepare the mesh for storm surge simulations. The mesh has 11023 no of computational nodes. The spatial resolution near land is 1km and 60km in the open ocean. ADCIRC model is primarily forced by tides, winds and wind-waves; during a cyclone, wind stresses are the dominant forcing. Coupling of the ADCIRC model with a wind wave model for capturing wave-induced setup has been established (Dietrich et al. 2011). The code has been parallelized for distributed memory and multicore computers and has been demonstrated to achieve excellent scalability on these platforms (Dietrich et al. 2011).

In SAC, we have used NCMRWF 0.25° spatial resolution winds as primary forcing. The ADCIRC+SWAN model was run for 10 days to accomplish model spin up. After that storm surge forecast was generated using NCMRWF 0.25° forecast wind fields. The model was run on SAC HPC facility using 288 cores which takes about 30 minutes to complete.

After IMD declared cyclogenesis in the Arabian sea on 23 May 2021, storm surge forecasts were generated. The forecast files were generated from 23 May 2021 till 25 May 2021 and updated daily. The NCMRWF forecast winds for 23 May 2021 was indicating landfall of cyclone YAAS on 26 May 2021 09UTC. During landfall the peak surge height forecast was around 3.5m near Digha region. The forecast wind from NCMRWF model on 24 May 2021 was indicating landfall again on 26 May 09UTC. Peak storm surge forecast for 24 May 2021 was about 3.5m-4m during Digha and Sagar Island areas. The storm surge forecast for 25 May 2021 is shown in Fig. 2.6a. From Fig. 2.6a, it is observed that the peak surge height was around 4m during landfall and about 3.5-4m just after landfall near Contai and Sagar Island region. Surge residual is the difference between model storm tide and model predicted tide. The surge residual validation is carried out at Dhamra port (86.95°E , 20.78°N) using tide gauge observation provided by INCOIS (Fig. 2.4b). The correlation coefficient between the forecasted surge residual and observed surge residual is 0.9.

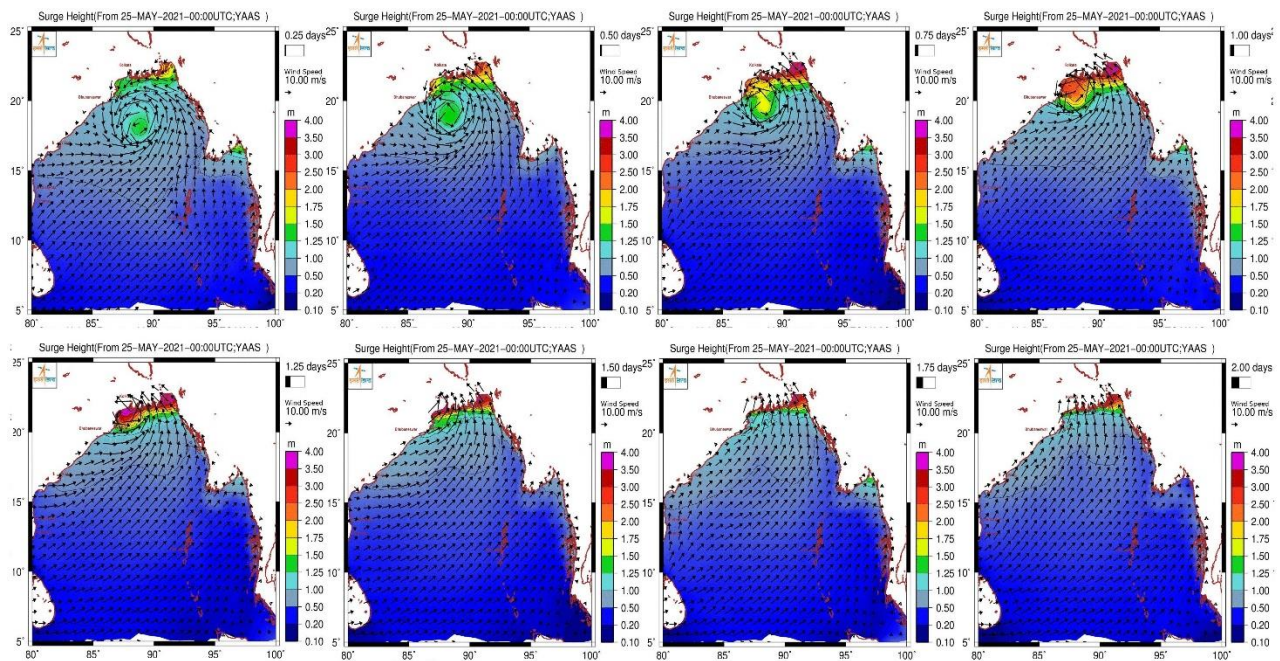


Figure 2.6a: Storm surge forecast starting from 25 May 2021 00UTC

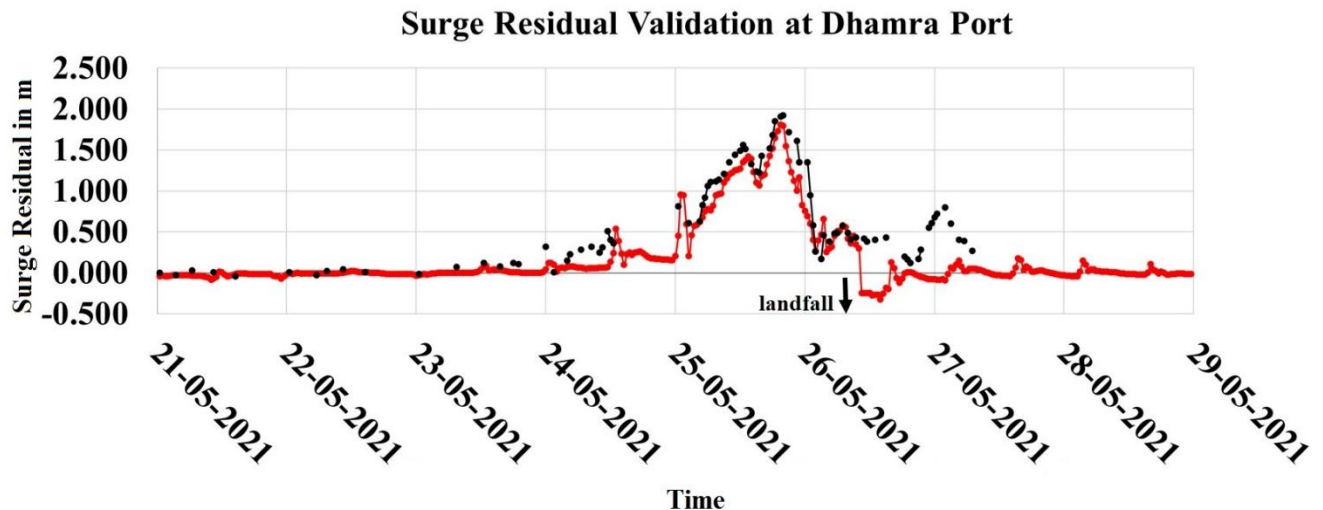
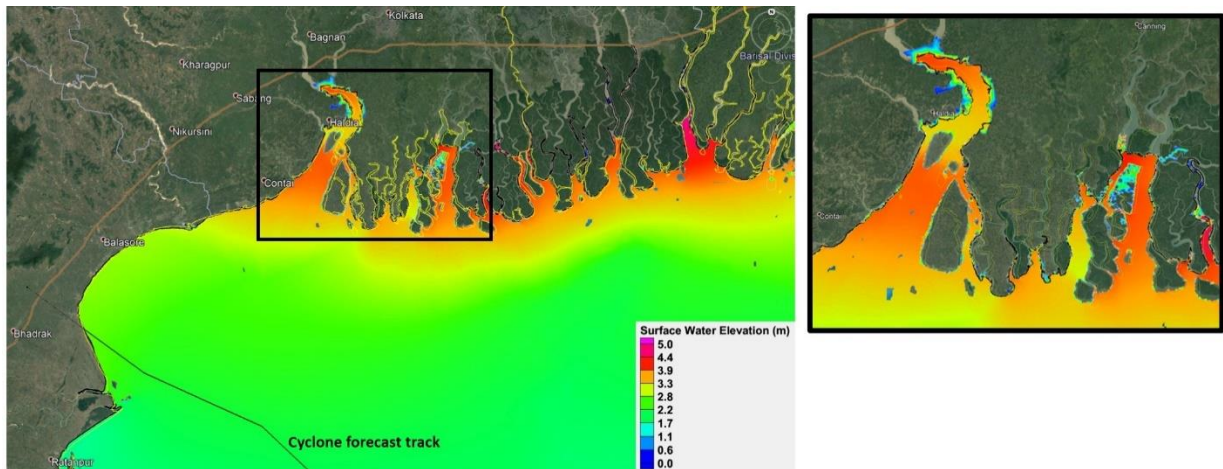


Figure 2.6b: The surge residual comparison with tide gauge observation provided by Dhamra port (86.95°E, 20.78°N)

The NCMRWF forecast winds from 23 May 2021 consistently showed landfall near West Bengal-Odisha border which lead to the fact peak value of storm surge came around Contai location in most of the forecasts. In the Fig. 6b, we have subtracted tide and therefore it is storm surge level without tide. These forecasts were disseminated via MOSDAC.

2.3.2 Coastal inundation forecast

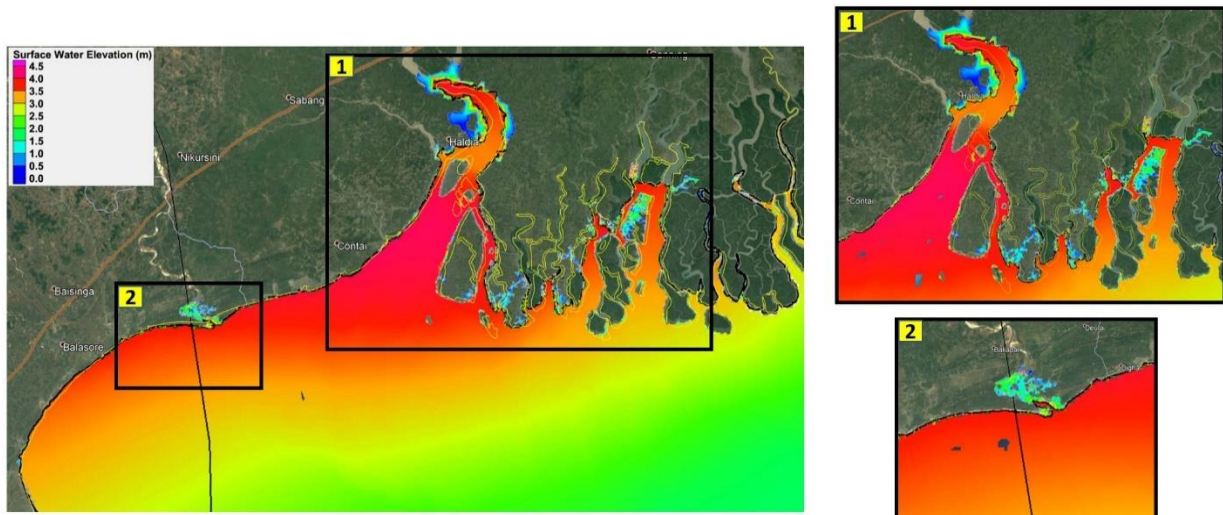
Coastal inundation occurs as a result of high storm tide during the landfall of a cyclone when the seawater enters in the low-lying areas near coastline. For effective coastal inundation forecast, coastal geometry must be well represented along with creeks, river-delta, islands etc. It must be also noted that for coastal inundation forecast a very high resolution mesh (near coast) is much needed so that the low lying areas are properly spotted. Coastal inundation forecast was generated in coupled ADCIRC+SWAN model using 100m fine resolution (near coast) mesh. The total water elevation as a combined effect of storm surge, wind waves and tides are simulated using NCMRWF 0.25° resolution forecast winds as primary forcing. This methodology was already verified for several past cyclones (Mandal et. al. 2019).



Coastal inundation forecast generated using coupled ADCIRC+SWAN model. Maximum storm tide is around 4m near Contai, 3.5m near Haldia and 4.2m near Sundarban area. Maximum inland coastal inundation extent is around 3.6km near Sutahata (Haldia), 0.5km near Lothian island and several other locations in Sundarban area. Expected landfall : (Longitude - 86.96, Latitude - 21.18) on 25 May 16 UTC
*Experimental

Figure 2.7: Coastal inundation forecast for 23 May 2021

The coastal inundation forecast for 23 May 2021 is shown in Fig. 2.7. From Fig. 2.7, it is seen that maximum storm tide was around 4m near Contai, 3.5m near Haldia and 4.2m near Sundarban area. Inundation was also forecasted in many low lying areas. Out of which maximum inundation was observed for three locations; 3.6km near Sutahata (Haldia), 0.5km near lothian Island and several other locations in Sundarban area.



Coastal inundation forecast generated using coupled ADCIRC+SWAN model. Maximum storm tide is around 4.2m near Contai, 3.5m near Haldia and 3.8m near Sundarban area. Maximum inland coastal inundation extent is around 3.8km near Sutahata (Haldia), 4.5km near Kumbhirkari, 1km near Bakkhali, 2.5km near and several other locations in Sundarban area. Expected landfall : (Longitude-87.33°E, Latitude: 21.50°N, Time: 26 May 08UTC)
*Experimental

Figure 2.8: Coastal inundation forecast for 24 May 2021

Coastal inundation forecast for 24 May 2021 is shown in Fig. 2.8. From Fig. 2.8, it is observed that maximum storm tide is around 4.5m near Contai and Sagar Islands, 3.5m near Haldia and

3.8m near sundarban areas. Maximum inland extent of coastal inundation is around 3.8km near Sutahata (Haldia), 4.5km near Kumbhigari, 1km near Bakkhali, and around 2.5km near several places in Sundarban area. The coastal inundation forecasts were disseminated via MOSDAC.

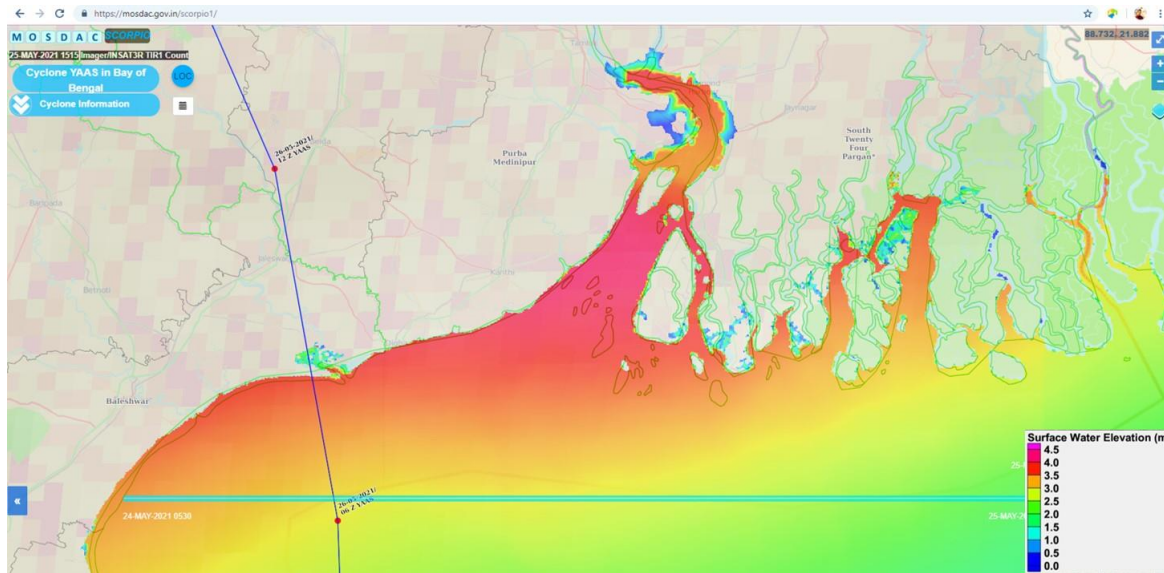


Figure 2.9: Coastal inundation over interactive platform hosted on MOSDAC

Another coastal inundation product, prepared in GEOTIFF format was also disseminated via MOSDAC, where user can zoom on a “street map” and check the corresponding coastal inundation as shown in Fig. 2.9. This product is available at dm.mosdac.gov.in/scorpio1/.

The summary of maximum storm tide, significant wave height and horizontal extent of coastal inundation are shown in Table 2.1.

Table 2.1. Summary of Storm tide height, significant wave height and horizontal extent of coastal inundation forecasts

Forecast date	Expected Landfall time (in UTC)	Storm tide height during landfall (in m) near			Significant Wave height during landfall (in m) near			Horizontal extent of coastal inundation during landfall (in km) near		
		Digha	Contai	Sagar Island	Digha	Contai	Sagar Island	Sutahata (Haldia)	Kumbhigari (Orisha)	Sundarban areas
23/05/2021	26 May 09z	3.5	3.8	3.8	1.8	2.8	1.8	3.6	0.5	0.5-1
24/05/2021	26 May 09z	3.5	4.0	4.0	2	2.5	2.0	3.8	4.5	2.5
25/05/2021	26 May 08z	3.5	4.0	4.0	2	2.5	2.0	3.8	4.5	2.5

2.3.3 Extreme wave prediction during ‘YAAS’

SAC operational wave forecasting system is based on WAVEWATCH III (WW3) model. It uses 10m analysis and forecast wind components obtained from the National Centre for Medium Range Weather Forecasting (NCMRWF) as the forcing field. The operational wave model runs one time in a day at the 0000 UTC model cycle and start with a 24 hour hindcast

for the previous day (using previous day's analysis winds). In order to improve the predictability of the model, SARAL/AltiKa, Jason3 and Sentinel measured wave heights are being assimilated into this 24-hr hindcast cycle. Updated model initial condition at the 24th hour of previous day (0000 UT of current day) is used for initialising the next 5 days (120 hours) forecast. Model forecasted wave parameters such as significant wave height (SWH), mean wave direction, swell height, swell direction and mean wave period are disseminated through LIVE MOSDAC (<https://live.mosdac.gov.in/>) and OCEAN EYE (<https://mosdac.gov.in/sci/>). For detailed description of the wave forecasting system, see Seemanth and Suchandra (2018).

WW3 simulated analysis fields of SWH during different development stages of 'Yaas' cyclone is shown in Fig. 2.10. As per IMD records, the deep depression over east central Bay of Bengal intensified into cyclonic storm 'Yaas' at 00 UTC of 24th May, 2021. During this period, maximum wave height simulated was ~5.5m (Fig. 2.10a). By 21 UTC on the same day, it further intensified into a severe cyclonic storm. SWH during this period (00 UTC of 25th May 2021) is also increased to ~8.5m in the northern Bay of Bengal (Fig. 2.10b). 'Yaas' then moved north-northwestwards and continued to intensify into a very severe cyclonic storm by 12 UTC of 25th May 2021. SWH up to ~9m is noticed in the northern bay during this time (Fig.2.10c). By 18 UTC on that day, 'Yaas' showed its maximum intensity with a maximum sustained surface wind speed of ~130-140 kmph (as per IMD record). Northern Bay of Bengal became very rough during this period with a wave height of ~9.2m (not shown). By 06 UTC of 26th May 2021, 'Yaas' moved north-northwestwards and crossed north Odisha coast around Latitude 21.35°N and Longitude 86.95°E, about 20 km to the south of Balasore as a very severe cyclonic storm. The maximum wave height during this time was ~5.5m in the northern part of Bay of Bengal and it generated waves of height ~2-2.5m along the Odisha coast (Fig. 2.10d). Fig. 2.11 shows the time-series evolution of model simulated SWH at different coastal locations along the east coast of India during 'Yaas'. At Dhamra coast, located south of the landfall location, the wave height was <0.8m till 24th May 2021. Then the SWH gradually increased up to ~2m during 18th UTC of 25th May 2021, i.e. 12 hours before the landfall of cyclone. It then reduced to ~0.7m by 29th May 2021. At the Digha coast (north of cyclone landfall region), maximum SWH of ~1.8m is simulated during the landfall of cyclone. Along the southern coast of Sagar island, the sea was more rough with a maximum SWH of ~2.7m during the landfall of cyclone. During non-cyclonic period, wave height over this region was <1.3m. Southern part of Sundarban region experienced higher waves from 24th May 2021 and

it reached up to ~4m, 12 hours before the landfall. It then gradually reduced to ~1.3m by 29th May 2021.

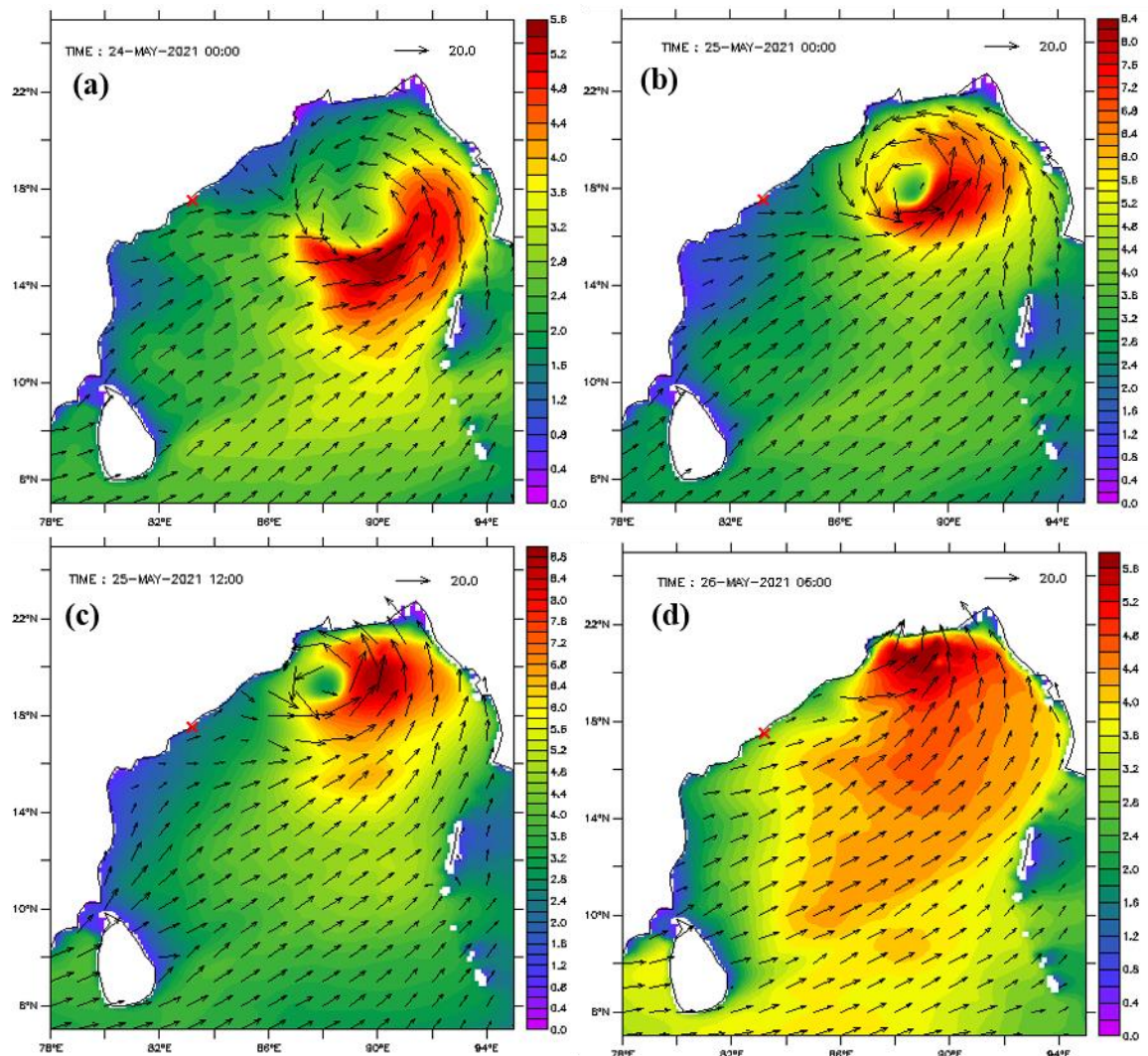


Figure 2.10: WW3 simulated analysis fields of SWH (m) and forcing wind vectors during Yaas. The red cross mark indicates the location of wave rider buoy at Visakhapatnam.

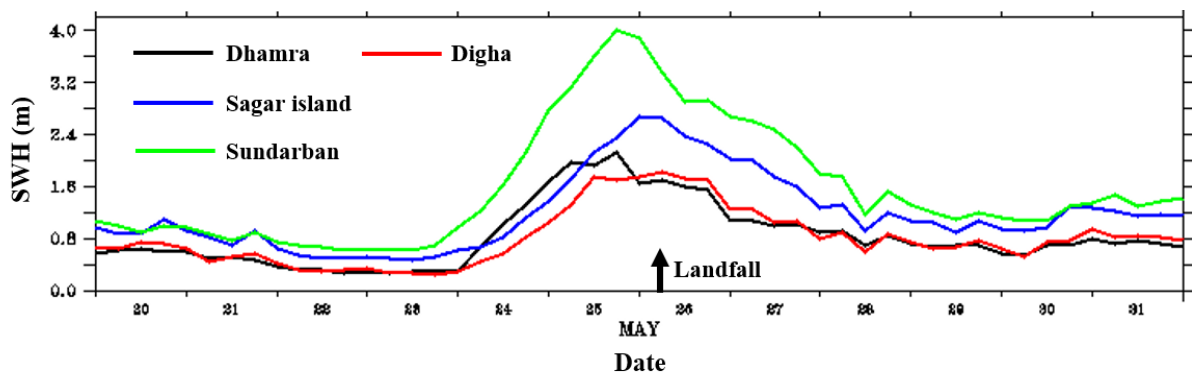


Figure 2.11: Time-series evolution of model analysis SWH at different coastal locations along the east coast of India during Yaas.

The analysis fields of simulated SWH during cyclone is compared with the SWH observation from the Indian National Centre for Ocean Information Services's (INCOIS) wave rider buoy available at Visakhapatnam (Fig. 2.12). Although this buoy is located (Red cross mark in Fig. 2.10) slightly far from cyclone passage, observed wave height shows a gradual increase because of the rough sea induced by the strong cyclonic winds. Observed SWH peaks during the landfall of cyclone with a magnitude of 2.36m. Time-series comparison of model simulated SWH with the buoy observation indicates that the simulation follows the observed SWH pattern reasonably well (Fig. 2.12). Maximum wave height simulated by the model was 2.48m at Visakhapatnam, which was very close to the observed value.

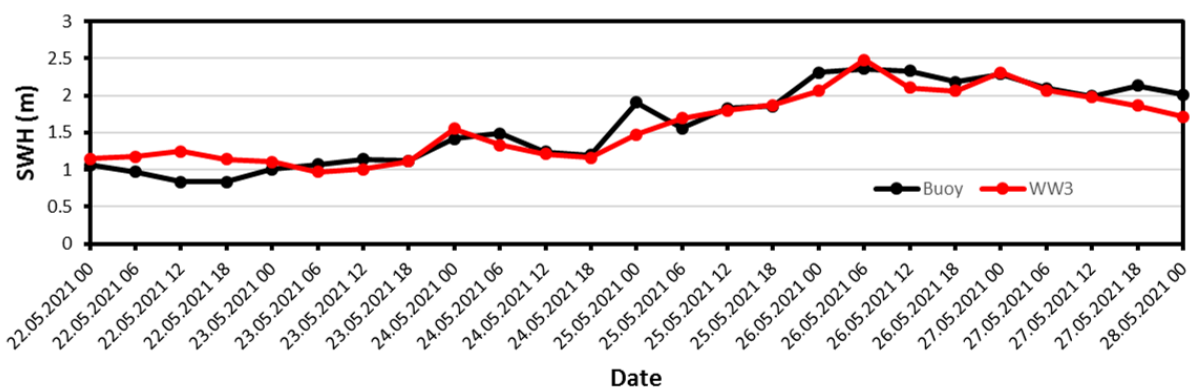


Figure 2.12: Time-series comparison of WW3 analysis SWH vs wave rider buoy observation during Yaas.

WW3 forecasted SWH initialised from 25th May 2021 is shown in Fig. 2.13. 6th hour forecast valid for 25th May 2021, 06 UTC showed a maximum SWH of about 9.2m in the northern part of Bay of Bengal (Fig. 2.13a). It is further increased to ~10.5m by 12 UTC (Fig. 2.13b) and then to ~11.5m by 18 UTC (Fig. 2.13c). During the landfall of cyclone, predicted wave height along the offshore region reached up to ~7.5m and near the coast of Odisha, it was around 2.5m (Fig. 2.13d).

Model forecasted SWH initialised from 23rd, 24th and 25th May is compared with the wave rider buoy observation at Visakhapatnam (Fig. 2.14). At this location, forecasts initialised from all the three days' initial conditions match reasonably well with the observed wave height pattern. However, the updated forecast from 25th May is slightly better most of the time, as compared to previous day's forecasts. For example, the maximum SWH observed (2.36m) during the landfall of cyclone (06 UTC of 26th May 2021) was closely predicted by the model initialised from 25th May (30th hour forecast). It indicates that the prediction with 1 –day lead time is better in such extremes.

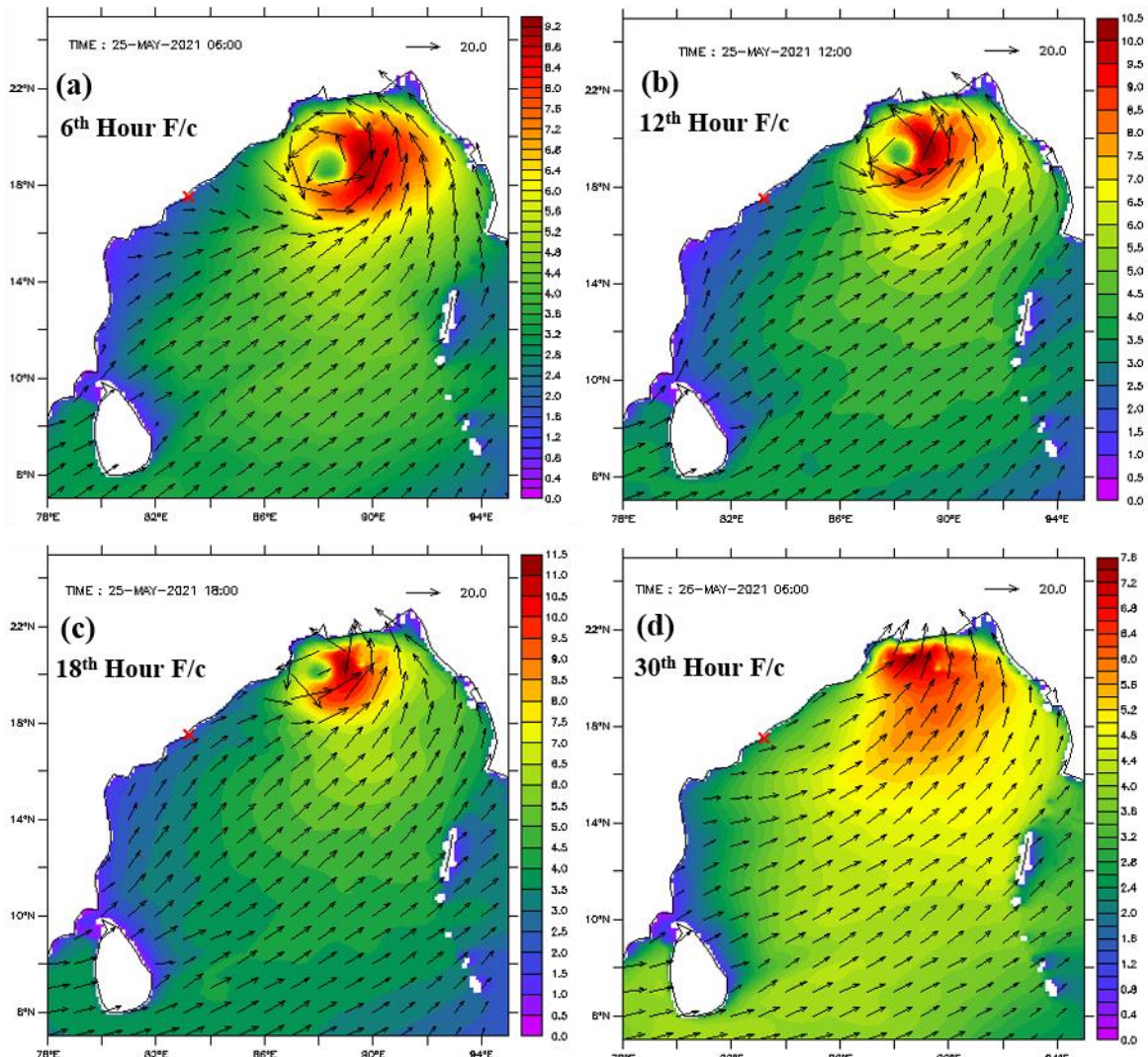


Figure 2.13: WW3 forecasted SWH (m) and forcing wind vectors initialised from 25th May 2021. The red cross mark indicates the location of wave rider buoy at Visakhapatnam.

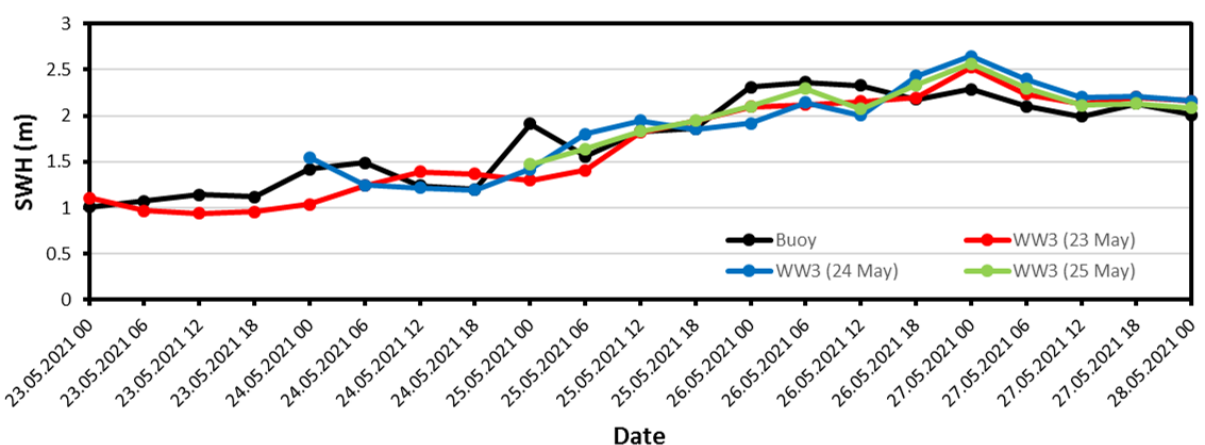


Figure 2.14: Time-series comparison of WW3 forecasted SWH for different initial conditions with wave rider buoy observation at Visakhapatnam.

2.4 Conclusions

In this report, cyclone ‘Yaas’ induced sea surface cooling is studied using INSAT 3D and GHRSST data. Satellite observations clearly show that the central Bay of Bengal had a high temperature (+1.2 °C) and TCHP anomaly (~ 60kJ/cm²) in the central BoB, just before the formation of cyclone. These conditions were conducive for cyclogenesis. After the passage of cyclone, large scale changes in SST, SSS and surface density were seen in the BoB. Surface cooling of around 2.25 °C was observed post cyclone and this mainly contributed to the surface density changes.

The current chapter also provided the details about various forecasts available from the operational models at SAC during ‘Yaas’. The storm surge forecast above astronomical tide during the landfall of ‘Yaas’ was ~4m, near Contai and Sagar Island region. The coastal inundation forecast generated on 24th May showed inundation of around 3.8km near Sutahata (Haldia), 4.5km near Kumbhigari, 1km near Bakkhali and around 2.5km near several places in Sundarban area. Similarly, extreme wave forecast during ‘Yaas’ cyclone was also generated routinely. Predicted wave height during the landfall of cyclone showed a maximum value of ~7.5m in the deep waters and ~2.5m near the Odisha coast. These forecasts were disseminated through MOSDAC.

References

1. Agarwal, N. et al., 2019. Geostationary satellite-based observations for ocean applications. *Current Science* (00113891), 117(3).
2. Dietrich, J. C., Westerink, J. J., Kennedy, A. B., Smith, J. M., Jensen, R. E., Zijlema, M., & Cobell, Z. (2011). Hurricane Gustav (2008) waves and storm surge: Hindcast, synoptic analysis, and validation in southern Louisiana. *Monthly Weather Review*, 139(8), 2488-2522.
3. Dietrich, J. C., Zijlema, M., Westerink, J. J., Holthuijsen, L. H., Dawson, C., Luettich Jr, R. A., & Stone, G. W. (2011). Modeling hurricane waves and storm surge using integrally-coupled, scalable computations. *Coastal Engineering*, 58(1), 45-65.
4. Gangwar, R.K. and Thapliyal, P.K., 2020. Variational based estimation of sea surface temperature from split-window observations of insat-3d/3dr imager. *Remote Sensing*, 12(19): 3142.
5. Luettich, R. A., & Westerink, J. J. (2004). Formulation and numerical implementation of the 2D/3D ADCIRC finite element model version 44. XX (p. 74). R. Luettich.

6. Mandal, A. K., Ramakrishnan, R., Pandey, S., Rao, A. D., & Kumar, P. (2020). An early warning system for inundation forecast due to a tropical cyclone along the east coast of India. *Natural Hazards*, 103, 2277-2293.
7. Mandal, A. K. and Ramakrishnan, R. (2019). Surge residual validation using INCOIS tide gauge data for past cyclones in the Bay of Bengal basin. SAC/EPSA/AOSG/SR/04/2019.
8. Price, J.F., 1981. Upper ocean response to a hurricane. *Journal of Physical Oceanography*, 11(2): 153-175.
9. Pudov, V., 1992. The ocean response to the cyclone's influence and its possible role in their track formation. ICSU/WMO international symposium on tropical cyclone disasters, p.^pp. 367-376.
10. Sadhuram, Y., 2004. Record decrease of sea surface temperature following the passage of a super cyclone over the bay of bengal. p.^pp.
11. Seemanth, M., and S.A. Bhowmick., 2018. Operational implementation of very high resolution data assimilative wave forecasting system for Indian ocean. Scientific report. SAC/EPSA/AOSG/SR/23/2018.
12. Walton, C., Pichel, W., Sapper, J. and May, D., 1998. The development and operational application of nonlinear algorithms for the measurement of sea surface temperatures with the noaa polar-orbiting environmental satellites. *Journal of Geophysical Research: Oceans*, 103(C12): 27999-28012.

3. Rainfall Estimation over Tropical Cyclone Yaas

Neerja Sharma and Atul Kumar Varma

3.1 Introduction

Rainfall structure of tropical cyclone (TC) is often complex and asymmetric in nature. Knowledge of its spatial and temporal variations can play a crucial role in understanding numerous facets of TC, which can be utilized significantly in disaster support decisions. Since surface rainfall observations are very sparse and limited to ground, rainfall products from satellites at high spatial and temporal resolutions can play vital role in this regard. Continuous monitoring of TC's rainfall is made possible from geostationary satellites, such as INSAT-3D/3DR using Infrared (IR) wavelength. Since rainfall measurements using IR band is not direct, it often suffers errors. These errors can be minimized by incorporating additional information of atmospheric parameters (e.g. relative humidity and total precipitable water) in the retrieval technique. Hydro-Estimator (H-E) is one of such rainfall retrieval technique from IR sensors which uses both satellite (brightness temperature) and model based (e.g. relative humidity, total precipitable water) inputs. Implementation of H-E rainfall retrieval technique on INSAT-3D IR observations is carried out by Varma and Gairola (2015). Since then technique is successfully providing rain estimates from INSAT-3D/3DR brightness temperature observations at $10.7\text{ }\mu\text{m}$ channel and products are operationally available on MOSDAC web portal of SAC, ISRO. Rain from INSAT-3D H-E is further validated and assimilated in WRF model for short-range weather forecasting, which showed a good improvement in the weather forecasting (Kumar and Varma, 2016). This technique is further applied to high-resolution IR observations from a polar orbiting satellite as a preparatory work for its operational implementation with Oceansat-3 SSTM observations (Sharma and Varma, 2020).

The main objective of this section is to show the usefulness and reliability of H-E rainfall products from INSAT-3D/3DR on very severe TC Yaas which formed in the Bay of Bengal and persisted from 21 May -28 May 2021. The section also provides validation statistics of H-E rain with surface rain gauges observations from Indian Meteorological Department (IMD) and other satellites products. In addition, a brief explanation of H-E rainfall retrieval technique is also provided.

3.2 H-E retrieval technique

The H-E method described herein is based on work by Kuligowaski (personal communication). In H-E method, convective and non-convective cores are identified, and different R-Tb relationships are provided for them. This allows higher precipitation rates for the convective cores. For convective core, rain (R_c) is given by,

$$R_c = a \exp(-bTb_{10.7}^{1.2}), \quad \dots\dots\dots(1)$$

Where, Tb_{10.7} is brightness temperature measured at 10.7 μm channel, and a and b are the regression coefficients which are precipitable water (PW) dependent. This makes the Tb versus R relationship dynamic in nature.

For a non-convective core, the relationship between Tb_{10.7} and R_n is given as:

$$R_n = (250 - Tb_{10.7}) * (R_{max}/5) \quad \dots\dots\dots(2)$$

R_{max} is again a function of PW. R_{max} is again PW dependent. R_n is not allowed to exceed - corresponding convective rain rate (R_c).

In H-E method, the precipitation at a pixel is allowed to be combination of both convective and non-convective core. This is worked out by considering a pixel box of 101X101 pixels surrounding the pixel of interest. The Z score at each pixel is determined as,

$$Z = (T_{mean} - Tb_{10.7}) / \sigma \quad \dots\dots\dots(3)$$

The maximum allowable value of Z is 1.5.

If Z < 0; R = 0, i.e., pixel either cirrus or inactive convective

$$\text{Otherwise, } RR = [R_c * Z^2 + R_n * (1.5 - Z)^2] / [Z^2 + (1.5 - Z)^2] \quad \dots\dots\dots(3)$$

R_c is the rain from the convective core given by (1) with coefficients determined by PW from NWP model. R_n is rain from non-convective core given by (2). If Z=1.5, the pixel rain rate RR reduces to convective type only (given by (1)). On the other hand, if Z=0, the pixel rain rate RR is determined by purely non-convective rain (given by (2)).

The (3) above provides the first guess precipitation amounts. The precipitation thus estimated is further modified to account for the wetness/dryness of the atmosphere and for the precipitation that comes from the warm clouds. The several steps involved for such modifications are as follows:

(a) Correction for Wet/dry Environment

A small correction in the brightness temperature (Tb_{10.7}) values is carried out to account for wetness of the environment. This adjustment is needed to account for evaporation of the precipitation in the dryer environment below the cloud.

(b) Warm-top modification

The equilibrium level is computed by following a parcel along a saturation adiabat upward (from lifting condensation level) to where the parcel temperature becomes equal to the environmental temperature. Strength of the convection is determined by comparing the temperatures of the convective tops with that of equilibrium level. This level comes before tropopause for the warm rain.

In H-E method, NCEP model derived temperature and relative humidity profiles are used in a atmospheric thermodynamic model to determine equilibrium temperature at a particulate pixel. This correction is applied to pixels that are warmer than the equilibrium level temperature.

- If the $(T_{eq} - T_{min}) < 10 \text{ K}$, then T_{min} in the pixel-area is used instead of $Tb_{10.7}$ of the pixel for warm top correction. The modification is as follows:

$$Tb_{10.7} - [(213 - T_{eq}) * 0.9] \text{ or } 25 \text{ K (whichever less)}$$

- If the $(T_{eq} - T_{min}) > 10 \text{ K}$, the modification is as follows

$$Tb_{10.7} - [(213 - T_{eq}) * 0.6] \text{ or } 15 \text{ K (whichever less)}$$

(c) Orography correction

Orography adjustment is carried out using 850 hPa Winds and topography from a digital elevation model at 4 km resolution (Vicente et al., 2002).

3.3 H-E rain during Tropical cyclone Yaas

TC Yaas was declared as tropical depression on 23rd May 2021. Fig. 3.1a shows spatial distribution of rainfall associated with TC Yaas on 23rd May 2021 at 0859 UTC. Widespread rainfall over Bay of Bengal is observed due to formation of tropical depression. On 24th May developed tropical depression strengthen its intensity and achieved a category of severe cyclone. Fig. 3.1b shows H-E rain on 24th May 2021 at 0300UTC. Compared to previous day, rainfall is more intense and occupied larger area of Bay. On 25th May TC further moved towards north eastern coast of India and gained its intensity to very severe cyclonic stage at 1200 UTC. H-E well captured intense rain and structure of TC on 25th May 2021 at 1830 UTC (Fig. 3.1c). Yaas maintained its intensity and remained in very severe cyclonic stage on 26th May also and made landfall on same day. Intensified rain on 26 May at 0930 UTC is shown in Fig. 3.1d. H-E rain fairly demonstrated intense rainfall during landfall. TC further moved deep inside the coast but with weaker intensity on 27th May. It wetted almost entire state of Odisha, Jharkhand and West Bengal. Spatial distribution of H-E rain over land regions on 27th May at 1200 UTC is shown in Fig. 3.1e.

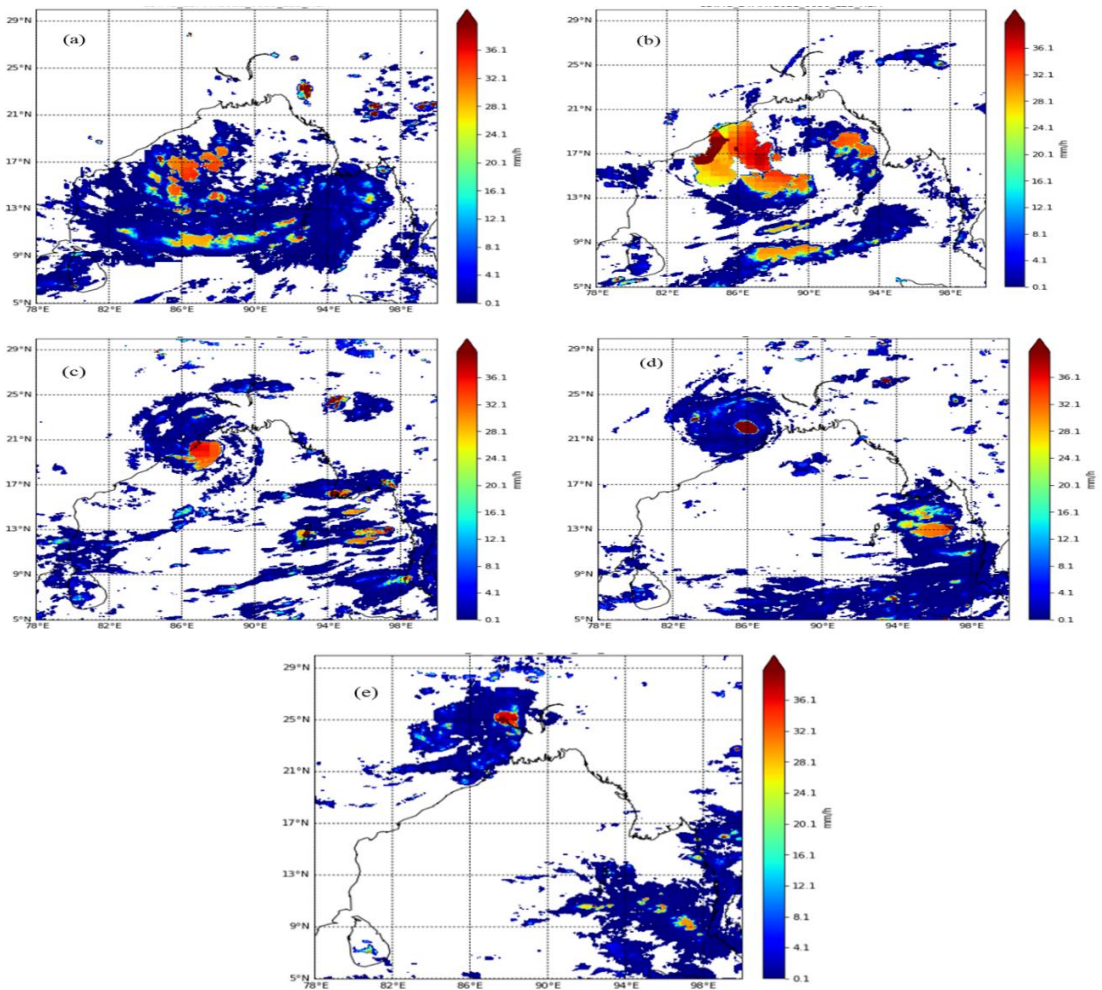


Figure 3.1: Spatial distribution of H-E rain from INSAT-3D on (a) 23rd May 2021 at 0859UTC, (b) 24th May 2021 at 0300 UTC, (c) 25th May 2021 at 1830UTC, (d) 26th May 2021 at 0930UTC and (e) 27th May 2021 at 1200 UTC.

3.3.1 Validation of H-E rain estimates

Validation of H-E rain from INSAT-3D during TC Yaas is carried out using rainfall data from two sources (surface rain gauges and satellites products).

A. Satellites products:

Fig. 3.2a, 3.2b and 3.2c. show spatial distribution of rain from H-E INSAT-3D, H-E NOAA and Integrated Multi-satellitE Retrieval for GPM (GPM-IMERG) on 25th May 2021 at 0700 UTC. Rainfall structure of H-E from INSAT-3D is well matched with the H-E NOAA and GPM-IMERG. High and low rainfall regions recorded by H-E INSAT-3D are coincide well with other two satellite products.

To compare H-E rain from INSAT-3D with IMERG, H-E rain is gridded to ~10x10 km spatial grid resolution in domain of 12°N-24°N and 80°E-95°E. Statistical comparison of hourly rain products from INSAT-3D H-E and GPM-IMERG from 25th to 26th May 2021 is shown in Table

3.1. The comparison shows a root mean square error (RMSE) of 3.41 mm/hr, R of 0.51 and bias of 0.32. Since IMERG final run products are not available analysis uses IMERG late run products where surface observations data is not blended. The statistics may further improve when generated with the IMERG final run products. As it is evident from Fig. 1 that expected intense rain in the eyewall region of cyclone is found missing in IMERG product.

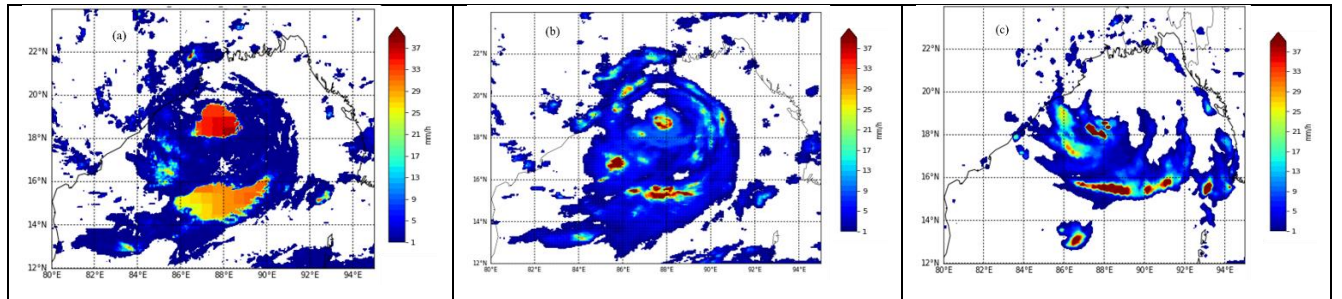


Figure 3.2: Spatial distribution of (a) H-E rain from INSAT-3D, (b) H-E NOAA and (c) GPM-IMERG on 25 May 2021 at 0700 UTC.

Table 3.1 Hourly statistics of H-E rain compared with GPM-IMERG during 25-26 May 2021.

RMSE (mm/hr)	Correlation	Bias
3.41	0.51	0.32

B. IMD surface rain gauges observations:

H-E is further compared with the surface rain gauge observations over Odisha, Jharkhand and Gangetic West Bengal meteorological subdivisions of India. Spatial distribution of district-averaged daily H-E rain over these subdivisions due to TC Yass is shown in the Fig. 3.3 (a), (b) and (c) for May 25, 26 and 27, respectively. Corresponding rain distribution recorded by surface observations is shown in Fig. 3.3 (d), (e) and (f). The figure shows a good trend in the distribution of rainfall over these states. Within these meteorological subdivisions, there are data void areas in the surface observations, which indicates missing or erroneous observations. Surface observations are just few measurements at certain point locations but continuous; on the other hand, H-E rain is a really-averaged instantaneously available with the sampling every 30 minutes.

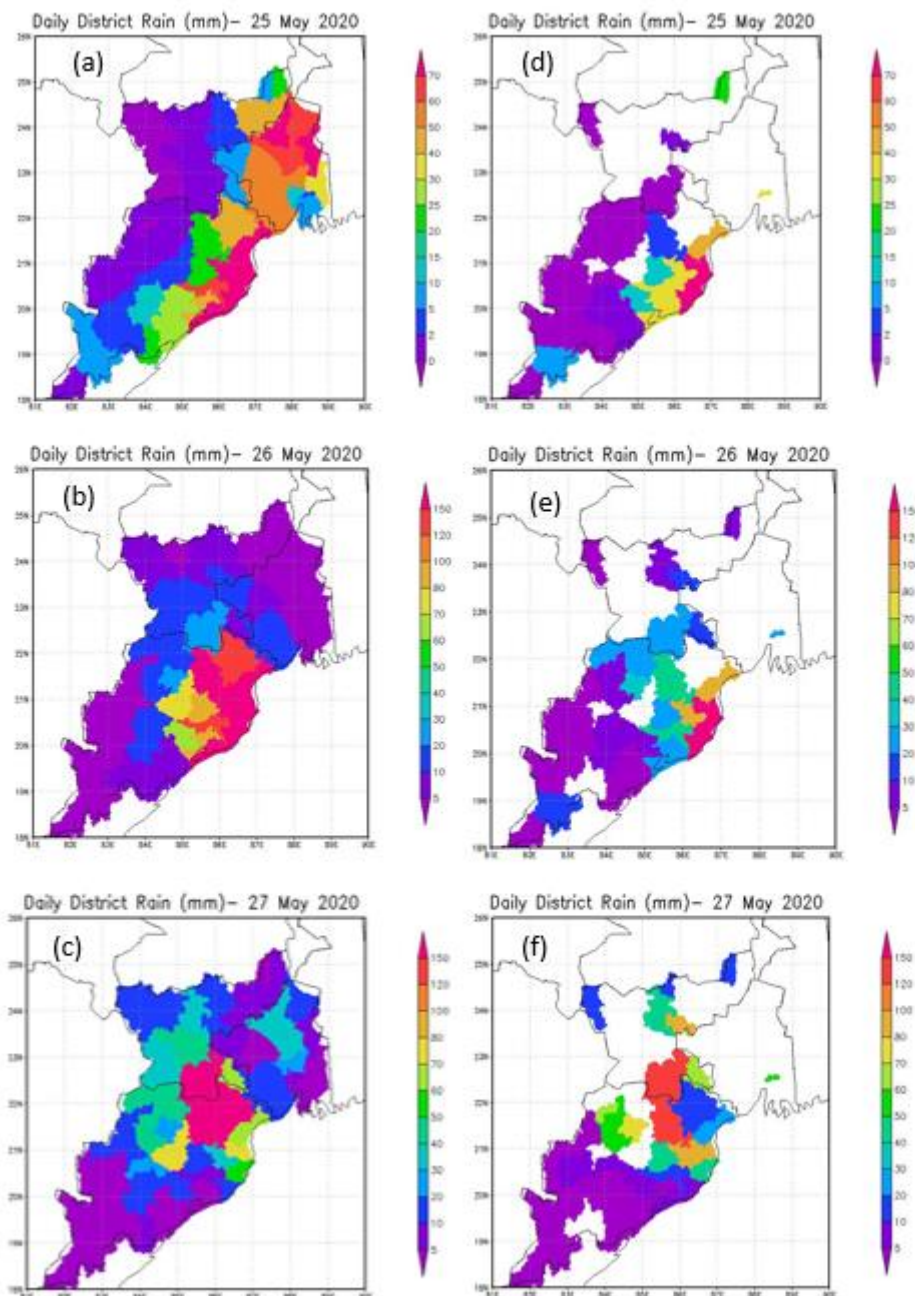


Figure 3.3: Distribution of district averaged daily rain (mm) for 25, 26 and 27 May 2021 associated with Yaas cyclone from INSAT-3D Hydro-Estimator (Left panels: Fig. (a), (b) and (c)) and Surface observations from IMD (Right panels: Fig. (d), (e) and (f)).

Table 3.2: Daily H-E rain from INSAT-3D over Odisha, Jharkhand and West Bengal during 21-28 May 2021.

	22May	23May	24May	25May	26May	27May	28May
Jharkhand							
BOKARO	4.3/9.7			1.5/14	19.26/190.3	86.6/103.4	38.6/54.4
DEOGHAR	4.7/7			8.7/14.8	5.6/168.7	7.8/1.8	7.0/17.4
DHANBAD	8.8/11			11.4/27.9	5.6/243	29.1/63.2	8/105.2
DUMKA	16.5/49.9			10.6/52.7	7.8/86	37.76/5.36	14.4/0.88
GARHWA						16.8/86.4	38.2/24.4
GIRIDIH	11.1/7.1				4.6/145.9	23.2/16.2	17.2/92.5
GODDA				23.3/11.6	7.6/19.9	12.0/4.8	38.4/63.2
GUMLA	2.7/88.3					37.3/232	6.9/34.2
HAZARIBAG	23.4/8.9					49.9/63.2	55.8/9.5
KODARMA)	1.6/17.3				7.7/112.2	13.2/14.3	62.4/1.53
LOHARDAGA					24.9/169	108.4/248.6	54.8/18.3
PAKAUR					7.2/0.19	26.4/3.9	
PALAMU)	0.7/49.6			1.4/81.7	6.2/144	56.2/147	40.1/35.5
PASHCHIMI-SINGHBHUM	50.1/28.8					139.2/344.4	10.1/61.7
PURBI-SINGHBHUM	9.9/28.3			7.4/4.8	19.1/120	67.3/303.2	8.9/1.6
RANCHI	19.4/45.9				11.9/293	91.3/272	24.9/17.4
SAHIBGANJ	22.4/119.1			10.4/3.3	3.2/6.5	30.2/7.8	228.6/29.5
ODISHA							
MAYURBHANJ	2.8/49	2.8/16.3		20.3/10.5	74.9/53.5	98.4/308.9	2.4/27
SUNDARGARH	17.8/97.2				24.9/84.5	98.5/205.5	13.3/20.5
SAMBALPUR	0.4/112.4				7.2/19.2	51.9/323.1	8.3/23.8
KEMNDUJHAR	10.7/63.9	2.0/33.4		3.5/44.5	47.5/29.8	144.9/198.8	5.0/32.3
JHARSUGUDA					8.5/6.4	67.3/325.3	8.7/39.4
BALESHWAR		11.2/15.5	0.03/7.6	43.8/6.4	90.3/13.1	22.8/223.2	
BARGARH	2.0/50.7				0.7/54.4	4.6/138.6	0.6/102.3
DEBAGARH	10.7/141				34.7/64.7	72.2/202.7	5.4/5.9
ANUGUL	9.2/66.6	0.8/17.8		4.3/20.4	23.5/36.5	40.1/110.3	3.0/7.6
BHADRAK				90/10.5	160/5	60.0/186.1	
DHENKANAL	4.0/44.8	11.1/31.1		14.1/82.1	25.3/19.8	46.4/13.5	0.7/9.9
JAJAPUR	0.2/51	0.7/46.8		36.1/38.8	100.3/5.3	79.3/69.9	0.3/7.1
SONPUR	0.2/63				2.3/10.2	3.5/193.3	0.4/40.4
BALANGIR	1.0/23				1.3/59.2	7.9/33	
BAUD	15.2/49.4				5.9/11.1	9.1/141.8	0.7/133.4
KENDRAPARA							1.0/16.5
CUTTACK	18.3/34.7	3.5/45.2		35.2/70.5	49.7/18.9	17.2/11	
KANDHAMAL	4.8/40.1			0.8/55.4	9.0/9.4	2.5/41.9	
NAYAAGARH	6.3/17.2	3/97.6		11.4/34.1	5.5/35.3	7.1/19.2	
KALAHANDI	6.0/22						
JAGATSINGHAPUR	5.9/10.5			44.9/87	95.5/10.7	13.0/8	1.5/16.6

KHORDHA	15.3/44	4.4/94.1		38.2/32.2	23.8/46.1	4.0/6.9	
GANJAM	1.1/47.2	2.9/167		0.4/21.7	2.3/30.2		
PURI	11.2/17.5			40.6/47.6	36.0/76.3	4.0/9.1	1.3/11.5
RAYAGADA	0.6/44.3						
GAJAPATI	9.2/70.5	10.1/89.8			0.1/7.2		
KORAPUT	8.2/19.1	5.8/36.4		7.7/22.4	12.4/18.9	1.4/3.7	
MALKANGIRI	7.8/11.9	16.2/45.9					
West Bengal							
MURSHIDABAD			27.7/15.1	27.7/7.6	3.5/68.8	24.5/4.2	40.7/29.9
BIRBHUM	4.3/42.1		30.3/12.8	30.3/15.1	9.8/67.1	36.4/37.7	19.3/61.8
NADIA			25.9/9.4	25.9/12.2	10.8/90.1	12.1/4	89.9/20.2
BARDDHAMAN	1.6/10.1	3.2/32.9	20.5/18.8	20.5/37.1	9.3/101.1	33.3/49.9	6.5/28.8
PURULIYA	13.5/25		6.9/33.1	6.9/9.9	6.8/211.3	37.4/121.5	3.1/52.1
BANKURA	16.0/22.3		0.3/40.6	0.3/8.3	12.4/137.1	78.7/74.9	2.2/20
HUGLI			14.8/21.4	14.8/55.4	15.6/144.7	60.6/81.4	67/9
MEDINIPUR	15.1/33.7		11.4/16.3	11.4/5.4	25.9/118.6	25.1/224.2	

To understand severity of rainfall that badly affected these three states, district-wise daily average value of H-E rain is calculated from 22 May to 28 May. Table 3.2 provides daily average rainfall from IMD and INSAT-3D H-E over the different districts of Jharkhand, Odisha and West Bengal.

Scatter between daily rain estimates from H-E and IMD stations of three states (Jharkhand, Odisha and West Bengal) from 21st May to 28th May 2021 is shown in Fig. 3.4. H-E found close agreement with IMD rain having R value of 0.45, RMSE of 40.5 mm/day and bias of 33.2 mm/day. Noteworthy, IMD rain gauges is a point measurement and not equally distributed in districts. Whereas, INSAT-3D rain product is an area average value.

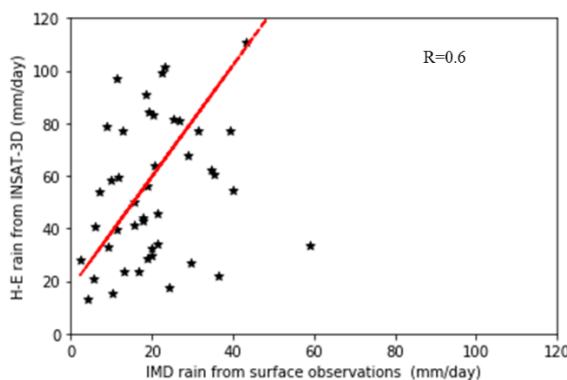


Figure 3.4: Scatter between rain estimates from IMD surface observations and INSAT-3D HE during 22May -28May 2021.

3.4 Conclusion

Present section of report provides a detail overview of H-E rainfall recorded by INSAT-3D satellite during TC Yass which formed in Bay of Bengal during 21-28 May 2021. H-E well

captured TC rain structure from genesis to dissipation. H-E recorded high-intensified rain on 25th and 26th May 2021, when TC reached to a category of very severe cyclonic storm. In addition, calm and warm TC eye successfully identified by rain structure with surrounded rain bands clearly distinguishable. H-E very clearly captured widely distributed rain occurred during landfall. Validation of H-E rain with surface based rain gauge observations over three states (Odisha, Jharkhand and West Bengal) is also presented here. Spatial distribution of H-E rain well matched with the surface observations. Further, comparison of H-E INSAT-3D rain products with GMP-IMERG and H-E NOAA products are also demonstrated. The shortcomings of other rain products, surface rain (point measurements with few observatories) and GPM IMERG (missing rain associated with eyewall region) discussed. Results infer that H-E rain estimates from INSAT-3D are in reasonably good agreement with other rain products.

References

1. Kumar P and A K Varma, Assimilation of INSAT-3D Hydro-Estimator Method Retrieved Rainfall on Short Range Weather Prediction, Quarterly Journal of Royal Meteorological Society, **143**: 384-394, DOI:10.1002/qj.2929, 2016.
2. Varma, A.K., R.M. Gairola, 2015, Algorithm Theoretical Basis Document Hydro-Estimator (Modified). SAC/EPSA/AOSG/SR/04/2015.
3. Vicente, G. A., J. C. Davenport, and R. A. Scofield, 2002, The role of orographic and Parallax corrections on real time high resolution satellite rainfall estimation. Int. J. Remote Sens., 23, 221-230.
4. Sharma, N., and A K Varma, 2020, Preparation of Rain Retrieval Technique for upcoming SSTM onboard OCEANSAT-3: Modified Hydro-Estimator, SAC/EPSA/AOSG/GRD/SR-37/2020, p 9.

4. Assessment of surface inundation and changes in water turbidity associated with Cyclone Yaas

Shard Chander, Amit K. Dubey, Vibhuti B. Jha, Rohit Pradhan,

Nimisha Singh and R.P. Singh

4.1 Introduction

Cyclone induced flash floods influence many low-lying areas in the coastal regions and changes the turbidity of the wetlands. Rise in sea levels, extreme groundwater withdrawal rates, land surface deformation, land use and land cover have further intensified the impact and extent of inundation following land falling tropical cyclones. Floods are temporary or permanent inundation of surface with or without vegetation canopy and can occupy vast expanses, causing widespread economic and sometimes loss of lives. Cyclones bring high intensity of rainfall with short duration and landmass with low to mild slope is also remain vulnerable to flooding. Rivers get swollen due to incessant rain under the influence of cyclone and turbidity of these inland water bodies changes due to inflow of nutrient loaded water from surrounding landmass. Remote sensing techniques are an effective source of information to understand various hydrological aspects related with cyclone induced flooding and so can be effectively used to map inundated areas with sufficient temporal and spatial resolution. Space borne measurements of terrestrial surface water have unique features, which can address some pivotal questions, which the in situ measurements find hard to answer.

Recently two major cyclones hit the country within a time span of fortnight. Cyclone Yaas that originates in Bay of Bengal has left behind a trail of disturbance in the East coast of India after Cyclone Tauktae that created havoc on the west Coast of India. Cyclone Yaas has formed in the North Bay of Bengal and shortly landfall to the East coast of India. Severe Cyclonic Storm Yaas made landfall south of Balasore in the Odisha state on 26 May 2021 and brought a high amount of rainfall that affected the many parts of Odisha, West Bengal and Bihar. Effect of cyclone was observed all the way up to Jharkhand, Bihar and Eastern parts of Uttar Pradesh (Fig. 4.1). Patna and its adjoining districts in Bihar also saw flooding due to heavy rains that continued to batter the region on 26-27 May 2021. Accumulated rainfall showed a high amount (> 300 mm) of precipitation received at the landfall location in Odisha during the period of 23 May 2021 to 28 May 2021.

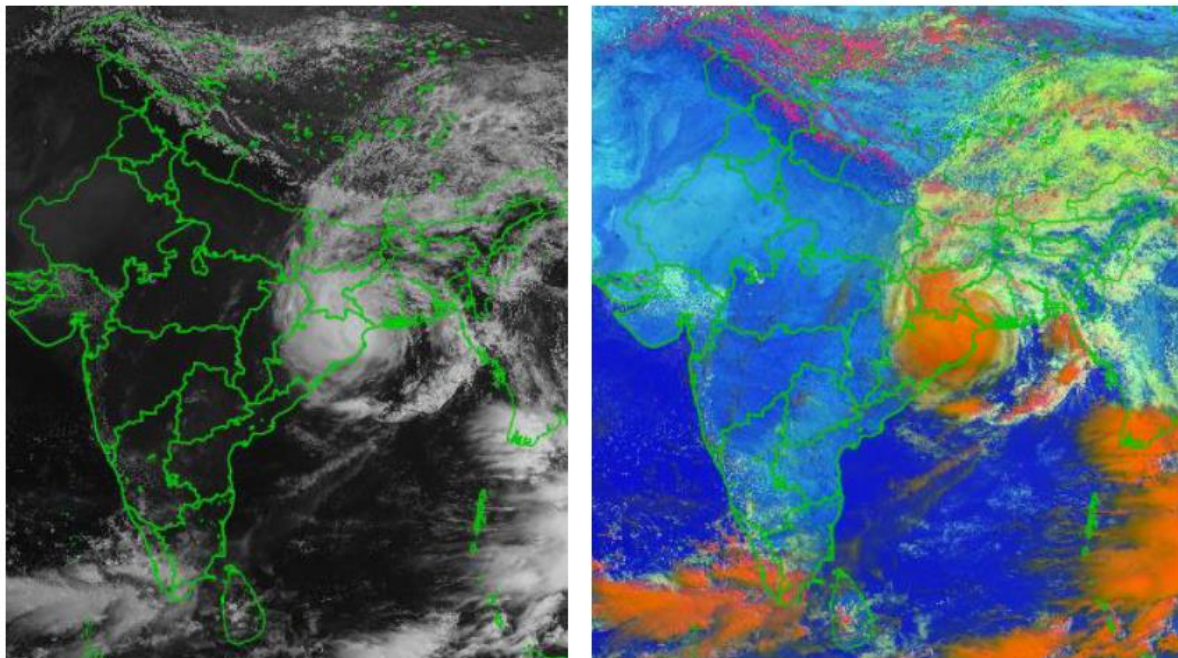


Figure 4.1: INSAT-3D Visible with Cloud Microphysics during landfall of TC Yaas on 26 May 2021

4.2 Data Used

Surface inundation was estimated using synthetic aperture radar Sentinel-1 and Advanced Microwave Scanning Radiometer AMSR-2 dataset. Optical dataset of Sentinel-2 was analysed to understand the changes in the turbidity of the nearby rivers and lakes.

Table 4.1: Dataset used to carry out assessment of Cyclone Yaas

Satellite	Sensor	Spatial Resolution	Temporal Resolution
Sentinel-1	Microwave Synthetic aperture radar- C band	10 m	12 days (6 days for Sentinel 1A and 1B)
AMSR-2	Passive Microwave Radiometer	0.1 degree	1-2 days
Sentinel-2	Optical Multispectral 12 bands (440-2200 nm)	10 m 20 m 60 m	10 days (5 days for Sentinel 2A and 2B)

4.3 Analysis of Cyclone Induced Flooding using Hydrological Modelling

Cyclones bring high intensity of rainfall with short duration and it generates instantaneous flooding conditions at low lying regions of coastal areas. Landmass with low to mild slope is also remain vulnerable to flooding due to high intensity of rainfall. These characteristics of cyclones are utilized here to derived flood inundation probability by making use of in-house developed SACHYDRO hydrological model. This model is a deterministic, distributed and unsteady flow model that simulates the hydrological fluxes at regional scale (5x5 km grid). The model takes care of several hydrological processes such as infiltration, surface runoff, evapotranspiration, runoff routing and snow melt runoff within the catchment. To solve different hydrological processes in these modules, different data set such as meteorological parameters from weather models and remote sensing data products for land surface variables are taken. Energy budget component of the model is solved using Weather Research and Forecasting (WRF) simulated fluxes. To perform hydrological simulations meteorological parameters such as temperature, wind speed, relative humidity and radiation fluxes are extracted from WRF forecast. WRF forecast of 24 hr were considered for the data set preparations with spatial resolution of 5 Km. Rainfall and Snow cover was taken from satellite derived product interpolated into model grid. Surface runoff is scaled to 0 to 1 based on amount of surface runoff and topography slope is also converted into 0 to 1 scale. By combining these two variables flood inundation probability is derived for cyclone induced flooding.

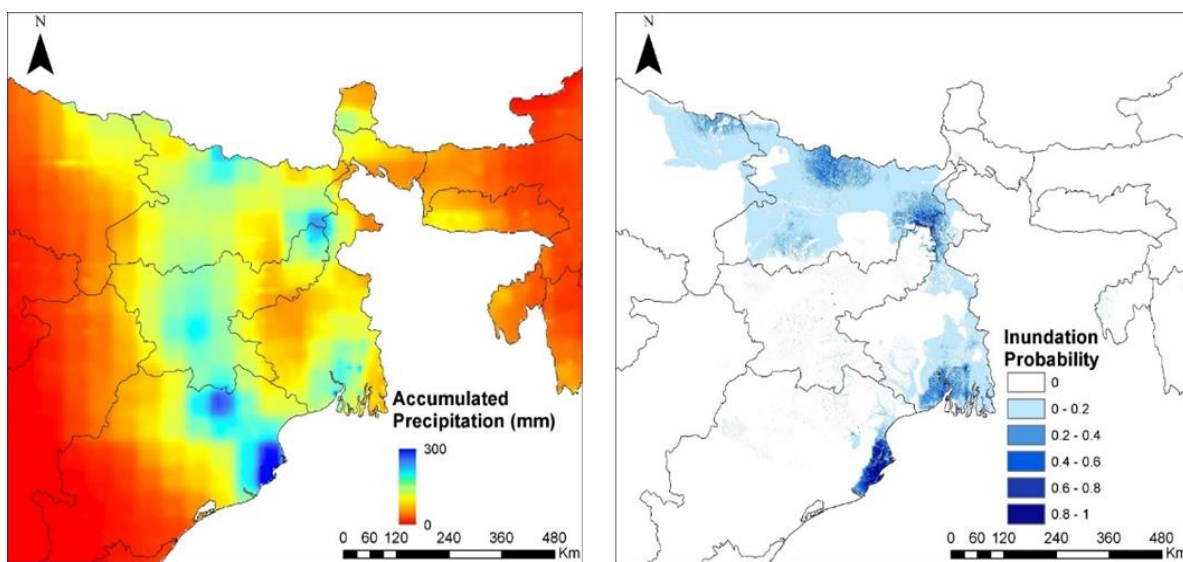


Figure 4.2: Cumulative precipitation and Inundation probability during TC Yaas (23-28 May 2021)

Very Severe Cyclonic Storm Yaas made landfall south of Balasore in the Odisha state and brought high amount of rainfall which affected the many parts of Odisha, West Bengal and Bihar. Hydrological modelling of Yaas cyclone was carried out to identify the high flood prone region. Accumulated rainfall showing high amount (> 300 mm) of precipitation received at the landfall location in Odisha during the period of 23 May 2021 to 28 May 2021. Large region of Jharkhand, West Bengal and Bihar also received the 100-150 mm of cumulative rainfall during this period. Many parts in these regions got inundation due to high intensity of rainfall. High amount of precipitation was observed at the Landfall location in Odisha state as highlighted by the satellite rainfall, which generated high inundation probability for the region (Fig. 4.2). Low-lying regions of Odisha and West Bengal found to be prone to Cyclonic floods and Cyclone Yaas affected these regions during the period of 23-28 May 2021.

4.3 Surface Inundation mapping using SAR

Synthetic Aperture Radars like RISAT, Sentinel-1 prove very useful in delineating inundated regions during cyclones and floods. SAR sensors emit electromagnetic pulses in the microwave region and receive the signal returned from the surface, termed as backscatter, in the form of amplitude and phase. The backscatter signal from a surface depends on the sensor parameters (wavelength and polarisation) and other parameters like dielectric constant, the geometry of the target, and surface roughness. The flooded regions appear dark with varying shades depending on the underlying heterogeneity and wind conditions. So the general idea is to find low backscatter regions in the SAR image which generally act as specular reflectors thus appearing as dark areas. Inundation after Cyclone Yaas in the Eastern Coast of India is shown in Fig. 4.3. Sentinel-1, C band SAR has been used to map inundation regions at a 10 m resolution.

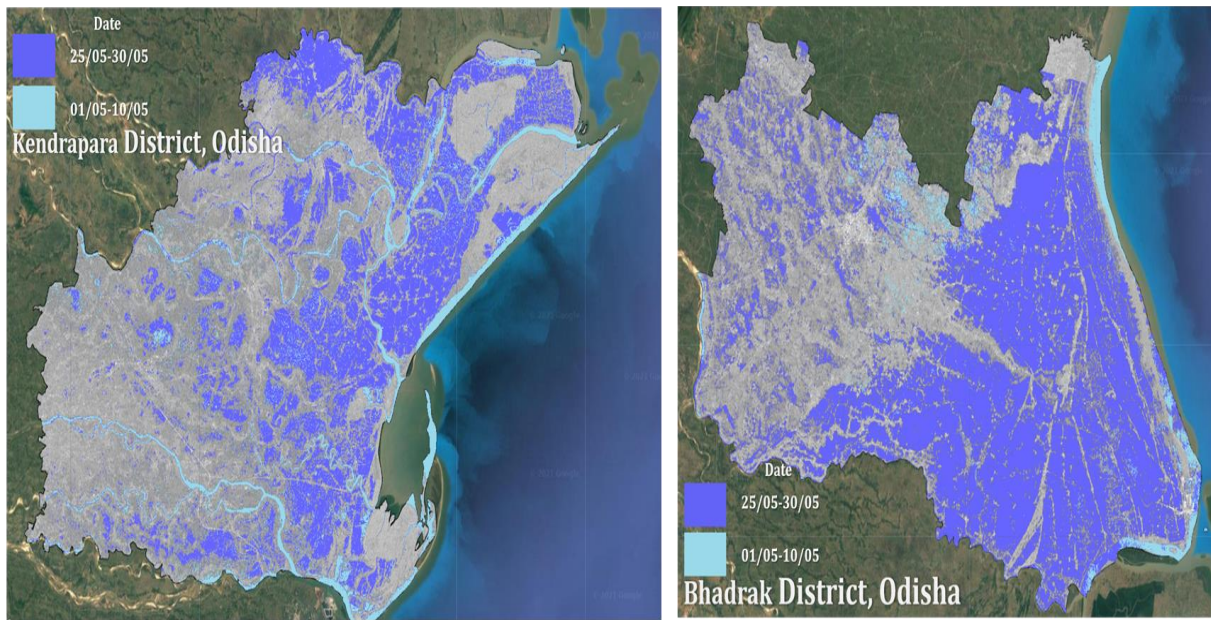


Figure 4.3: Inundation after Cyclone Yaas in the Kendrapara district, Odisha and Bhadrak district, Odisha using Sentinel-1 C band 10 m spatial resolution dataset

The regional threshold was determined based on the histogram backscatter values to delineate the still water surface and quasi inundated areas. Generally, the backscattering value for flooded regions is below -14 dB, the precise value of which can be found using various image segmentation techniques. Heavy flooding was observed in the coastal districts of Orissa. For cyclone Yaas, we have done the delineation exercise for the districts of Bhadrak, Kendrapara, Baleshwar, Jagatsinghpur and Purba Medinipur. The post cyclone flooding was carried out on datasets of the period 25th – 30th June for cyclone Yaas. District wise analysis of inundated surface area is shown in Table 4.2.

Table 4.2. Inundated area in affected districts after Cyclone Yaas

District	Inundated Area Post Cyclone (sq.km)	Percentage of total area
Bhadrak	1280	52 %
Kendrapara	933	38 %
Baleshwar	413	11 %
Purba Medinipur	530	13 %

4.5 Surface Inundation mapping using Microwave Radiometry

Microwave indices obtained from multi-frequency radiometry have been used in detecting characteristics of land and water surfaces (Paloscia et al., 2018). Brightness Temperature

Polarization Ratio (PR), also known as Microwave Polarisation Difference Index (MPDI), at a particular frequency is one such index that is used to study soil moisture, surface inundation and vegetation characteristics (Gupta et al., 2019; Njoku et al., 2003; Zheng et al., 2016) Generally, wet soil that has high soil moisture is associated with high dielectric constant and lower emissivity. Hence High soil moisture reduces the brightness temperature. This principle is used to derive surface inundation during cyclones and floods. Further to improve the temporal period of the analysis radiometry brightness temperature (BT) difference at 36 GHz from Advanced Microwave Scanning Radiometer (AMSR2) at 0.1-degree spatial resolution was utilized for estimating the inundated areas at a much finer temporal resolution. This frequency is suitable to assess surface flooding and avoid signals due to wet soil. Although microwave radiometers have a coarse resolution, it provides repeat observations of the entire country with 1-2-day repetitivity, which makes it suitable for analysis of regional scale inundation from extreme events.

Long-term MDPI statistics (mean and standard deviation) was computed using AMSR-2 36 GHz Brightness temperature dataset. Water bodies and inundated regions show high value of MPDI. Desert regions and barren land too have high MPDI and these needs to be separated from the true flood signal using LULC maps and appropriate thresholds. Flood Index for pixels with MPDI in the range of 0.01 and 0.1 is computed on a linear scale of 0 to 1. Pixels with $\text{MPDI} < 0.01$ are represented as non-flooded. AMSR2 36GHz MPDI based flood index maps were generated for Cyclone Yaas during 27-28 May 2021. The BT difference and Surface flooding map (Fig. 4.4) using AMSR2 36 GHz MPDI clearly shows the affected regions of Orissa, Bihar, Jharkhand and West Bengal.

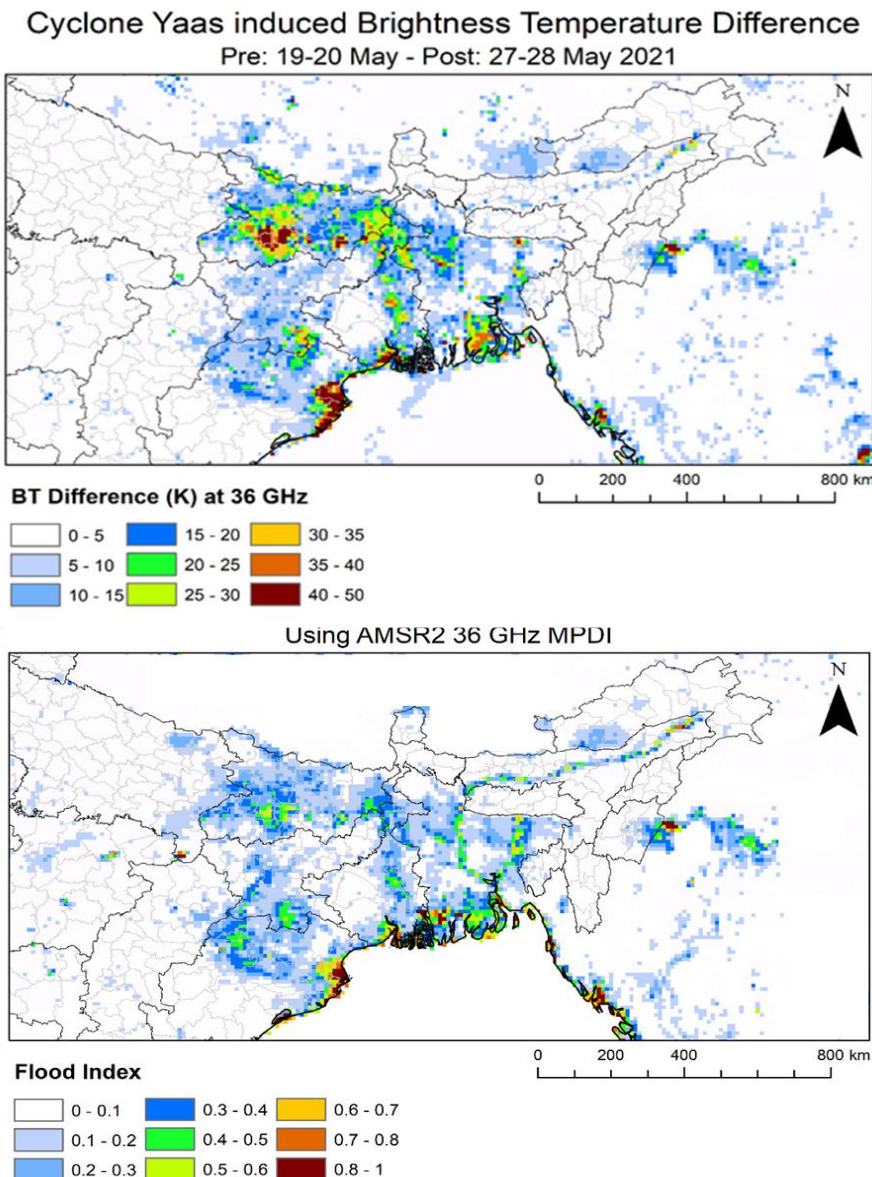


Figure 4.4: Surface flooding map after Cyclone Yaas using AMSR -2 36 GHz dataset

4.6 Impact assessment of Water Quality using optical dataset:

Extreme events like cyclones, floods, landslides are associated with changes in turbidity and water quality in coastal regions, wetlands, lakes, rivers and reservoirs. Historically datasets acquired by optical sensors have been widely used for natural hazard and disaster management. Algorithms based on reflectance's in the green and NIR bands can be utilized to map the water surfaces whereas reflectance's in the green and red bands are used for mapping of turbidity. However, these extreme events are usually associated with high cloud cover in which inundation mapping is difficult from optical datasets. In the present study, optical satellite datasets were used to understand these changes in turbidity levels during pre and post cyclonic event. Here, we look at the changes in the level of turbidity,

an important water quality parameter, through Sentinel-2 multispectral dataset. Cloud free images of 9 May (Pre cyclone) and 29 May (post cyclone) were analysed to understand the changes in the turbidity. Normalized difference turbidity index (NDTI) was used to estimate the spatial distribution of turbidity. Near Digha coast (Fig. 4.5) a high amount of river discharge at the ocean mouth was observed in comparison to pre cyclone time. The turbidity of the water was observed to be high due to sediments carried by the river.

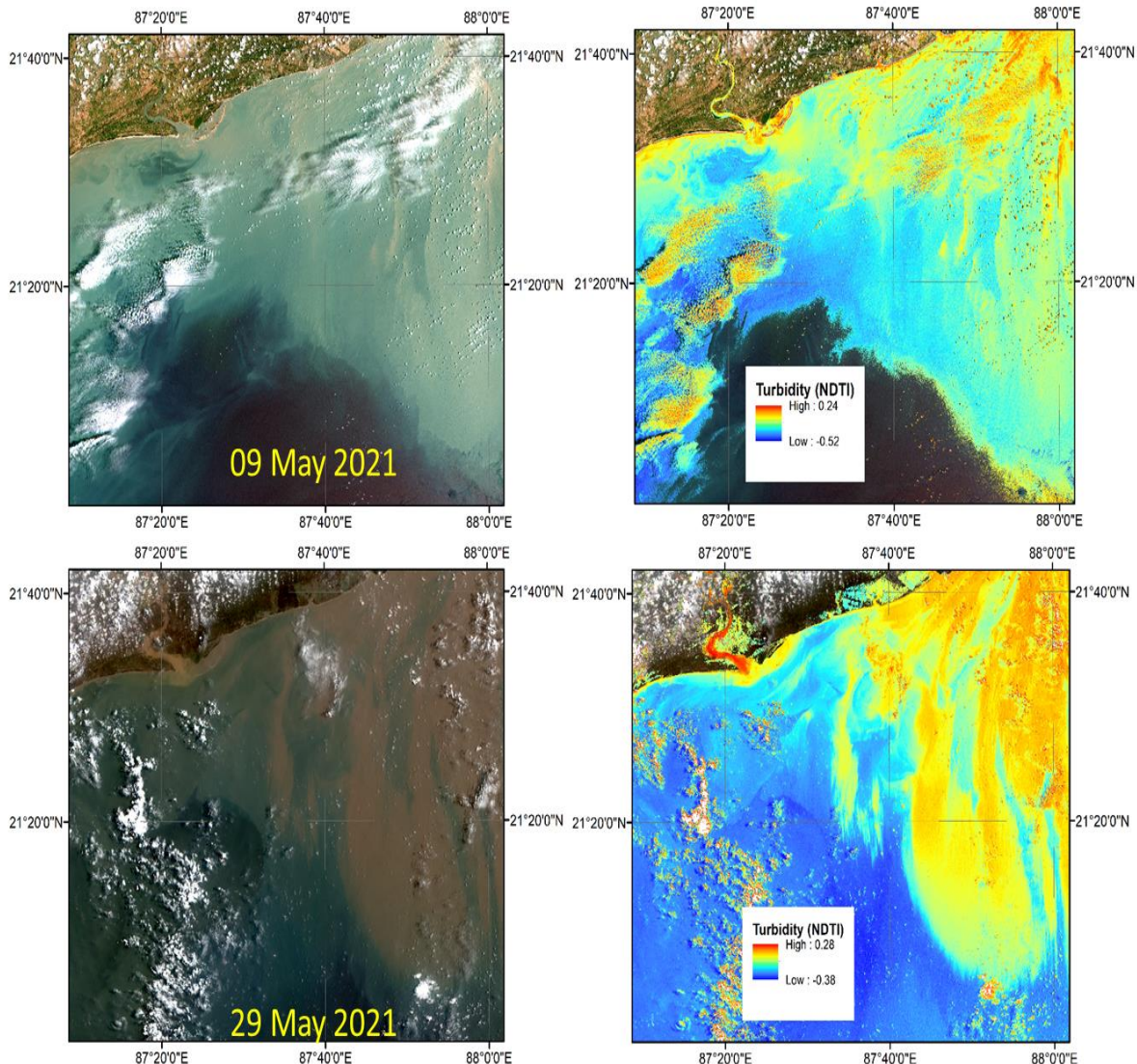


Figure 4.5: Natural colour composite and derived turbidity variation during pre and post cyclone at the East coast of India using Sentinel-2 multispectral dataset of 10 m spatial resolution

4.7 Conclusion

Heavy rain from Cyclone Yaas created flood like situation in the coastal districts of Orissa and West Bengal. Effect of Cyclone Yaas was observed all the way up to Jharkhand, Bihar and Eastern parts of Uttar Pradesh. Coastal districts of Orissa including Bhadrak, Kendrapara and Balasore saw heavy flooding due to Cyclone Yaas. Patna and its

adjoining districts in Bihar also saw flooding due to heavy rains from Cyclone Yaas that continued to batter the region on 26-27 May 2021. Various hydrological aspects were analysed with the help of remote sensing dataset. Better understanding of these hydrological aspects can further help to outline the susceptibility of different localities to potential floods based on analyses of the impacts from earlier events.

References

1. Paloscia, S., Pampaloni, P., and Santi, E. (2018). Radiometric Microwave Indices for Remote Sensing of Land Surfaces, *Remote Sens*, 10, 1859.
2. Njoku, E. G., et al. (2003). Soil moisture retrieval from AMSR-E, *IEEE Trans. Geosci. Remote Sens.*, 41, 215–229.
3. Gupta, P.K., Pradhan, R., Singh, R. P. and Misra, A. (2019). Scatterometry for land hydrology science and its applications. *Current Science*, 117(6), 1014-1021.
4. Zheng, W., Sun, D. and Li, S. (2016). Coastal flood monitoring based on AMSR-E data. *IEEE International Geoscience and Remote Sensing Symposium (IGARSS)*, Beijing, 4399-4401. DOI: 10.1109/IGARSS.2016.7730146.

5. Cyclone Yaas induced upwelling and changes in ocean biological productivity

Debojyoti Ganguly, R.K. Sarangi, N. Jaiganesh, Arvind Sahay

5.1 Introduction

Tropical cyclones are extreme weather events that can have profound influence on the marine ecosystem. The strong forcing of tropical cyclone produces two kinds of dynamic responses in the upper ocean, namely turbulent mixing and upwelling, both of which can induce a decrease of sea surface temperature (Pan et al. 2018). The wind stress and the rotating wind system can cause nutrients from below the mixed layer to be uplifted to the surface, a process called upwelling, thus enhancing the biological productivity. Upwelling, which is driven by the wind stress curl, is the most important process causing density changes in the thermocline through divergence of upper layer transport (Dickey et al. 1998). In this study, we investigate the impact of extremely severe cyclonic storm Yaas on the oceanic parameters like SST, Sea Level anomaly (SLA) and chlorophyll concentration.

5.2 Data Used

Parameters	satellite/data source	Scale/Product resolution	Source link
Chlorophyll concentration (Chl, mg m ⁻³)	ESA's GlobColor project – merged data – weighted average of MODIS AQUA, VIIRS and OLCI data (optical channels, 400-700 nm) Ocean Colour Monitor (OCM-2) Local Area Coverage data	Globcolor: Daily/8day – 4 Km OCM-2 : daily -360 m	https://hermes.acri.fr http://10.61.143.36:8080/SDIS_2.0/
Sea Surface Temperature (SST, °C)	Global High Resolution Surface temperature (GHRSSST)	Sea	Daily-4km http://apdrc.soest.hawaii.edu

Sea Level Anomaly (SLA, cm) and surface currents	AVISO product - processed data from all altimeter missions: Jason-3, Sentinel-3A, HY-2A, Saral/AltiKa, Cryosat-2, Jason-2, Jason-1, T/P, ENVISAT, GFO, ERS1/2	Daily – 25 Km	https://resources.marine.copernicus.eu/
Wind velocity(m/s) and direction	Advanced Scatterometer (ASCAT)	Daily-25km	http://apdrc.soest.hawaii.edu

5.3. Methodology

- Wind stress and Ekman suction velocity are computed on a daily basis from 17 May 2021 to 9 June 2021 using following equations:

$$\tau = \rho * C_d * W^2. \quad (1)$$

$$v = \frac{\nabla \times \tau}{\rho f}. \quad (2)$$

Where τ is the wind stress, ρ is the density of water and f is the Coriolis parameter, rho is the density of air taken as 1.25 kg/m³, W is the wind speed and C_d is the wind dependent drag coefficient given by (Sun et al. 2010).

$$C_d = (0.73 + 0.069W) * 10^{-3} \quad (3)$$

- Daily SST data from GHRSST is procured from the period 17 May 2021 to 9 June 2021 and 8-day composites generated for the 24-day period.
- 8-day composite images of chlorophyll are obtained from Globcolor multi-sensor merged products from 17 May 2021 to 9 June 2021. Single day OCM-2 Local Area Coverage (LAC) images from 17 May to 31 May are also obtained. OCM-2 data are processed for atmospheric correction and chlorophyll is obtained from remote sensing reflectance using OC2 algorithm (O'Reilly et al. 1998; O'Reilly et al. 2019).
- 8-day composites of sea level anomaly (SLA) and geostrophic current velocity components have been generated and current vectors overlaid on SLA data. Mesoscale eddies appear as rotating (clockwise or anticlockwise) vortices with depressed or

elevated sea surface heights. Eddies are detected using outermost closed contours of sea level anomalies using the methodology of Faghmous et al. (2015).

- Every 6-hour position of cyclone track point is obtained from Indian Meteorological Department (IMD). Cyclone translation speed is calculated as the average speed during the 6-hour period from the 6-hour track position.
- The thermocline displacement due to the cyclonic wind stress is computed along cyclone track using the following equation (Price et al. 1994; Walker et al. 2005).

$$\eta = \frac{\tau}{\rho * f * U_T} \quad (4)$$

Where, η is the thermocline depth (in metres), τ is the wind stress, ρ is the water density, f is the Coriolis parameter and U_T is cyclone translation

5.4 Results

The data are divided into three 8-day periods. The first 8-day period from 17-24 May, 2021 is the pre-cyclone period. The next 8-day period from 25 May to 1 June, 2021 is the during cyclone period and the next 8-day period from 2 June to 9 June, 2021 is the post-cyclone period. SST, chlorophyll and sea level anomaly are analysed for each of these three periods. Ekman suction velocity is analysed during all these three periods using 4-day averaged products. In this case, 4-day averages are considered because the cyclonic storm was active only for 4 days (23-26 May 2021) and 8-day averaged data cannot pick up cyclone induced wind stress curl. The pre-Yaas, during Yaas and post-Yaas Ekman suction velocities are shown in Fig. 5.1.

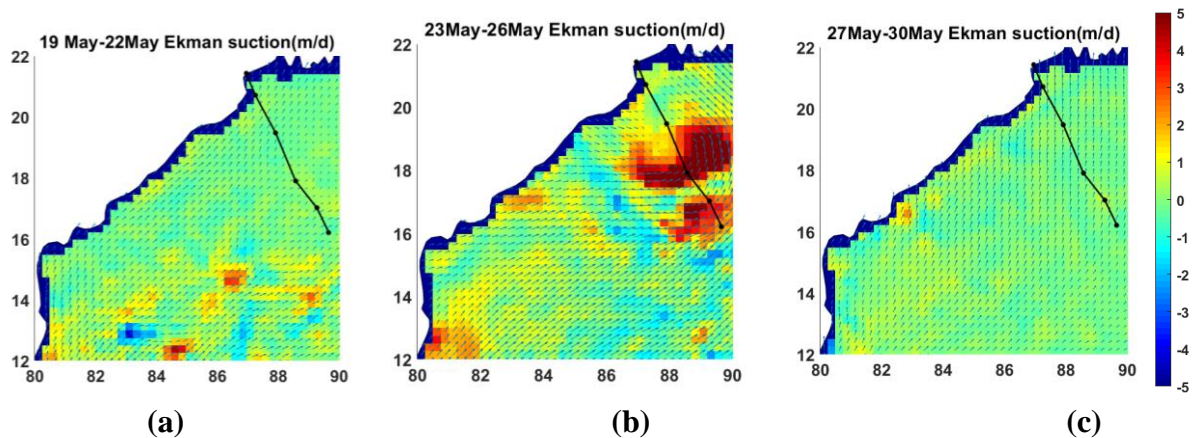


Figure 5.1: (a) Ekman suction velocity(m/d) during 19-22 May 2021 (Pre Yaas), (b) Ekman suction velocity(m/d) during 23-26 May 2021 (during Yaas), (c) Ekman suction velocity during 27-30 May 2021 (post Yaas).

It can be observed from Fig. 5.1 that the period from 23-26 May is characterized by high Ekman suction velocities ranging around 5m/day. The rotating storm system causes Ekman

mass divergence and upwelling due to the wind stress curl. Ekman suction velocities in pre-Yaas and post-Yaas period are significantly lower (<1m/day).

The impact of Yaas cyclone has been observed in the 8-day averaged chlorophyll concentration (CC) images (Fig. 5.2). A region of high chlorophyll plume is observed left of the track in the coastal and offshore waters with CC (0.5 mg/m^3 and more). The data was masked due to cloud cover during cyclone and post-landfall week. In post-cyclone week (2-9 June 2021), the image showed high chlorophyll patches and it is spreading in the north-west Bay of Bengal (BoB) (Fig. 5.2). 8-day composite images of SST showed significantly reduced SST during 25 May-1 June and 2-9 June 2021 due to cyclonic storm induced upwelling and entrainment. Ekman suction velocities of 1-2m/day is observed in the bottom half of the image (Fig. 5.1 b). A coastal plume of increased chlorophyll concentration is seen in the post-Yaas chlorophyll image (Fig. 5.2i) between $12\text{-}17^{\circ}\text{N}$ indicating the possibility of coastal upwelling.

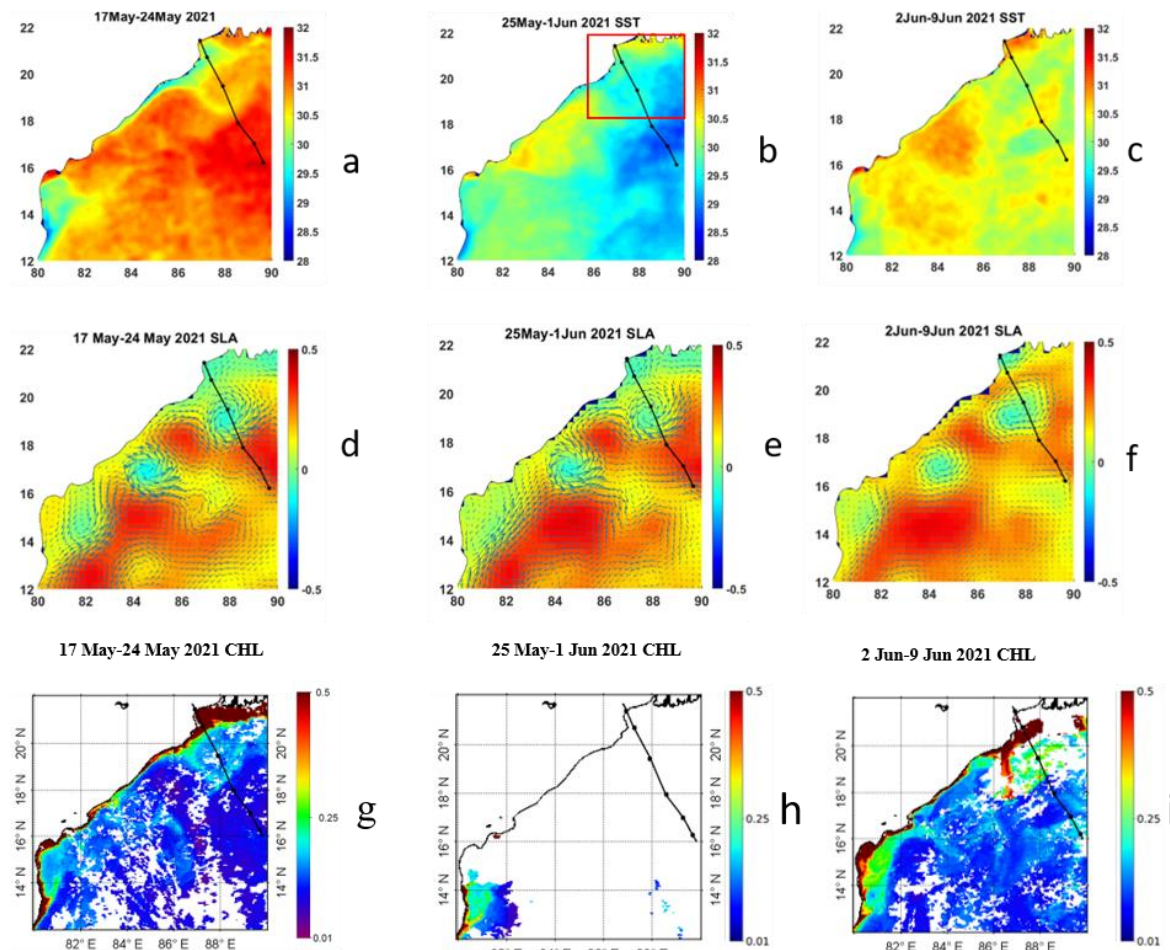


Figure 5.2: SST, SLA and chlorophyll concentration (mg/m^3) for pre Yaas period (17-24 May 2021), during Yaas period (25 May-1 Jun 2021) and post Yaas period (2-9 Jun 2021).

To investigate the change in chlorophyll after the cyclonic event images of pre-cyclone and post-cyclone period were analysed by differencing. The difference images are shown in Fig. 5.3.

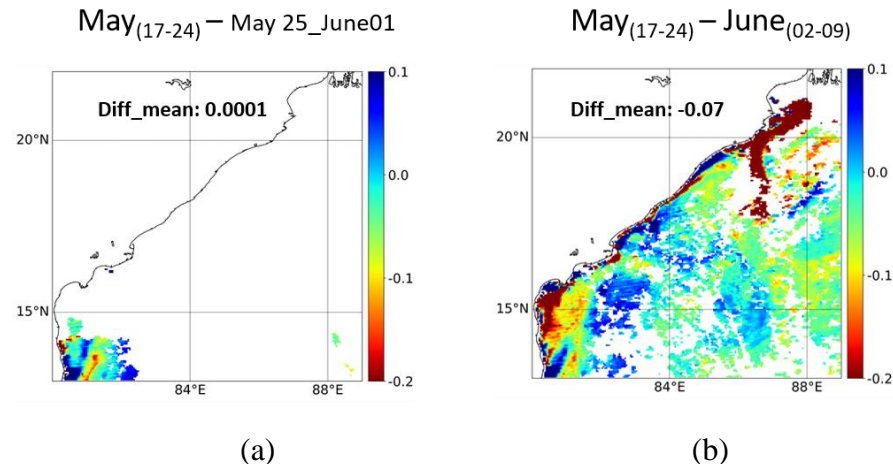


Figure 5.3: (a) Chlorophyll difference image between pre cyclone (May 17-24) and during cyclone (May 25-June 1), (b) Chlorophyll difference image between pre cyclone (May 17-24) and post cyclone (June 2-9)

The chlorophyll difference images show increase in chlorophyll concentration in the June 2-9 image as compared to May 17-24 image. A plume of increased chlorophyll concentration is visible in Fig. 5(b) which extends into offshore waters. Chlorophyll increase of up to 0.2 mg/m³ is observed along the plume.

The average SST and chlorophyll in a rectangular box (shown in Fig. 3b) around cyclone path for the three 8-day periods was also analysed. It is observed that the average SST drops by up to 1.1°C and an average chlorophyll increase of 0.09mg/m³ is observed in the rectangular region. The results are presented in Table 5.1.

Table 5.1: Average chlorophyll and SST for pre Yaas (17-24 May 2021), during Yaas (25 May-1 June 2021) and post Yaas (2-9 June 2021) and percentage change after Yaas.

Parameter	17 May- 24 May	25 May- 1June	2 June-9 June	Percent change
Chlorophyll concentration (mg/m³)	0.26	0.22	0.35	34.6
Sea surface Temperature (°C)	31.01	29.9	30.23	-2.51

The daily time series of SST and SLA over the rectangular box is shown in Fig. 5.4. It can be observed that the SST drops drastically from 24 May, reaches minimum of 29.2°C on May 30 and increases thereafter. There is a slight drop in SLA from 26 May to 30 May.

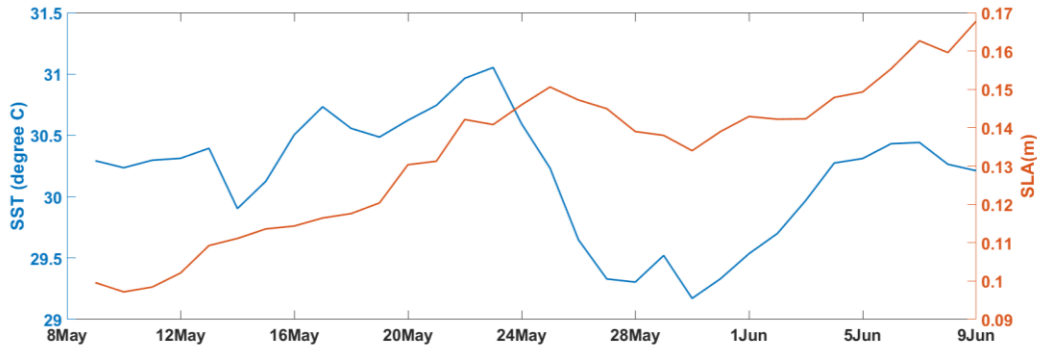


Figure 5.4: Daily time series of SST and SLA in the rectangular box (Figure 5.2b).

5.4.1 Chlorophyll from Ocean Colour Monitor (OCM-2) imagery before and after TC Yaas

We investigated OCM-2 single day passes over Bay of Bengal in order to assess if chlorophyll data could be obtained due to higher spatial resolution of OCM-2 (360 m). OCM-2 scenes before and after cyclone Yaas were inspected for cloud-free data availability. Finally, two scenes were selected, one dated 17 May and other dated 29 May. The OCM-2 scenes are processed and chlorophyll are retrieved using OC-2 algorithm (O'Reilly et al. 1998; O'Reilly et al. 2019). The images are shown in Fig. 5.5.

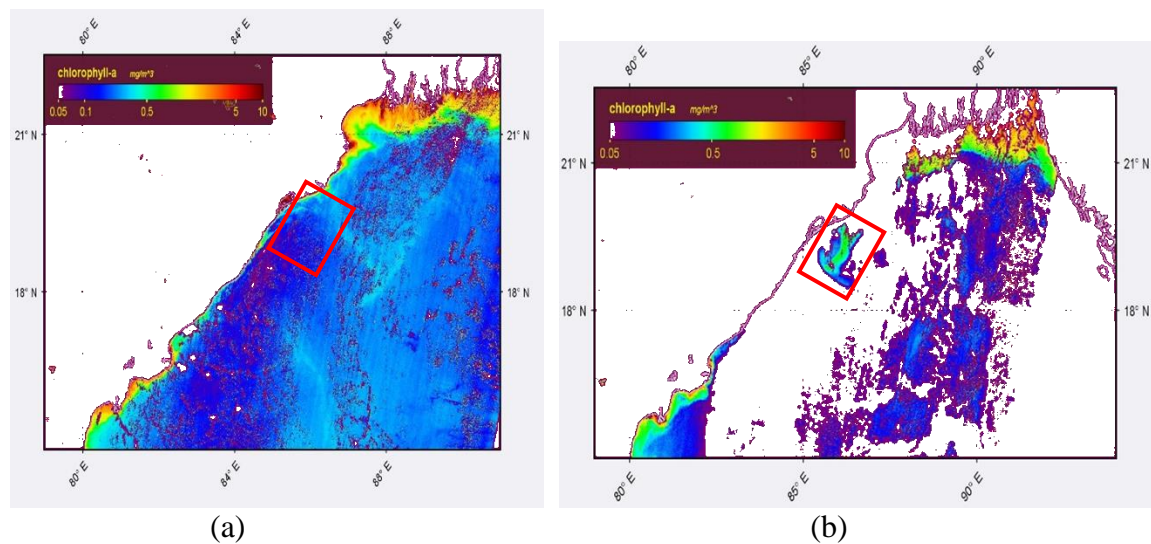


Figure 5.5: Oceansat-2 OCM derived chlorophyll for (a) May 17, 2021, and (b) May 29, 2021.

A patch of increased chlorophyll concentration is observed in OCM-2 imagery on May 29, 3 days after cyclone Yaas landfall. This patch of increased chlorophyll occurs in coastal and offshore waters near Chilka lake, left of cyclone track. The average chlorophyll concentration in the rectangular box was 0.16 mg/m^3 on 17 May, 2021 and 0.6 mg/m^3 in the post-cyclone image of May 29, 2021. Thus, for this region a more than 3-fold increase in chlorophyll concentration was observed. 8-day composite chlorophyll imagery of GlobeColor could not detect this increase because the high chlorophyll patch dissipated in the post landfall week.

5.4.2 Thermocline displacement following the passage of cyclone Yaas

Thermocline displacement is evaluated along the track for every 6 hourly position of cyclone. The results are illustrated in Table 5.2.

Table 5.2: Cyclone Yaas position and thermocline displacement

Date	Time (UTC)	Lat	Lon	Thermocline vertical Displacement(m)
24.5.21	00	16.21	89.65	16.09
24.5.21	06	16.5	89.6	7.75
24.5.21	12	17.01	89.26	13.54
24.5.21	18	17.6	89	19.87
25.5.21	00	17.9	88.56	13.21
25.5.21	06	18.7	88	15.75
25.5.21	12	19.47	87.91	24.14
25.5.21	18	20.1	87.8	20.39
26.5.21	00	20.71	87.24	20.41
26.5.21	06	21.43	86.94	22.77

Thermocline displacement ranging from 7-24 m was observed along the track based on equation 1. Thermocline displacement along the track was also calculated using modelled temperature profile data obtained from Copernicus marine environment monitoring service and found to be in similar range.

5.5 Discussion

Sarangi et al. 2015 reported that for cyclone Phailin, the post-cyclone chlorophyll was around $0.80\text{--}1.50 \text{ mg/m}^3$ in the offshore water, which is quite high as compared to pre-cyclone concentration ($<0.60 \text{ mg/m}^3$). The post-Yaas chlorophyll concentration enhancement is of lesser magnitude and appears only in a small patch close to coast. The intensity of wind speed and wind stress during Phailin was higher (180-200km/hr) before the landfall, which is lesser (~130km/hr) in case of Yaas cyclone before its land fall in northern Odisha coastal region, between Dhamra and Balasore.

Another cyclone named Sidr made landfall during November 2007. The impact of this cyclone on phytoplankton biomass in the western Bay of Bengal (BoB), off Andhra coast was documented with high chl-a range $2.5\text{--}3.5 \text{ mg/m}^3$ (Srinivasa et al, 2009; Maneesha et al, 2011). Chacko et al. 2017 reported well defined chlorophyll bloom all along the track of cyclone Hudhud (October 07-12, 2014). with chlorophyll concentration exceeding 3 mg/m^3 . The monsoon and post monsoon cyclones impact on chlorophyll and ocean productivity is observed to be of higher magnitude as compared to the summer season cyclone impacts. It is reported that the post cyclone increase in chlorophyll is more pronounced in the presence of cyclonic eddies and for slow moving cyclones (Gierach and Subrahmanyam 2008; Chacko et al. 2017; Ganguly et al. 2020). Cyclone Yaas resulted in a 200% increase in chlorophyll concentration in a localised patch close to coast. In other regions the increase is not significant. This needs to be investigated in light of above mentioned facts.

5.6 Conclusion

- Upwelling velocity of 4-6 m/day was observed during Cyclone Yaas. This dropped to less than 1 m/day in the post landfall week. SST decrease of up to 1.8°C was observed in daily data.
- A localised patch of enhanced chlorophyll concentration was observed near Chilka which extended offshore up to 100 kms. Chlorophyll increase of 200-250 percent was observed in this region. This patch has subsequently dissipated and thus absent in 8 day composite image of 2-9 June, 2021.
- A ribbon-like patch of increased chlorophyll concentration was observed left of the track in 8-day composite image. This patch extends from coast to offshore waters and appears to be in the direction of surface currents.
- Thermocline displacement of up to 24m was observed along cyclone track.

References

1. Chacko, N. 2017. Chlorophyll bloom in response to tropical cyclone Hudhud in the Bay of Bengal: Bio-Argo subsurface observations. *Deep Sea Research Part I: Oceanographic Research Papers*. 124:66-72. doi: 10.1016/j.dsr.2017.04.010
2. Dickey, T., D. Frye, J. McNeil, D. Manov, N. Nelson, D. Sigurdson, H. Jannasch, D. Siegel, T. Michaels and R. Johnson. 1998. Upper-ocean temperature response to Hurricane Felix as measured by the Bermuda Testbed Mooring. *Monthly*

- Weather Review.* 126: 1195–1201.doi: 10.1175/1520-0493,126<1195:UOTRTH>2.0.CO;2.
3. Ganguly, D., K. Suryanarayana, and M. Raman. 2020. Cyclone Ockhi induced upwelling and associated changes in biological productivity in Arabian Sea. *Marine Geodes.* 44 (1): 70-89.
 4. Gierach, M.M., B. Subrahmanyam. 2008. Biophysical responses of the upper ocean to major Gulf of Mexico hurricanes in 2005. *J. Geophysical Research.* 113 (C04029).
 5. Jansen, M.F., R. Ferrari and T.A. Mooring. 2010. Seasonal versus permanent thermocline warming by tropical cyclones. *Geophysical Research Letters.* 37(3). doi: 10.1029/2009GL041808.
 6. Maneesha, K., et al., 2011, Meso-scale atmospheric events promote phytoplankton blooms in the coastal Bay of Bengal, *J. Earth Syst. Sci.*, vol. 120, no. 4, pp. 773–782.
 7. O'Reilly, J.E., Maritorena, S., Mitchell, B.G., Siegel, D.A., Carder, K.L., Garver, S.A., Kahru, M., and McClain, C. 1998. Ocean color chlorophyll algorithms for SeaWifs. *Journal of Geophysical Research.* 103 (C11): 24937-24953.
 8. O'Reilly, J.E., and Werdell, P.J. 2019. Chlorophyll algorithms for ocean color sensors-OC4, OC5 & OC6. *Remote Sensing of Environment.* 229: 32-47.
 9. Pan J., L. Huang, A.T. Devlin, and H. Lin. 2018. Quantification of Typhoon-Induced Phytoplankton Blooms Using Satellite Multi-Sensor Data. *Remote Sensing.* 10.318.doi: 10.3390/rs10020318.
 10. Price, J.F. 1981. Upper ocean response to a hurricane. *Journal of Physical Oceanography.* 11: 153–175. doi: 10.1175/1520-0485(1981)011<0153:UORTAH>2.0.CO;2.
 11. Sarangi, R.K., Mishra, M. and Chauhan, P., 2015, Remote Sensing Observations on Impact of Phailin Cyclone on Phytoplankton Distribution in Northern Bay of Bengal, *IEEE Journal of Selected Topics in Applied Earth Observations and Remote Sensing*, 8(2):539-549. doi:10.1109/JSTARS.2014.2347036, February 2015.
 12. Srinivasa, K.T., Nayak, S.R., Mupparthy, R.S., and Nagaraja, K.M., 2009, Phytoplankton bloom due to Cyclone Sidr in the central Bay of Bengal,” *J. Appl. Remote Sens.*, vol. 3, no. 1, p. 033547.

13. Walker, N.D., R.R. Leben, and S. Balasubramanian. 2005. Hurricane-forced upwelling and chlorophyll-a enhancement within cold-core cyclones in the Gulf of Mexico. *Geophysical Research Letters*. 32. L18610.doi: 10.1029/2005GL023716.

6. Damage Assessment of Agricultural Crops and Forest in Coastal Regions of Odisha and West Bengal

**Saroj Maity, Rojalin Tripathy, Nikhil V. Lele, Ayan Das, Mukesh
Kumar, Mehul Pandya and Bimal Bhattacharya**

6.1. Introduction

A detailed study has been carried out to assess the damage of agricultural crops and forest region due to Yaas cyclone in the coastal regions of Odisha and West Bengal. The study included use of microwave and optical sensor data to explore the region affected by cyclone. Cyclone namely Yaas hit the Southern region of the town Chandipur of Odisha (Balasore district) on 25th May 2021. The cyclone further crossed over Simlipal forest and entered Jharkhand, by crossing over Jamshedpur. Cyclone track from IMD is shown in Fig 6.1.

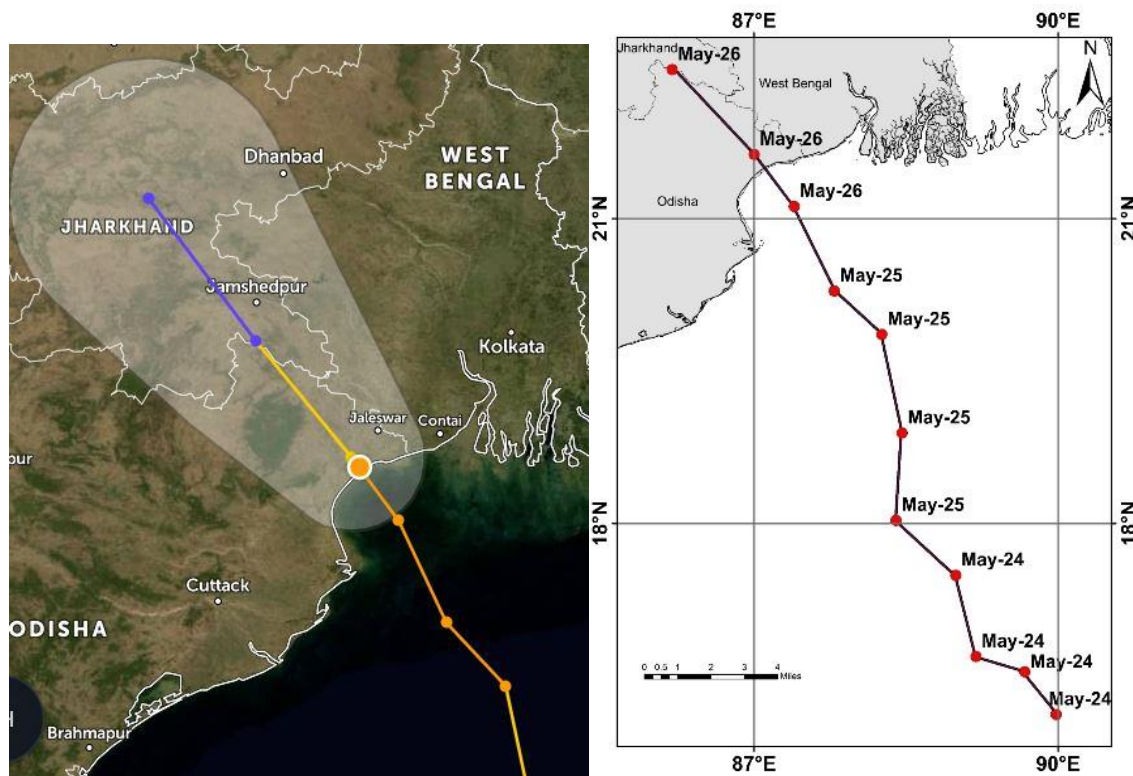


Figure 6.1: sowing location and track of cyclone Yaas in Odisha and West Bengal (source: IMD 2021 and Zoom earth (2021)).

Following sections provide details of two major studies carried out for assess the damage due to cyclone on crop and forest.

A. Damage assessment study for crop using Opti-SAR

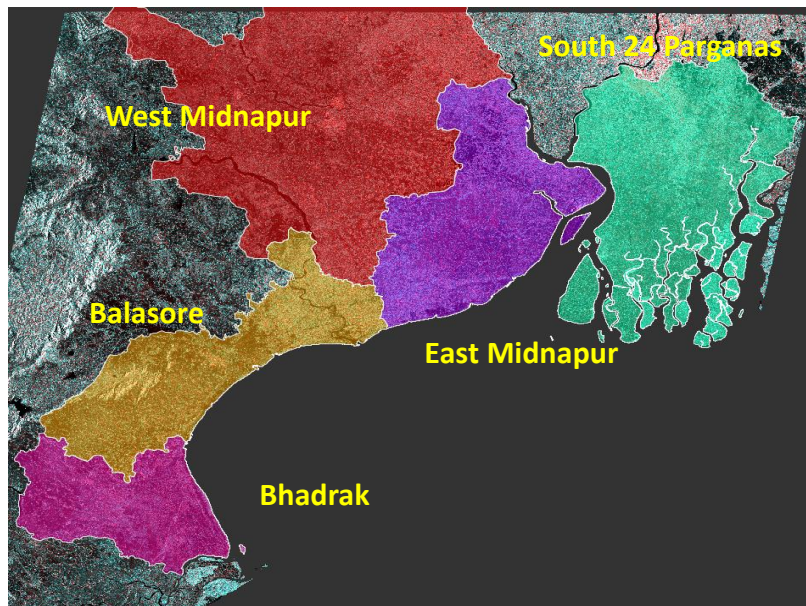
Synthetic Aperture Radar (SAR) plays an important role among the advanced instrument used in remote sensing. It provides complementary information with respect to the optical system and thus simultaneous use of both, helps immensely in vegetation health / growth monitoring. Amplitude

and phase information of Single Look Complex (SLC) SAR imageries of multiple channels, provide good amount of information of the health status of vegetation targets.

Due to the ingress of saline water from sea into the agricultural land in recent Yaas cyclone that fell near Basudevpur, Odisha on 26th May 2021, crop / forest damage, water logging and wide area inundation of fishery land occurred. To assess and monitor these damages, satellite based approach is adopted that used optical and microwave data. The presence / growth of vegetation can be monitored by observing the long-time NDVI profile, while co- and cross-polarised backscatter of SAR data with phase can provide the structural information of the vegetation targets. Using these complementary information, a joint approach has been adopted to map the affected areas.

A.1. Study Area

Coastal region of Odisha and West Bengal comprised of Bhadrak, Balasore, East Midnapore, South 24 Parganas districts have been identified as shown in figure below.



A.2. Data Used

Optical as well as Sentinel -1A SAR data of pre and post-cyclone dates, have been used for the study. Two types of SAR data i.e., GRD (Ground Range Detected) and SLC (Single Look Complex) have been used in this case. The list of data used in our study is tabulated below (Table 6.1).

Table 6.1: Data Used

Sensor type	Sensor name	Data type	Date of Pass	Parameters used	Pixel Spacing
Optical	Sentinel 2A/2B	Multi-spectral	2021-04-27, 2021-04-29, 2021-05-01, 2021-05-02, 2021-05-06, 2021-05-07, 2021-05-09, 2021-05-11, 2021-05-12, 2021-05-14, 2021-05-16, 2021-05-17, 2021-05-21, 2021-05-22, 2021-05-29, 2021-06-01, 2021-06-03, 2021-06-05, 2021-06-06	NDVI	10 m
SAR (Microwave)	Sentinel 1A	GRD	17, 22, 23, 27, 29 May, 3, 4 June, 2021	Sigma_0 (VV,VH)	10 m
	Sentinel 1A	SLC	17 th May & 29 th May, 2021	Entropy	10 m
Ancillary data	Global forest Mask (30 m Landsat derived) ver 1, 2020 (Hansen et al, 2013)				

A.3. Scientific Approaches

Sentinel 2 derived NDVI images were composited using Maximum Value Compositing (MVC) method from both Pre and post-cyclone. From the pre-cyclone NDVI composite image active vegetation mask was generated using NDVI value thresholding (NDVI greater than 0.25 marked as active vegetation). Another set of data pertaining to Landsat derived global forest mask was used to mask out forest area from the active vegetation layer.

(a) *Opti-SAR based approach:*

This active agricultural mask (before cyclone) is then applied on all the S1A derived GRD data for further analysis. Sentinel 1A derived VH and VV backscatter over agricultural active vegetation pixels are analyzed for any changes in frequency distribution histograms before and after cyclone using skewness and kurtosis. Differences in VH and VV backscatter between pre and post-cyclone are mapped over the agriculture pixels. Similarly, pre and post-cyclone NDVI difference image has also been generated. Based on these two images of NDVI difference and backscatter difference probable affected area mapping is done. Those pixels with positive NDVI difference (decrease in NDVI from pre to post) as well as positive backscatter difference (increase in backscatter from pre to post-cyclone resulting in decrease in backscatter dB values) are mapped as probable affected areas. Probable affected areas are further classified into three damage classes of less affected, moderately affected and highly affected areas using equi-quantile segregation of the 95 percentile values. The flowchart of optical and SAR data processing is shown in Fig. 6.2.

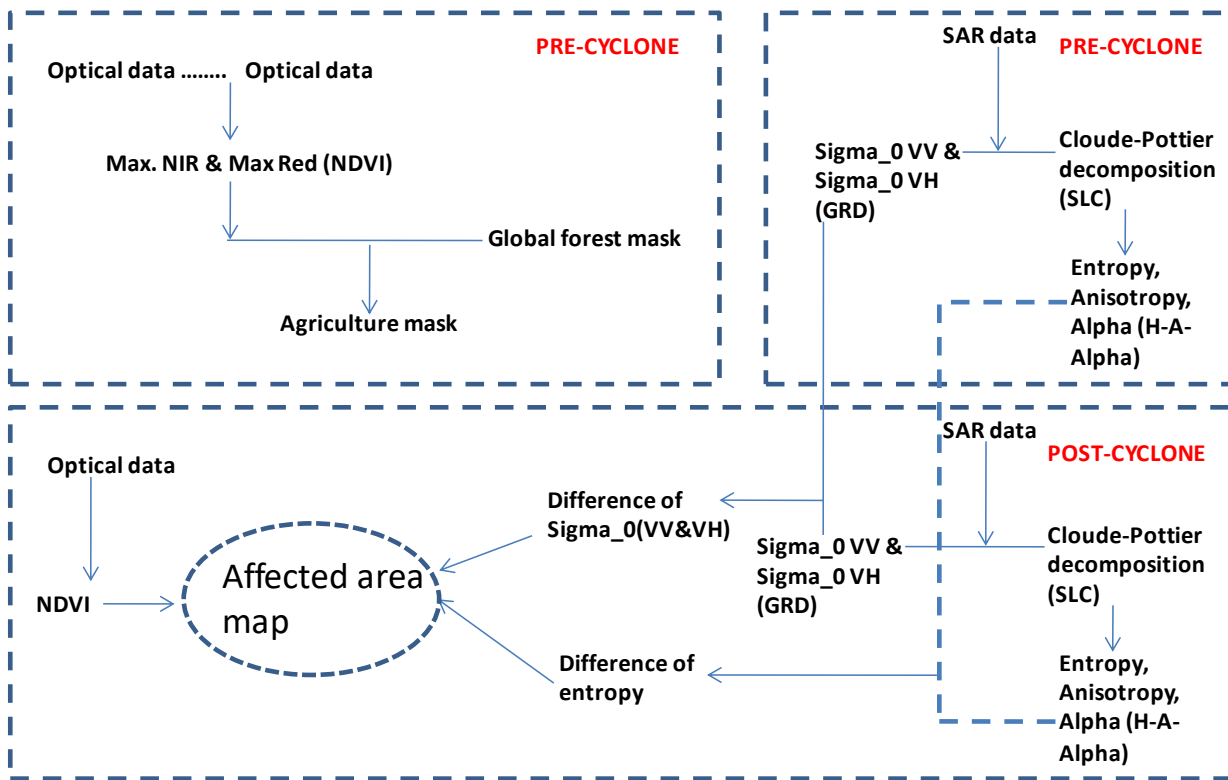


Figure 6.2: Data processing flow chart for optical and SAR imageries.

(b) Polarimetric SAR approach:

Sentinel-1A SAR SLC data sets, dated 17th and 29th May 2021 has also been used to study the effect of cyclone on different polarimetric parameters like entropy, anisotropy and alpha. Eigen value/Eigen vector decomposition is done on two dualpol SAR data sets as proposed by Cloude-Pottier. Decomposed image contains three channels i.e., entropy, anisotropy and alpha. Out of these three parameters, entropy of the image is selected as it signifies the randomness of the targets. This parameter picks up any sort of small disturbance in target geometry. It scales between 0 and 1. Lower value signifies the surface scattering and higher value signifies the more and more volume scattering. It is observed that due to cyclone, the randomness in crop geometry is increased hence increases the value. False colour composite of SAR data sets of pre and post cyclone dates are shown in Fig. 6.3. From the image, the water logged areas has been clearly picked up by backscatter shown in red colour. Using proper threshold, the water covered area has been masked and is shown in Fig. 6.4.

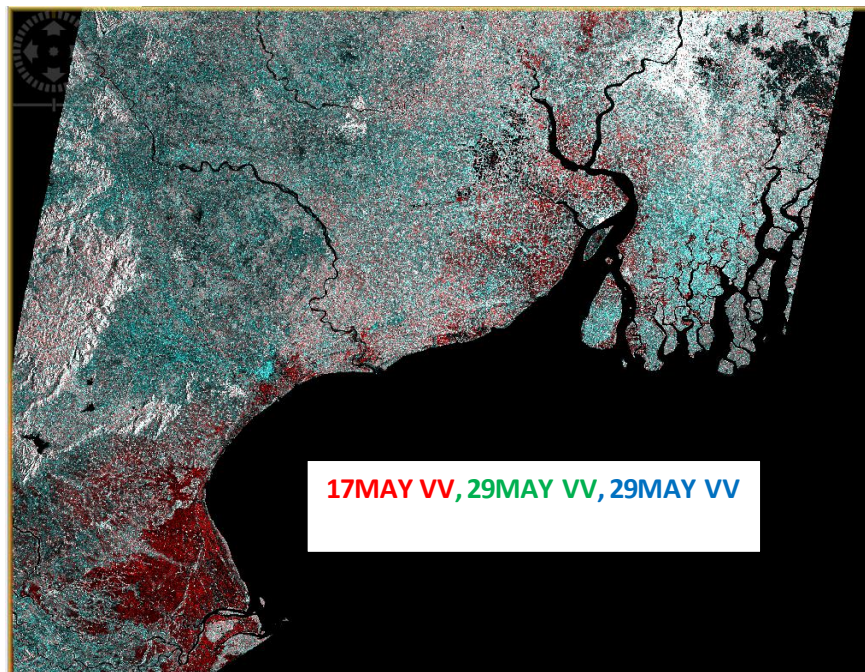


Figure 6.3: FCC of VV channels of Sentinel 1A SAR images (Pre and Post event).

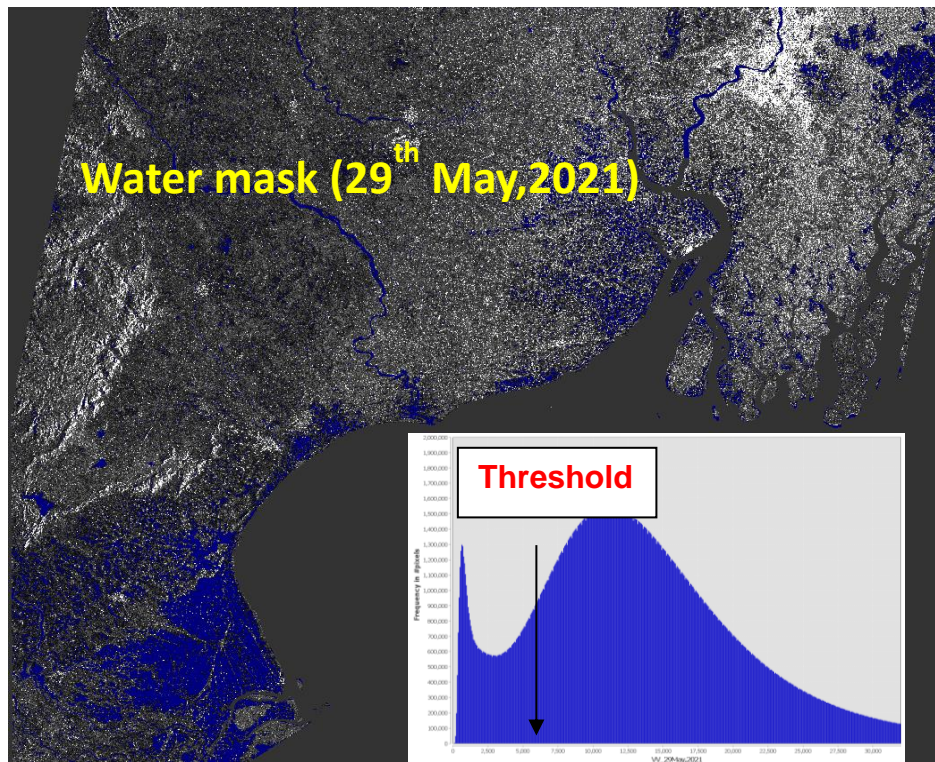


Figure 6.4: Water logged area has been shown as mask. It has been mapped after using the backscatter threshold of 29th May, 2021 image. Threshold value has been calculated from the bi-modal distribution of image statistics.

A.4. Results

From the results, it can be seen that both VH and VV backscatter (in dB) increased from pre to post-cyclone in parts of Balasore, Mayurbhanj, Bhadrak, East Midnapore and South 24 Parganas districts. However, the increase in dB is more profound in VH channel rather than VV (Fig. 6.4). From the VH and VV backscatter difference, it could be found that, both VH and VV backscatter decreased (positive dB difference as shown in red to magenta color) near Basudebpur (place of landfall), Bhadrak district and Chandipur of Balasore district after Yaas cyclone (Fig. 6.5 a). This might be due to inundation of crop fields resulting in lowering of backscatter values. However, interestingly in rest of the parts, particularly near Simlipal forest and parts of West Midnapore district, the backscatter difference between pre and post-cyclone are found to be negative. This could be due to increase in backscatter values either due to increase in surface soil moisture (exposed soil between crop rows) or increase in surface roughness due to crop canopy disturbances. From the table in Fig. 6.6b, it could be seen that both skewness and kurtosis of frequency distribution of histograms varied between pre and post cyclone for both VH and VV polarizations. However, the δ changes in both the parameters are higher in case of VH backscatter than VV backscatter. Therefore, VH backscatter difference over the study sites is used for further mapping of affected areas. In mapping of the affected areas, NDVI difference image from pre to post cyclone has also been employed.

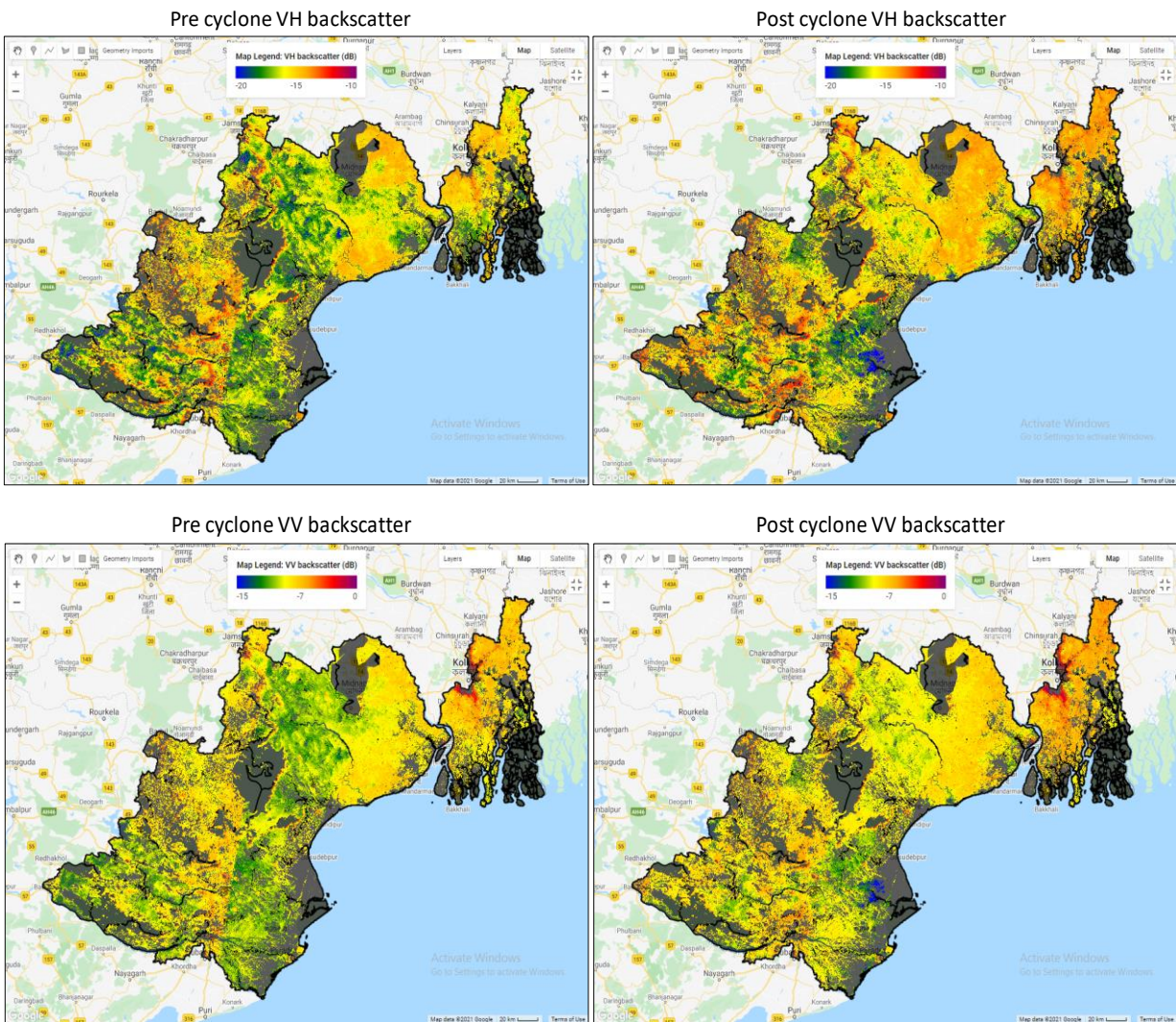
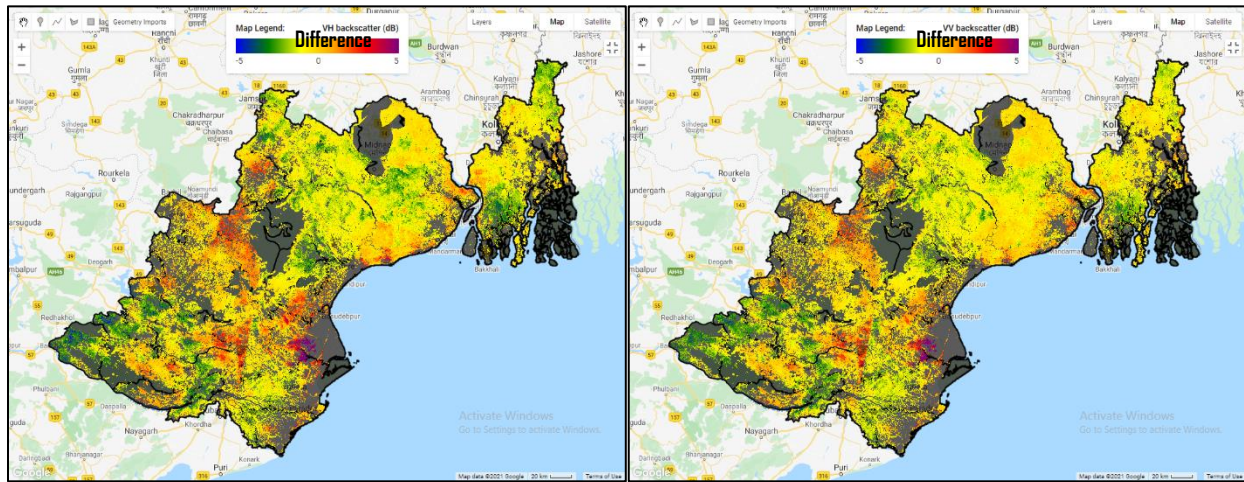
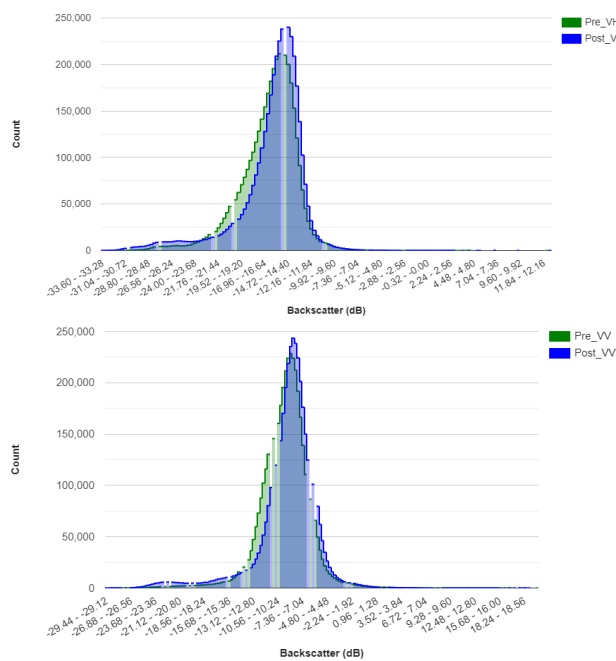


Figure 6.5: Pre and post-cyclone VH and VV backscatter images over agricultural patches. Those pixels with positive VH difference vis-a-vis positive NDVI anomaly were retained as probable affected areas. From the inset in figure 4, it can be seen that VH difference over the probable affected areas varied from 0 to 5 dB. Backscatter difference of -1 to -4.5 dB (coming within 95 percentile) were classified through equi-quantile segregation into three classes of affected areas. Low affected areas are having dB difference of -1 to -1.6 dB, moderately affected areas are having dB difference of -1.61 to -3.2 dB and highly affected regions are having dB difference of -3.21 to -4.5 dB.

(a) VH Backscatter Difference



(b)



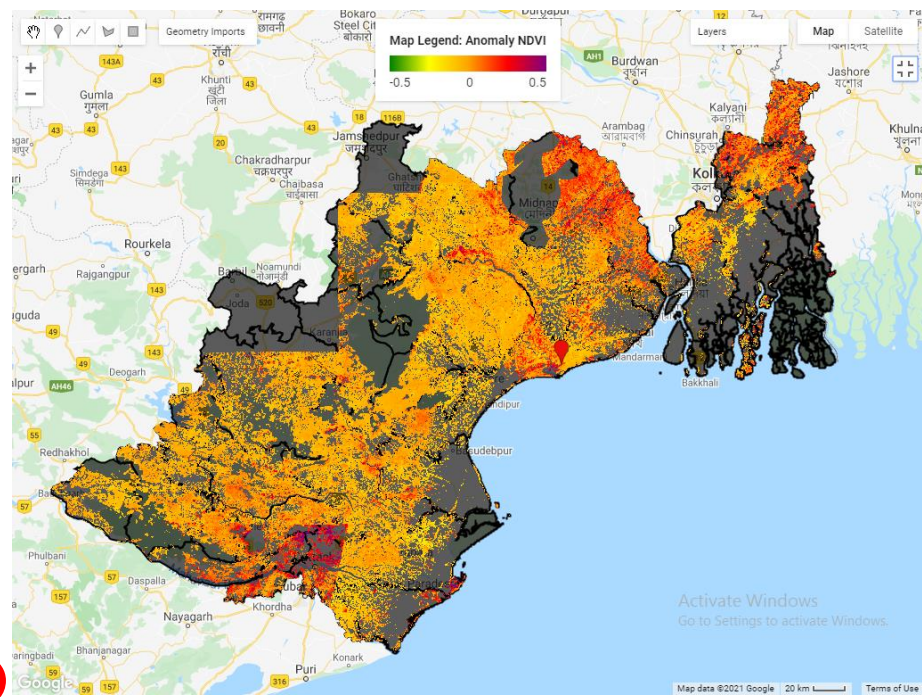
Skewness		
Polarizations	Pre cyclone	Post cyclone
VH	-0.15	-1.58
VV	-0.59	-0.39

Kurtosis		
Polarizations	Pre cyclone	Post cyclone
VH	1.19	7.85
VV	3.36	6.88

δ Change (Pre – Post) in backscatter frequency distribution		
Polarizations	Skewness	Kurtosis
VH	1.43	-6.66
VV	-0.20	-3.52

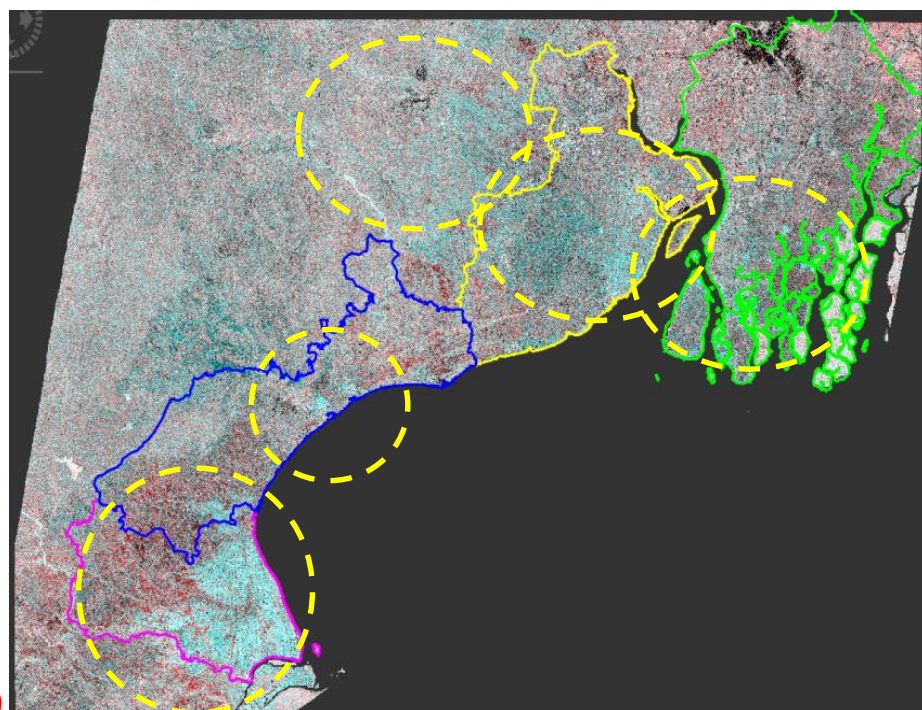
Maximum change in skewness and kurtosis in VH polarization

Figure 6.6: (a) VH and VV backscatter difference (Pre – Post) (b) Frequency distribution histograms of Pre and Post cyclone VH and VV backscatter and change in Skewness, Kurtosis.



(a)

R: 17 May; G: 29 May; B: 29 May



(b)

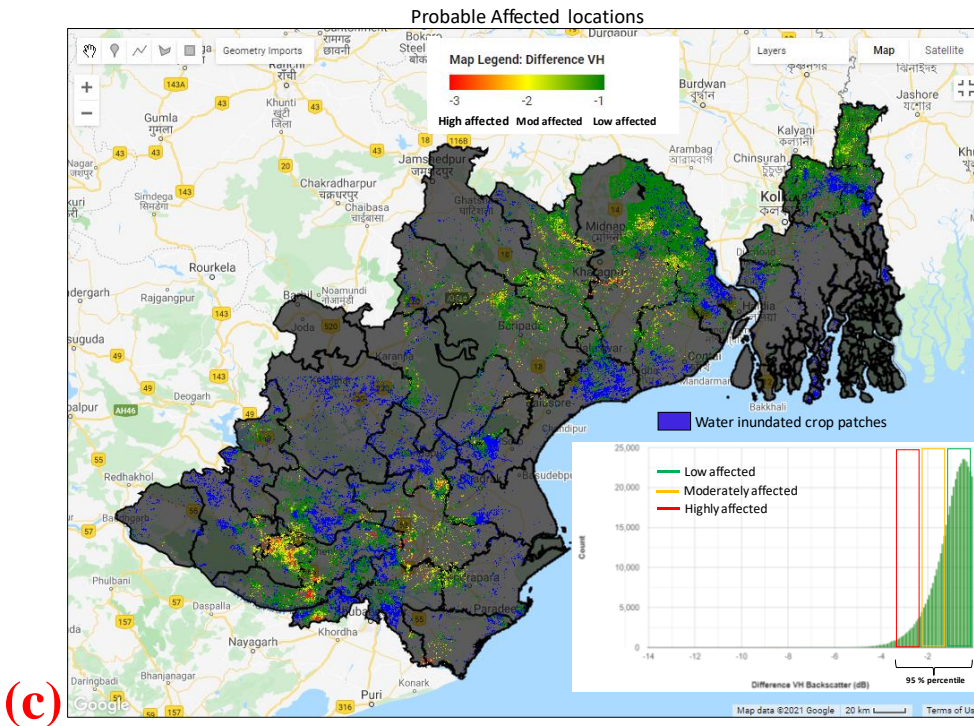


Figure 6.7: (a) NDVI Difference between Pre and Post cyclone. (b) Pre and post-event entropy is shown as FCC. It is clear from the colour of the image that entropy has been increased in Bhadrak, Balasore and eastern side of East Midnapore district. The highly affected area has been marked in dotted circle. (c) Affected area maps over active agricultural patches. Affected areas are mapped from Green (low affected) to yellow (moderately affected) to red (highly affected). Water inundated areas over active agricultural patches are shown in blue color.

B. Damage assessment study for forest region

Many of the coastal areas of the world are vulnerable to tropical cyclones and their associated storm surges (Klemas 2009). Particularly in tropical countries of the world, cyclones are one of the major natural disturbances to forest ecosystems, typically generating sustained high winds, storm surges and heavy rainfall. These disasters often cause significant loss of life, property and environmental damage in large-scale and are expected to increase in intensity and frequency due to a warming climate (Knutson et al. 2010). A severe cyclone can extensively influence the composition, structure and succession of forests, and consequently affect the terrestrial carbon sink (Foster, 1988; Boutet and Weishampel, 2003). Remote sensing can be a cost-effective, accurate and potential tool for mapping the damages of tropical cyclones from small to large regions to support the management approaches (Vatsavai et al. 2011).

Majority of the studies are based on optical remote sensing, in which the change or standardized change of various vegetation indices are adopted as damage indicators with few efforts to evaluate their quantitative relationship with forest damage at the pixel level, and with few comparative analyses on the performance of these vegetation indices.

B.1. Study area and datasets

Study area includes forest regions of Balasore, Bhadrak and Kendrapara districts of Odisha. Study area also includes forest regions of Simlipal wildlife sanctuary and mangrove vegetation of coastal Odisha, particularly Bhitarkanika national park.

Simlipal sanctuary is situated in Mayurbhanj district of Odisha that comprises of moist deciduous and semi-evergreen forests, while Bhitarkanika region is dominated with mangrove vegetation, with various species such *Avicennia*, *Excoecaria*, *Heritiera* etc. Bhitarkanika region particularly, is close to mouth of the river and is comprised of several low-lying areas such as Satabhaya.

In the present study analysis-ready data (ARD)(surface reflectance product) from Sentinel-2 optical MSI instrument were acquired to asses vegetation affected due to cyclone. Pre-cyclone data during 1st May to 20 May 2021 were used and maximum NDVI composite was generated for the entire region. Similarly, to understand the impact of cyclone, post-cyclone data from 26 May to 1st June was processed in similar way to prepare maximum NDVI composite. Cloud mask with QA 60 band from Sentinel-2 data was used to mask cloud from each of the image. Entire procedures were implemented through Google Earth Engine (GEE).

B.2 Methodology

Research on satellite remote sensing of hurricane-induced forest damage started in the 1990s, because satellite data have high temporal and spatial resolution, and extensive coverage relative to ground and aerial measurements.

Several remote sensing based indices such as NDVI, NDII, or variations of NDVI and NDII are used to assess damage in vegetation. The image differencing method is used to derive the change of damage indicators before and after a cyclone. NDVI is a well-known and most popular vegetation index, though some studies also indicate better results from use of NDII, due to its better sensitivity to vegetation modifications. Yet, NDVI is more commonly used due its simple, easy to implement and interpret for largescale investigations (Muhammad Al - Amin Hoque, 2015).

In the present study, NDVI difference for pre-cyclone and post-cyclone data was used to identify forest areas affected due to cyclone. In order to eliminate possible errors due to phenological changes during this period, vegetation phenology in few representative areas were also checked.

Vegetation phenology plays important role particularly in deciduous and semi-evergreen forest regions and need to be carefully studied before concluding vegetation changes across the months. As mentioned earlier, vegetation phenology from representative areas in Simlipal forest was first analysed using time-series data of year 2019. Time-series NDVI of Senitinel-2 data is shown in Fig 6.7. The profile of NDVI clearly explains increasing trend in NDVI during month of May and June. This implies that the subtraction ($NDVI_{May} - NDVI_{June}$) will result in negative values. Therefore, as mentioned earlier, all positive values resulting from $NDVI_{Pre-cyclone} - NDVI_{Post-cyclone}$ are likely to be vegetation changes due to cyclone and need not be attributed to phenological changes.

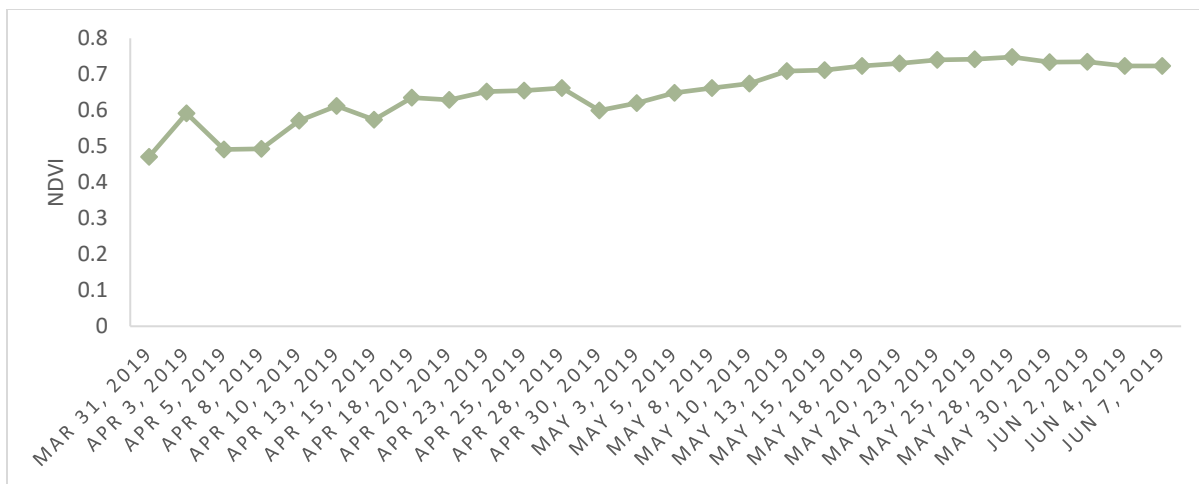


Figure 6.8: NDVI profile indicating vegetation phenology during April to June 2019, indicating increasing trend of NDVI between month of May and June.

Further, district-level forest mask was used to remove non-forest areas from the data. There were patches of intermittent clouds which are also masked out. Areas shown as ‘not affected’ in the subsequent results is summation of all non-negative constituents in the data such as- areas with increase of vegetation (increase in post-cyclone period), non-forest areas, cloud areas and NDVI difference as zero.

B.3 Results

(i) Assessing affected forest patches in selected districts

Balasore district

Landfall of cyclone occurred in Balasore district. Total forest area affected due to cyclone is 10% of total forest area of the district, corresponds to 10,100 sq m area. Among the affected areas, not only the areas close to coast were affected but also in-land forests areas such Kulhadia sanctuary was also affected. Thin strip of mangrove vegetation along the Balasore coast indicates minor changes in NDVI. Overall, less affected area was 9% of total forest area of the district and moderately affected was 1 % (Fig 6.8).

Bhadrak district

Forests area in Bhadrak district is more of scattered forests. Total forest area affected due to cyclone is 31% of total forest area of the district, corresponds to 93,800 sq m area. Remaining

69 % remains unaffected due to cyclone. Results showed less affected area was 26% of total forest area of the district, moderately affected was 4 % and heavily affected was 1 % (Fig. 6.9).

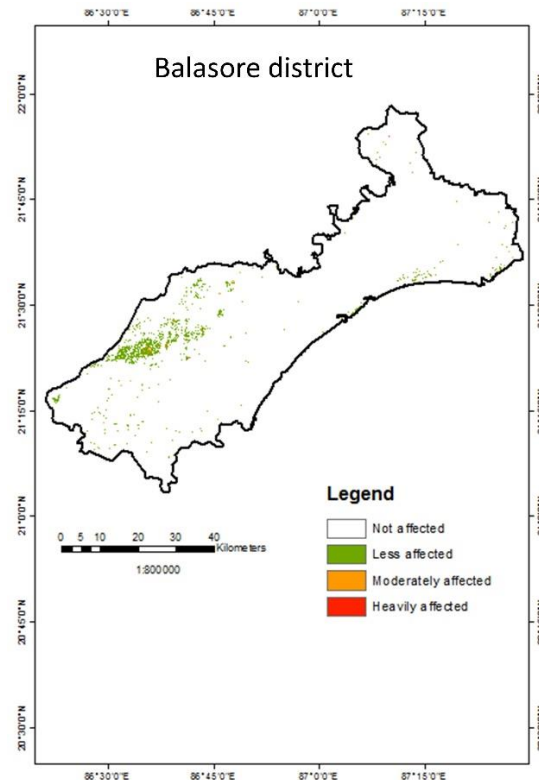


Figure 6.9: Cyclone affected forest areas of Balasore district

Kendrapara district

Kendrapara district comprises of mangrove areas of Bhitarkanika, which is one of the largest continuous stretch of mangroves in the country. Western part of the district has few pockets of forests as well. It was found that in all 1.57 sq km (1572000 sq m) of forest vegetation was affected, that corresponds to 30 % of forest area of the district. Results showed less affected area was 18% of total forest area of the district, moderately affected was 7 % and heavily affected was 5% (fig 10).

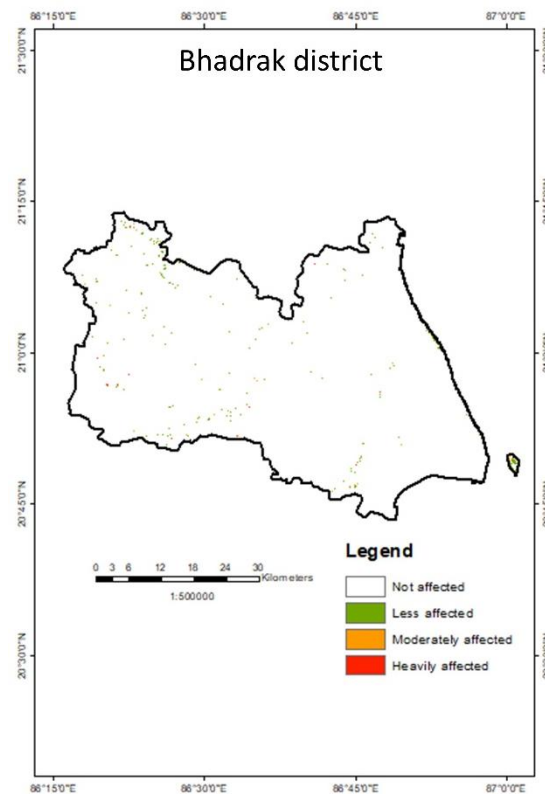


Figure 6.10: Cyclone affected forest areas of Bhadrak district

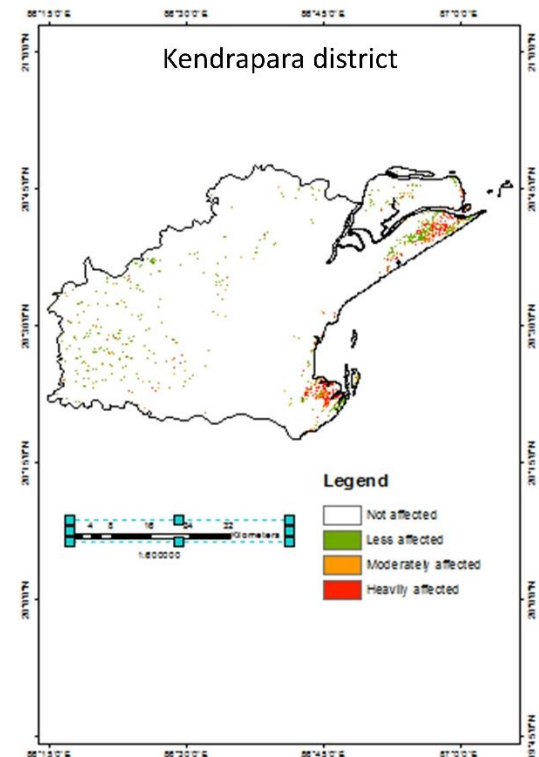


Figure 6.11: Cyclone affected forest areas of Kendrapara district

(ii) Changes in Bhitarkanika mangroves

Bhitarkanika mangroves and surroundings were considered for assessing impact of cyclone on mangroves, showed few patches of mangroves affected in Dangmanl and Kalibhanjdiya island (Fig. 6.11). Overall, less affected and moderately affected area constitute 12 % each while heavily affected area is 15%. Large patches of decrease in NDVI (heavily affected patches) are particularly seen in Satabhaya area, it is important to note that, these patches are currently inundated with water. This area is a low-lying area dominated with *Suaeda* species, that is one of the typical low-heighted mangrove associate. Being a low-lying area, water inundation is frequent in this region and cyclonic conditions with heavy rainfall in this region may lead to surge of water, further leading to inundation in Satabhaya region. The same also has been reported in news article highlighting falling of trees in Bhitarkanika and saline water inundation in Satabhaya (Down to Earth, 2021).

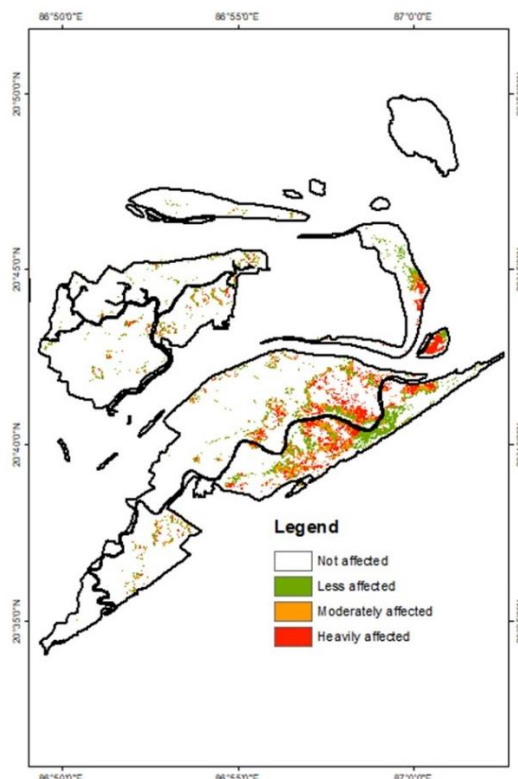


Figure 6.12: Cyclone affected forest areas of Bhitarkanika and surroundings

(iii) Changes in Simlipal forest and surroundings

As per the track of cyclone, it precisely crossed over Simlipal forest in Mayurbhanj district of Odisha. Total affected area in Simlipal forest is nearly 46%, that consists of 39 % less affected, 5 % less affected and 2 % heavily affected. This corresponds to 3.67 sq km area.

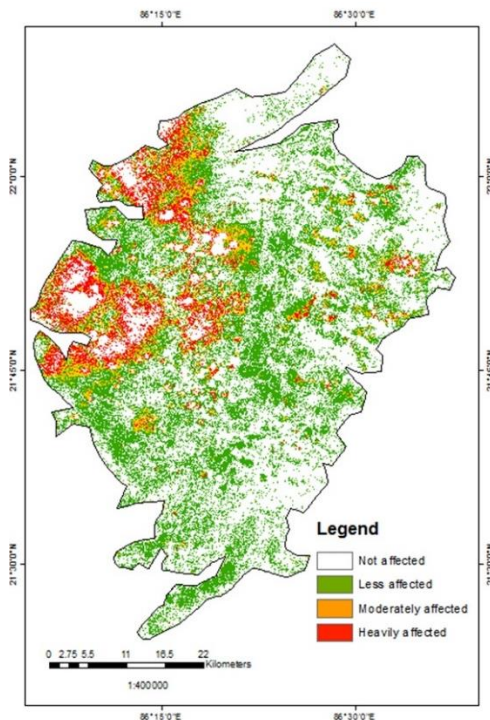


Figure 6.13: Cyclone affected areas in Simlipal forest

Table 6.2: Summary of various affected forest areas

Area	Total forest affected (%)	Less affected (%)	Moderately affected (%)	Heavily affected (%)
Balasore district	10	9	1	0
Bhadrak district	31	26	4	1
Kendrapara district	30	18	7	5
Bhitarkanika and surroundings	41	12	12	15
Ssimlipal forest	46	39	5	2

In summary, it can be noted that not only the coastal mangrove vegetation, but also the in-land forests such as Simlipal, negative changes in vegetation as a result of cyclone were seen. Ground reports from Bhitarkanika and Simlipal also confirm the same. In this region, strong winds were the main reason for uprooting / felling-off of forest trees.

(iv) Sources of uncertainties

Through forest areas are showing negative changes as impact of cyclone, it is also important to mention that some of the areas in the data are also water-logged or having cloudy situations,

leading to blurring of the data and may not clearly indicate vegetation affected due to cyclone. In addition, increase of forest vegetation such as shrubs/ grasses due to rain were also observed. Overall analysis with available datasets indicating negatively affected forests are presented here.

6.2 Conclusions

The systematic data from optical Mx and SAR instruments in the form of Analysis Ready Data and polarimetric signatures at 10m spatial resolution at 6-day interval from twin satellites of Sentinel-1A/1B and Sentinel-2A/2B have shown the potential of possible damage detection and mapping affected areas with various levels of possible disturbances. However, EO-based disaster impact and risk reduction support requires quicker and repetitive assessment of the affected areas within a very short period (7 – 10 days) of time after landfall. Therefore, there is a need of constellation of high-resolution (~ 5-10m) optical and C-band SAR instruments onboard India's space-based platform and daily high-resolution analysis ready data for quicker damage assessment. This possibility needs to be explored with other application requirements where highly dynamic and frequent monitoring at this resolution are required even in areas not affected by disaster.

References

1. Boutet Jr., J.C., Weishampel, J.F., 2003. Spatial pattern analysis of pre- and posthurricane forest canopy structure in North Carolina, USA. *Landscape Ecology* 18, 553–559.
2. Down to Earth, 2021. <https://www.downtoearth.org.in/news/natural-disasters/months-after-forest-fire-cyclone-yaas-threatens-flooding-in-similipal-77150>. Accessed 18 June 2021.
3. Foster, D.R., 1988. Species and stand response to catastrophic wind in central New England, USA. *Journal of Ecology* 76, 135–151.
4. Klemas, V. V., 2009. The role of remote sensing in predicting and determining coastal storm impacts. *Journal of Coastal Research*, pp.1264-1275.
5. Knutson, T. R., McBride, J. L., Chan, J., Emanuel, K., Holland, G., Landsea, C., Held, I., Kossin, J. P., Srivastava, A., and Sugi, M., 2010. Tropical cyclones and climate change. *Nature Geoscience*, 3 (3), pp. 157-163.

6. Muhammad Al - Amin Hoque, 2015. Assessing tropical cyclone damage using moderate spatial resolution satellite imagery: Cyclone SIDR Bangladesh 2007. *Proceedings of ACRS 2015*.
7. Vatsavai, R., Tuttle, M., Bhaduri, B., Bright, E., Cheriyadat, A., Chandola, V., and Graesser,.2011. Rapid damage assessment using high-resolution remote sensing imagery: Tools and techniques. In: Proceedings Geoscience and Remote Sensing Symposium (IGARSS), IEEE International 2011, IEEE, pp.1445-1448.